The Pennsylvania State University

The Graduate School

Department of Electrical Engineering

BROADENING SPECTRAL RESPONSE IN SOLID-STATE DYE-SENSITIZED SOLAR CELLS VIA FÖRSTER RESONANCE ENERGY TRANSFER

A Dissertation in

Electrical Engineering

by

James Ian Basham

Submitted in Partial Fulfillment
of the Requirements
for the Degree of

Doctor of Philosophy

December 2011

The Dissertation of James Ian Basham was reviewed and approved* by the following:

James Breakall
Professor of Electrical Engineering
Dissertation Advisor
Chair of Committee

Thomas Mallouk
Dupont Professor of Materials Chemistry and Physics

Suman Datta
Associate Professor of Electrical Engineering

Qiming Zhang
Distinguished Professor of Electrical Engineering

Kultegin Aydin
Professor of Electrical Engineering
Interim Head of the Department of Electrical Engineering

*Signatures are on file in the Graduate School

Abstract

Dye-sensitized solar cells (DSSCs) are a promising renewable energy technology. However, in the 19 years since the dye solar cell was first popularized by O'Regan and Gratzel there has been little improvement in efficiency. A major hurdle to increasing the efficiency of both solid and liquid dye-sensitized solar cells is the fact that these cells can only convert light in a relatively narrow spectral region. For example, the most popular dye used in DSSCs, N-719 dye only responds to wavelengths of light between 350-650 nm. Its competitor, crystalline silicon will convert light all the way to 1100 nm. While DSSCs can have conversion efficiencies near unity for the light which is absorbed, the fact that they are unable to process a large fraction of the solar spectrum creates a fundamental limit on their overall efficiency.

Without a broader spectral response, DSSCs cannot achieve efficiencies high enough to displace other more expensive technologies. While many different solar dyes have been synthesized in the past two decades, the most efficient cell realized to date, possessing an 11.5% conversion efficiency, still uses a dye with a structure very similar to that used in the original Gratzel cell published in 1991 and has the same spectral response in the range from 350-650 nm. Thus far, efforts to increase efficiency by extending the response of dyes have been unsuccessful. It seems that there is a tradeoff between having a high absorption coefficient and having a broad absorption range. Many of the strongly absorbing red and NIR dyes have narrow response windows which are insensitive to much of the blue and green light. The problem becomes more significant when we consider the case of solid state dye sensitized solar

cells (SDSCs). The active layer of an SDSC is required to be very thin due to transport limitations of the low-mobility hole transport materials used. In order to completely absorb light using such a thin layer, we are restricted to using only the aforementioned high absorbing dyes with narrow spectral response windows.

The question then becomes “what can we do given the materials available to us?” The obvious solution is to employ two or more sensitizers with complementary absorption spectra which can together create a solar cell with a broader spectral response. Historically, the most successful examples of this concept have been dye cocktails, in which two or more dyes are absorbed onto titania and work in parallel. To date, however none of these dye cocktails has demonstrated a performance better than if the best constituent dye was used alone.

The focus of this dissertation is a newly developed approach which relies on Förster Resonance Energy Transfer (FRET). In this scheme two dyes work in series instead of in parallel. A short wavelength absorbing donor material dispersed in the hole transport material is coupled with a long wavelength absorbing acceptor material anchored to the surface of titania. The donor material absorbs the short wavelength light, becomes excited, and transfers this excitation to the acceptor dye. In addition to the energy transferred from the donor, the acceptor also absorbs the long wavelength light matching with its own absorption spectra, which would be its only energy source in the absence of the donor material. Combining the materials in this way overcomes several of the losses inherent in the dye cocktail system, and because the donor and

acceptor are not in physical contact they are insensitive to many of each other's properties.

FRET has the potential to overcome current efficiency limitations for SDSCs yet, at the inception of this work, FRET had not yet been demonstrated in SDSCs. The purpose of this dissertation is to develop and demonstrate efficient FRET systems, and indentify appropriate donor and acceptor materials. Herein, efficient working systems are demonstrated using off-the-shelf laser dyes as donors and commercially available solar cell dyes as acceptors.

Table of Contents

List of Figures

List of Tables

Acknowledgements

First and foremost, I would like to thank Dr. Craig Grimes, under whose guidance I performed the majority of my research. I would like to thank Dr. Thomas Mallouk for his great assistance in the assembly of my dissertation, and Dr. James Breakall for his proactive role in assuming responsibility for my committee. I would like to thank Dr Thomas Jackson for finding the time to teach the majority of my graduate classes.

I would like to thank all of the members of my lab with which I had the pleasure of working, including Dr Karthik Shankar who taught me all of the fundamentals in my first year, Dr Gopal Mor who taught me the fine art of solar cell fabrication and supplied unwavering optimism and motivation, and Drs. Oomman Varghese and Maggie Paulose whose complete abstinence from sleep has kept our lab running smoothly and productively for years.

Finally, I would like to thank all of my friends and family who have provided support in my effort and balance in my life.

1. Introduction

1.1 Powering the Planet

It requires a staggering amount of energy to power our planet. The global average rate of electrical energy consumption is 2.1 terawatt[1]. All other energy uses such as transportation, heating, agriculture and industry bring the total primary power load to 16 terawatts.[1] For a large and still growing faction of the world population, the modern way of life is predicated on cheap and abundant energy. As the world population continues to increase and developing countries start on the path of American-style consumerism this power load is expected to increase exponentially with time at an estimated rate of 1.4% per year, perhaps reaching 24 TW by 2035.[1] About 80% of this energy currently comes from burning fossil fuels. The damage that the extraction and utilization of these resources does to both the environment and human health is becoming increasingly visible and undeniable. Furthermore, as these resources become scarcer their market value is likely to increase substantially as competition over them increases. There is some debate about how long it will take us to run out of fossil fuels. In almost all cases though the forecasts[2,3] agree that it will be quite soon, they argue only about a few years sooner or later. However, long before we burn the last lump of coal it will be economically unfeasible to extract and refine progressively deeper, smaller and poorer quality deposits.[3] The end of the cheap energy which enables our way of life will be upon us much sooner than the end of fossil fuel reserves.

Clearly, we must drastically cut global dependence on finite fossil fuels. We must replace current technologies with new ones that have the potential to produce power on the terawatt scale. But that is much easier said than done. So far, no renewable energy technology can compete with coal which is cheap, abundant and easily utilized. People will continue to burn coal for electric power until a cheaper alternative is presented to them. Despite the fact that we already have the ability and manufacturing capacity to produce several forms of affordable renewable energy technologies, and existing solar technologies can already pay back their embodied energy in 1-4 years,[4] market forces dictate that they will not be widely adopted until they are the cheapest forms of energy available. The solution to this problem is to develop inexpensive, efficient solar energy conversion devices. No other renewable energy source even comes close to being able to fulfill our total energy needs[5]. The total power that could feasibly be derived from hydroelectric dams is estimated to be about 0.9 TW, although we already produce about 0.6 TW of hydropower today.[5] The amount of power derivable from wind energy may be up to 2-4 TW, assuming that turbines were placed on all suitably windy locations on Earth.[5] Biofuels have been the focus of much hope, although a large fraction of the world's arable land is already used to produce food. Biofuels may be able to produce up to 5 TW averaged over the year, although it would require the farming of all remaining land with sufficient rainfall, including national forests and preserves, rainforests, etc.[5]

The power delivered to the surface of the Earth by the Sun is 120,000 terawatts.[6] Enough energy falls on the surface of the Earth in just one hour to power humanity for an entire year. In fact, all of the energy that could ever be produced from our total

reserves of coal, oil, gas, and mined uranium amounts to only 6 months worth of the solar energy hitting earth.[6] And, this energy comes free. The obvious choice is to harness the sun, as that is where the real potential lies. The challenge is only to find a way to harness it in an affordable and scalable manner .

1.2 The Solar Resource

As with any instance where energy is converted from one form to another, we may be concerned about the specifics of the raw form of energy. The solar energy which reaches the Earth leaves the sun as black body radiation, fueled by the heat produced by fusion at the core. Measured at the edge of the earth's atmosphere, the solar spectrum is very similar to black body radiation with a temperature of about 5800 K. The intensity is about 1366 W/m^2. By the time the light hits the surface of the Earth some has been lost due to scattering, as well as absorbed by compounds in the atmosphere, notably water, ozone and carbon dioxide. The intensity at the surface of the earth for a collector directly facing the sun, at a latitude of about 37 degrees is about 1000 W/m^2, of which approximately 900 W/m^2 is direct and 100W/m^2 is diffuse on a clear day. [7] This ratio is highly dependent on local conditions however, with greater cloud cover resulting in more diffuse light. The ratio of diffuse to reflected light is important when considering which type of technology to use, as solar concentrators collect only the direct component, due to the nature of concentrating optics, while thin film photovoltaics can collect both the direct and diffuse components.

Access to sunshine is not equal, being based on local conditions such as latitude, season and weather patterns. Maps of average irradiance have been made, and areas of high development potential have been identified. Typically one looks for areas with a high number of clear days per year as there are no economical means of storing large amounts of electrical energy. Areas such as the American southwest and the Sahara Desert have been identified as prime locations for utility scale power, although it is worth noting that areas with high population density but less solar irradiance become economical as the price of solar modules decreases. It is also interesting that Germany, which has a rather modest amount of average irradiance, is perhaps the biggest market for solar panels. Canada currently has one of the world's largest single PV installations at 80 MW consisting of over one million CdTe panels. **Figure 1** and **Figure 2** show the average amount energy reaching the earth's surface per day across the United States. Values are given for both the flux across a fixed plane facing south and tilted from the vertical by an angle equal to the local latitude, which is the typical way to mount a conventional photovoltaic panel, and for a plane whose normal is directed to the sun and tracks it through the day, which maximizes power density on the collector and is the typical way that concentrated solar power trackers work. The flux relative the surface normal is also important to consider when calculating how much land is to be used to collect a required amount of energy, while the energy incident on a tilted collector is important to consider when calculating the area of solar panels to install.

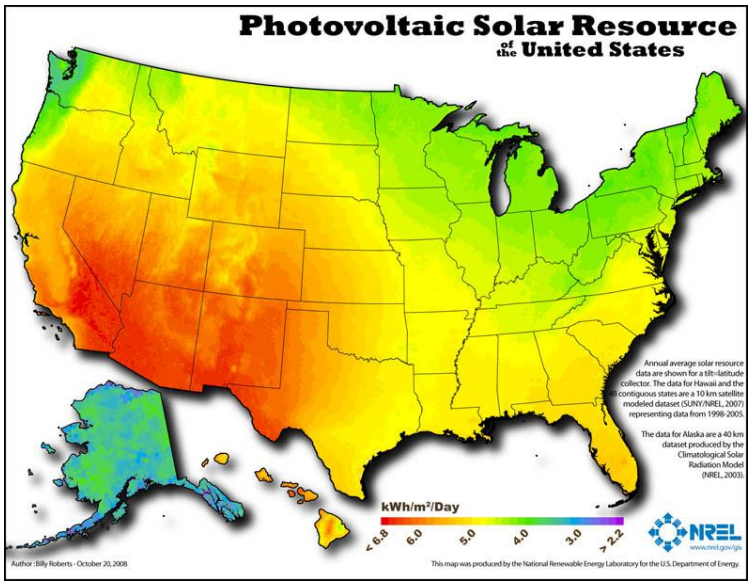

Figure 1: Average daily insolation for a fixed flat panel facing south and tilted at an angle from the vertical equal to the local latitude. [8]

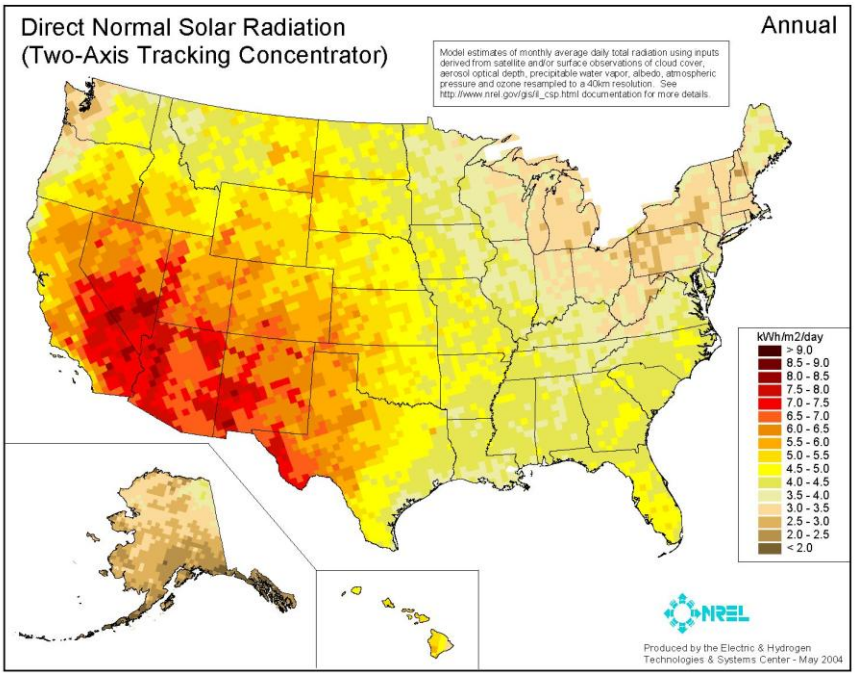

Figure 2: Yearly average insolation for an absorber which tracks the sun throughout the day. Includes direct radiation only: excludes diffuse radiation. [8]

These raw power values can be further broken down to a power density as a function of wavelength. About 42% of the total solar power lies in the visible region between 350 nm – 650 nm. 33% of the total is found between 650 nm – 1000 nm, leaving most of the remaining 25% at wavelengths longer than 1000 nm. This distribution is significant as it is easier to harvest higher energy photons using a PV device, while generally more difficult and less beneficial as wavelength increases. Because the open circuit voltage of a device diminishes as the bandgap lowers, there is an optimum bandgap value of about 1.1 – 1.3 eV for a single junction cell limiting efficiency to a maximum theoretical value, the Shockley-Queisser limit of about 30% efficiency.[9] This means that, in order to be as efficient as possible, a single-absorber solar cell must ideally be able to absorb out to 950-1100 nm.

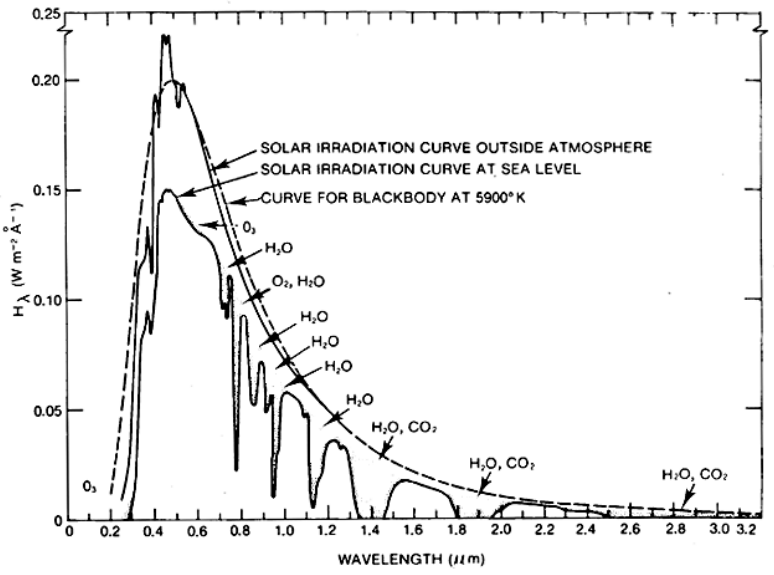

Figure 3: Power spectrum for a black body at 5900 K, sunlight measured at Earth's upper atmosphere, and of sunlight incident on earth's surface, showing several absorption bands. [10]

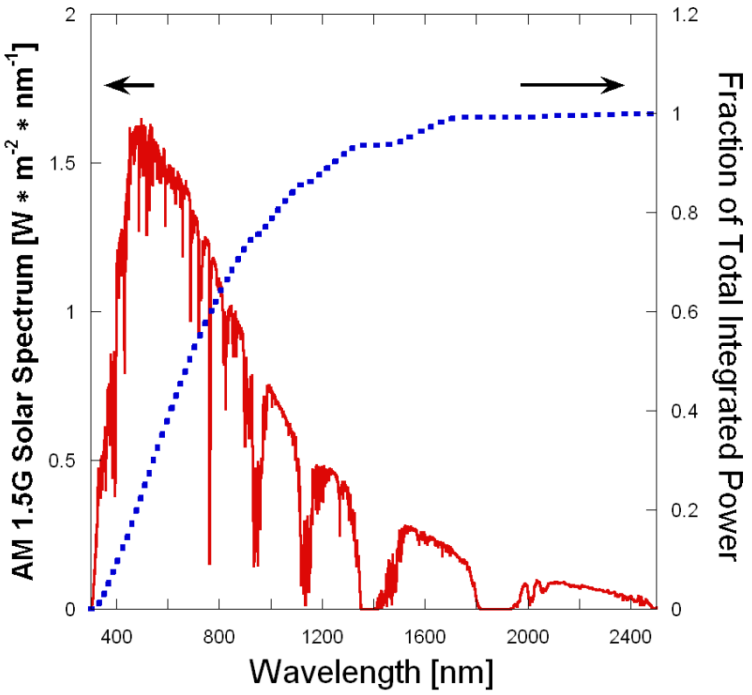

Figure 4: The solar spectrum of power density vs wavelength, overlaid with total power integrated from short to long wavelengths. [11]

1.3 Current Technologies

The first generation of solar cells was based on p-n junctions in single crystalline semiconductors. This technology can be quite efficient, but also quite expensive. Because the amount of energy required to produce single-crystalline materials is quite

high, it takes a longer time in operation for the cell to repay this initial investment in energy. The most common type of first generation cell is the crystalline silicon cell, although any single junction, crystalline type of cell could be said to belong to this family.

Second generation solar cells attempt to reduce the cost of production, including the energy used, by using techniques to grow thin layers of highly absorbing direct bandgap semiconductors over large areas. Some examples include Copper Indium Gallium Selenide (CIGS), Cadmium Telluride (CdTe), and amorphous silicon technologies. These techniques do reduce costs, but are still not considered quite cheap enough to become a dominant source of power. They still require high vacuum processes and high purity materials. Some of the materials important today in second generation solar cells, such as indium and tellurium, are in insufficient supply to fulfill a very large fraction of the world's energy needs.[12] Currently the module price for first generation technologies are $1.84 per watt peak and $1.37 per watt peak for second generation technologies.[13] technologies such as water heaters, concentrators and steam turbines are also considered to belong to the second generation.

In recent years much attention had been focused on developing new types of ultra-low cost solar cells which have the ability to provide energy at a cost well below that of a coal-fired power plant. These technologies have been collectively termed third generation solar cell technologies. The goal is to achieve efficiencies comparable to high-end second generation devices, but at greatly reduced cost per watt.[14] One way of achieving this may be to use technologies which enable efficiencies beyond the

thermodynamic limit for a single junction device, such as multijunction cells, up/down converters, multiple exciton generation, and hot carrier harvesting.[15]

Another proposed method to achieve low cost per watt is to develop technologies which can utilize established, high throughput industrial production methods such as screen printing, roll-to-roll processing or Gravure printing which are of special interest due to their low cost per area. The use of inexpensive plastic sheets or films as the substrate would further lower cost. Such cells would likely initially offer modest efficiencies, but drastically reduced cost per area.

In the search for the ideal solar cell architecture there are several factors to consider. First and foremost it is important that over the lifetime of the cell it produces several times more energy that it required to manufacture it. This means that the processing steps must be very short and cannot require a clean room or high vacuum steps, such as are used in VLSI manufacture. It must also utilize cheap and abundant raw materials such as plastics and abundant elements. For example, indium and tellurium are important elements in CIGS and CdTe solar cells, repectively, but are actually quite scarce.[16] There is not nearly enough of these elements to satisfy the world's energy need using those technologies. Ideally we should be able to supply most of the world's power requirement without exhausting the supply of any important materials.

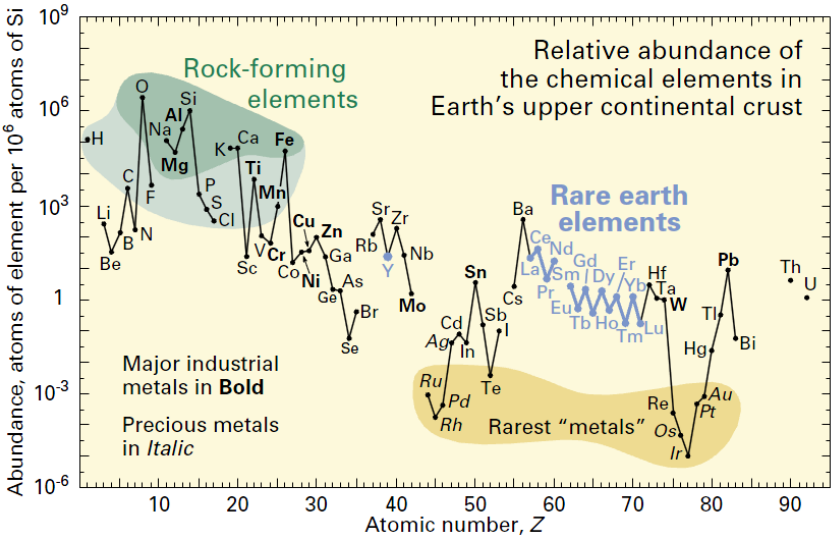

Figure 5: Abundance of various elements in the Earth's crust.[16]

It is also preferable that these cells do not contain any hazardous materials and can be easily recycled at the end of their lifetime. They must also be durable enough that they can have a long operational lifetime. They must also be cheap and easy to install so as to keep overall costs down. One of the most promising technologies, which fulfills all of these requirements, is the Gratzel Cell, or Dye-Sensitized Solar Cell (DSSC) in which the absorbing material is a dye adsorbed onto a nanoporous titania electrode. It uses low cost processing methods and has a reasonably high record efficiency of 11.5% for a liquid-junction device.[17] It is made of cheap and abundant materials, with the exception of the very small amount of ruthenium used in many dyes. They have been shown to be quite stable[18] and can be manufactured using high throughput processes such as doctor blading or screen printing.

1.4 Current Limitations to Dye-Sensitized Solar Cells

While liquid junction DSSCs have efficiencies that are competitive with many thin-film technologies, solid state devices are preferred because they do not have the worry of leakage or evaporation of a liquid electrolyte. They are also easier to fabricate on a flexible substrate. Unfortunately, at present the efficiency of solid state dye-sensitized solar cell (SDSC) devices lags behind that of the well-studied liquid junction devices having a record efficiency of only about 6%,[19] mainly because light absorption is less complete in solid state devices as well as faster back electron transfer. Solid state hole transport materials have low carrier mobilities,[20,21] which requires the use of very thin active layers. The thickness of a solid state device is restricted to 2 μm while a typical liquid junction device has an optimized active layer of about 12 μm.[22,23] Because the absorber thickness is much reduced a great deal of the incident light is allowed to pass through an SDSC without being converted. One obvious remedy would be to make the cell thicker and use a higher mobility hole transport material, but no suitable material currently exists. Another would be to use a dye capable of absorbing light more strongly while maintaining a broad absorption spectrum. Unfortunately, again there are no dyes currently available that fulfill this requirement. There is a tradeoff between strong absorption and a broad absorption spectrum. There are, however, many dyes available which can absorb a narrow frequency band completely with an active layer of only 2 μm, though do not absorb outside of this band. Perhaps by combining several such dyes with complementary absorption spectra the goals of both strong and broad absorption could be met. Such an approach has been used before with dye cocktails

and organized dye layers, usually with a resulting device that was equivalent to or less efficient than if the most efficient dye had been used alone.[24,25]

1.5 Förster Resonance Energy Transfer as a Path to Improvement

Further progress hinges on the development of a method to combine multiple strong absorbers without adversely affecting device performance. In this work, Förster Resonance Energy Transfer (FRET) is investigated as a means to this end. FRET is a phenomenon by which one absorber transfers energy to an acceptor molecule through a resonance between the absorber's fluorescence and the acceptor's absorbance. This process can have close to unity efficiency and has been the main mechanism of light harvesting in photosynthetic organisms for billions of years. When using FRET in SDSCs only one type of dye is adsorbed onto the nanostructured titania electrode, while complementary absorbers may be dissolved in the electrolyte. This adds almost no complication to the production process. These added absorbers may transfer their excitation to the dye while having limited participation in the rest of the chemistry of the cell. Because relatively little is required of these added absorbers, it should be possible to find compatible pairings of materials which exhibit efficient energy transfer. By matching the absorption spectra of these added absorbers to the gaps in the absorption of the original dye, we hope to achieve the goal of both strong and broad light absorption in a SDSC.

Because we are concerned with low-cost, commercially scalable technologies, we consider only purely organic materials. Only the elements carbon, oxygen, nitrogen, sulfur and hydrogen are used in the absorbers. This is important because all of the compounds in this study can be manufactured via organic synthetic chemistry, and are not reliant on expensive or scarce metals. The rest of the cell also contains titanium, silicon, tin, fluorine and traces of lithium, which are all abundant industrially available materials. Gold contacts are used because of the ease of depositing noble metals, but could be substituted for aluminum or other metals on a production line. Therefore, utilizing FRET provides a pathway to overcoming active layer thickness limitations by significantly raising absorbance over a wide spectrum, while still maintaining scalability.

1.6 Scope of Thesis

At the time this dissertation was begun there was only one paper published on the subject of FRET used in DSSCs.[26] For this reason the goal of this work is to provide a basic investigation into the feasibility and proof of concept of the employment of FRET in DSSCs by surveying and characterizing several possible materials systems. Chapter 2 discusses the relevant background material including the operating principles of DSSCs, limitations, and a survey of important literature. Chapter 3 provides a theoretical treatment of Förster resonance energy transfer and its relevance and applicability to DSSCs. Of special concern are the requirements for compatibility imposed by the existing DSSC system on FRET donor materials. Chapter 4 concerns the fabrication procedure of an SDSC from start to finish, including fabrication of the substrate, staining, deposition of hole transport material, and deposition of the back

contact. Chapter 5 concerns the various candidate materials that were investigated. These materials were all off-the-shelf commercially available products which were believed to have potential for FRET enhanced SDSCs. In order to confirm their compatibility absorption and emission spectra were collected and the quenching due to lithium salt and the acceptor dye was measured. Materials were also tested for stability in a completed cell. Chapter 6 includes the characterization of SDSCs employing various donor materials. Included are electronic and efficiency measurements, and most importantly incident photon to collected electron (IPCE) yields. Chapter 7 summarizes the important results of the work and discusses the outlook for the future. In short, this work aims to introduce the use of FRET into the field of SDSCs and seek out new donor-acceptor systems

1.7 References

(1) Energy Information Association International Energy Outlook 2010 http://www.eia.doe.gov/ (accessed Mar 20, 2011).

(2) Tsoskounoglou, M. Ayerides, G.; Tritopoulou, E. The end of cheap oil: Current status and prospects. *Energy Policy* **2008**, *36*, 3797-3806.

(3) Heinberg, R.; Fridley, D. The end of cheap coal. *Nature* **2010**, *468*, 367-9.

(4) Pearce, J.; Lau, A. *Net Energy Analysis for Sustainable Energy Production From Silicon Based Solar Cells*; ASME, 2002; pp. 181-186.

(5) Lewis, N. S. Powering the Planet. *MRS Bulletin* **2007**, *32*.

(6) Hermann, W. Quantifying global exergy resources. *Energy* **2006**, *31*, 1685-1702.

(7) *ASTM standard G-173-03*.

(8) NREL htp://www.nrel.gov/gis/solar.html (accessed Feb 4, 2011).

(9) Schokley, W.; Quiesser, H. Detailed Balance Limit of Efficiency of p-n Junction Solar Cells. *Journal of Applied Physics* **1961**, *32*.

(10) Online http://www.nasa.gov/.

(11) Basham, J. I. Mor, G. K.; Grimes, C. A. Förster resonance energy transfer in dye-sensitized solar cells. *ACS nano* **2010**, *4*, 1253-8.

(12) Wadia, C. Alivisatos, A. P.; Kammen, D. M. Materials Availability Expands the Opportunity for Large-Scale Photovoltaics Deployment. *Environmental Science & Technology* **2009**, *43*, 2072-2077.

(13) Solar Buzz http://solarbuzz.com (accessed July 7th, 2011).

(14) Conibeer, G. Third-generation photovoltaics. *Materials Today* **2007**, *10*, 42-50.

(15) Green, M. Third generation photovoltaics: Ultra-high conversion efficiency at low cost. *Progress in Photovoltaics: Research and Applications* **2001**, *9*, 123-135.

(16) Sound, S. Of, M.; Mineral, O. U. R. Rare Earth Elements — Critical Resources for High Technology. **2002**.

(17) O'Regan, B.; Gratzel, M. A low-cost, high-efficiency solar cell based on dye-sensitized colloidal TiO_2 films. *Nature* **1991**, *353*.

(18) Kroon, J. M. Bakker, N. J. Smit, H. J. P. Liska, P. Thampi, K. R. Wang, P. Zakeeruddin, S. M. Gratzel, M. Hinsch, A. Hore, S. Würfel, U. Sastrawan, R. Durrant, J. R. Palomares, E. Pettersson, H. Gruszecki, T. Walter, J. Skupien, K.; Tulloch, G. E. Nanocrystalline dye-sensitized solar cells having maximum performance. *Progress in Photovoltaics: Research and Applications* **2007**, *15*, 1-18.

(19) Cai, N. Moon, S.-J. Cevey-Ha, L. Moehl, T. Humphry-Baker, R. Wang, P. Zakeeruddin, S. M.; Grätzel, M. An Organic D-π-A Dye for Record Efficiency Solid-State Sensitized Heterojunction Solar Cells. *Nano letters* **2011**, *11*, 1452-1456.

(20) Poplavskyy, D.; Nelson, J. Nondispersive hole transport in amorphous films of methoxy-spirofluorene-arylamine organic compound. *Journal of Applied Physics* **2003**, *93*, 341.

(21) Snaith, H. J.; Gratzel, M. Electron and Hole Transport through Mesoporous TiO_2 Infiltrated with Spiro-MeOTAD. *Advanced Materials* **2007**, *19*, 3643-3647.

(22) Barbe, C. J. Arendse, F. Comte, P. Jirousek, M. Lenzmann, F. Shklover, V.; GRATZEL, M. Nanocrystalline Titanium Oxide Electrodes for Photovoltaic Applications. *Synthesis* **1997**, *71*, 3157-3171.

(23) Wamg, Z. Significant influence of TiO_2 photoelectrode morphology on the energy conversion efficiency of N719 dye-sensitized solar cell. *Coordination Chemistry Reviews* **2004**, *248*, 1381-1389.

(24) Chen, P. Yum, J. H. De Angelis, F. Mosconi, E. Fantacci, S. Moon, S.-J. Baker, R. H. Ko, J. Nazeeruddin, M. K.; Gratzel, M. High open-circuit voltage solid-state dye-sensitized solar cells with organic dye. *Nano letters* **2009**, *9*, 2487-92.

(25) Lee, K. Park, S. W. Ko, M. J. Kim, K.; Park, N.-gyu Selective positioning of organic dyes in a mesoporous inorganic oxide film. *Nature materials* **2009**, *8*, 665-71.

(26) Shankar, K. Feng, X.; Grimes, C. A. Enhanced harvesting of red photons in nanowire solar cells: evidence of resonance energy transfer. *ACS nano* **2009**, *3*, 788-94.

2. Dye Sensitized Solar Cells

2.1 Introduction

Dye Sensitized Solar Cells (DSSCs) have recently attracted much attention due to their low cost, ease of manufacture and high efficiency. DSSCs, also called Grätzel cells after their inventor Michael Grätzel, were first described in 1985,[1] and by 1991 with an efficiency of 7.1%[2] DSSCs are a type of photoelectrochemical cell which seek to mimic a part of the photosynthetic process. In this chapter the mechanics of a dye sensitized solar cell are explained, emphasizing elements which are pertinent to the following chapters and specific SDSC design investigated in this work.

2.2 Dye-Sensitized Solar Cell Architecture

DSSCs consist of an electron collecting electrode and a hole-collecting electrode connected via a liquid redox electrolyte. The electron-collecting electrode is coated in a monolayer of photoactive dye. Upon absorption of a photon, the dye molecule becomes excited. The electron is injected into the electron collecting electrode, made of nanostructured titanium dioxide. The dye molecule is regenerated as the hole is injected into the redox electrolyte, typically an iodide/triiodide couple (I^-/I_3^-) with performance-boosting additives. Iodide is oxidized by the dye to form triiodide (I_3^-). Triodide then travels across the liquid junction to the hole collecting (electron injecting)

electrode to be reduced again to iodide, completing the circuit. A band diagram for the particular design used in this work is depicted in Figure 13.

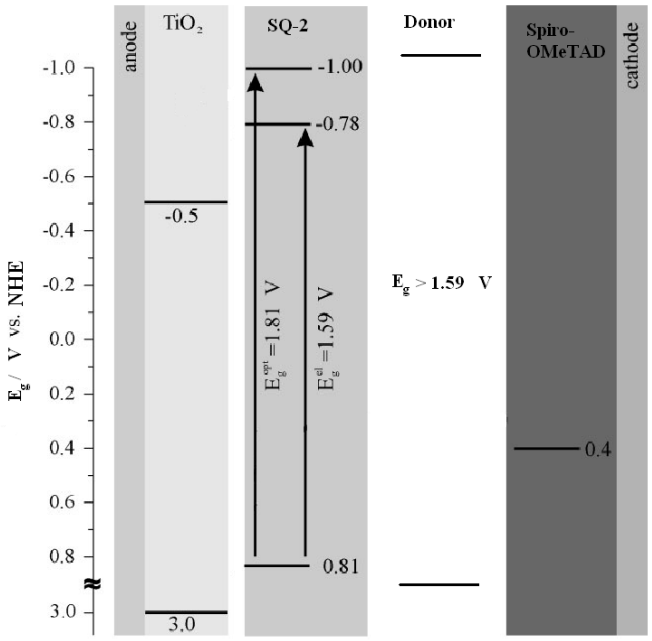

Figure 6: Band diagram for SDSCs used in this work.

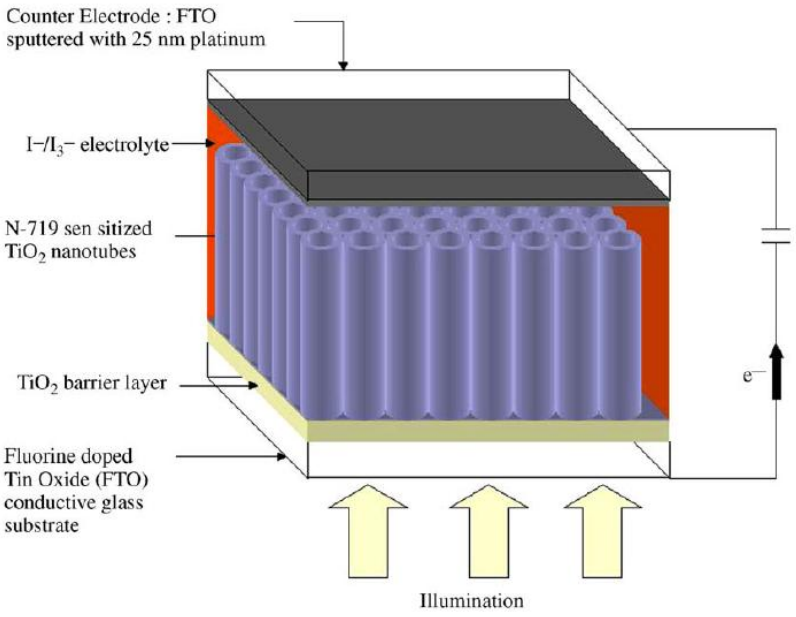

Figure 7: Layout of liquid junction DSSC. Reprinted from ref.[3]

Possible loss mechanisms include reflection of light at the air/glass interface, absorption of light by the glass substrate, transport losses through the TiO_2 substrate, back injection of electrons from TiO_2 to the electrolyte, decay of the excited state of the dye without electron injection, transport losses through the hole transport material, and lost light transmitted through the cell without being absorbed. Luckily, many of these losses can be kept in check, allowing for near unity collection of photons of specific wavelengths. For efficient dyes the excited dye molecule will inject charge on picoseconds time scales, while recombination lifetimes are measured in micro- or milliseconds.[4] The main limiting factor is the inability of DSSCs to absorb photons in the infrared region.

DSSCs can nonetheless be quite efficient; up to 11.5% power conversion efficiency has been demonstrated at the laboratory scale.[5] The evolution of efficiency increases from 7.1% to 11.5% over the course of almost 20 years has not been due to any radical changes in DSSC design, but rather the understanding and optimization of many small elements of the process. DSSCs were originally hailed as the long-awaited solution to low-cost solar power. Commercial adoption has been very slow however, due to concerns over lifetime due to evaporation of the liquid electrolyte. The most efficient solvent so far, acetonitrile, has a boiling point of 82 °C. Although it allows for excellent diffusion of charge carriers due to its low viscosity it is volatile at a temperature it will likely experience in operation on a roof on a hot summer day. For this reason, focus has shifted away from high volatility liquid electrolytes to low volatility liquids or gels, or near zero volatility ionic liquids.[6-15] This solves the problem of electrolyte

evaporation, although a ruptured cell may still leak. The ultimate goal is to develop an efficient solid-state DSSC (SDSC) where the electrolyte is replaced with an organic solid hole-transporting material. By and large, the material of choice is Sprio-OMeTAD,[16-23] although notable attention has also been given to the other transparent hole conducting materials copper iodide[24-27] and copper thioyanate (CuSCN).[28-32]

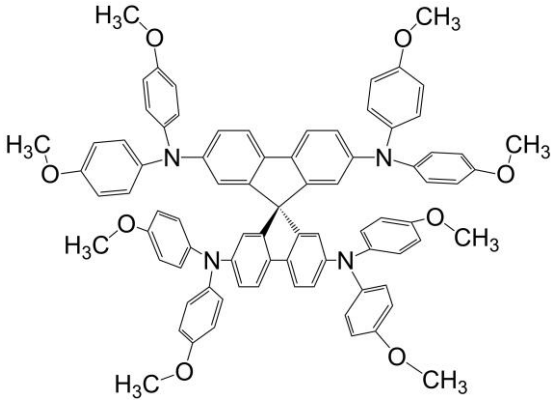

Figure 8: Chemical structure of Spiro-OMeTAD, $C_{81}H_{68}N_4O_8$

Spiro-OMeTAD (2,2',7,7'-tetrakis(N,N-di-p-pethodyphenyl-amine)-9,9'-spiro-bifluorene) is a glassy small molecule hole conductor, pictured in Figure 8. It is usually deposited via spin coating from chlorobenzene, although doctor blading is also possible.[33] Due to its relative stability in ambient atmosphere, it is preferred over other materials which can be very sensitive to oxygen or water vapor. Hole mobility in Spiro-OMeTAD is inherently low, as is typical for organic compounds. Pristine Spiro-OMeTAD has a mobility of roughly $1x10^{-4}$ $cm^2V^{-1}s^{-1}$.[34] Unfortunately, films of Spiro-OMeTAD infiltrating nanoporous titania electrodes can have their mobility reduced by an order of magnitude due to disorder.[17] Doping is required to improve device performance. The preferred method is to add a small amount of lithium bis(trifluoromethylsulfonyl)imide,

$Li(CF_3SO_2)_2N$, a lithium salt also used in lithium ion batteries to enhance conductivity. Upon adding this lithium salt, mobility is increased by more than an order of magnitude.[17] The net result is that Spiro-OMeTAD film incorporated into an SDSC will exhibit a hole mobility of about 1-5x10^{-4} $cm^2V^{-1}s^{-1}$.[17] This makes it suitable for use in SDSCs where the active layer is kept quite thin, not more than 2 µm. Above this value transport losses will be high. For this reason practical devices are kept quite thin, even though thicker active layers (~12 µm) are used in optimized liquid junction DSSCs. The result is that incident photon to collected electron (IPCE) efficiencies are well below unity across the whole spectrum due to incomplete light absorption.

2.3 Dyes used in DSSCs

2.3.1 Requirements

Dyes must perform several functions in a DSSC. They are of course responsible for light absorption. But because they form the barrier between the hole and electron transporting materials, they are also in effect the junction across which charges must be separated. To avoid losses they must be able to quickly inject an electron into TiO_2 upon excitation, which efficient dyes have been shown to do on sub-picosecond timescales. They must the localize the hole far away from the TiO_2 surface until it can be transferred to the hole transport material. This process must also be quite fast to avoid recombination losses. Additionally, the dye must prevent direct contact of the hole transport material and TiO_2 surface to avoid back injection of electrons from TiO_2 to the hole transport material, which can otherwise be a significant loss mechanism. Dyes

form a closely packed self-assembled monolayer across the TiO2 substrate to prevent interaction of the substrate and electrolyte.

From their inception, DSSCs have very commonly used ruthenium-based sensitizers due to their high efficiency. In these dyes a single ruthenium atom forms the core of a coordination complex. Upon excitation an exciton will form, localized on the metal core of the dye molecule and surrounding ligands. For efficient operation, it is very important than an electron is very quickly injected into TiO_2 on a time scale much shorter than decay of the photogenerated exciton. Therefore, the dye molecule contains carboxylic acid functional groups which provide a fast pathway for charge transfer to the substrate. Upon adsorbing to TiO_2, the carboxylic acid groups will transfer protons to the TiO_2 surface giving it a slight positive charge. This, along with the π-conjugated linkage between the ligand and TiO_2 provides an impetus for fast electron injection by excited dye molecules.

2.3.2 Ruthenium-Based Dyes

After electron injection it is important to inhibit the back reaction of returning the electron to the oxidized dye molecule. The solution is to add large electron-donating groups to the side of the molecule opposite the anchoring groups. In this way, the hole is physically separated from the electron-rich substrate and the excited state of the dye can have a very long lifetime. It also provides a large structure for easy regeneration by the electrolyte. This general structure is typical of many dyes and is exemplified in Figure 9 by the dye N-719, the most popular among ruthenium dyes.

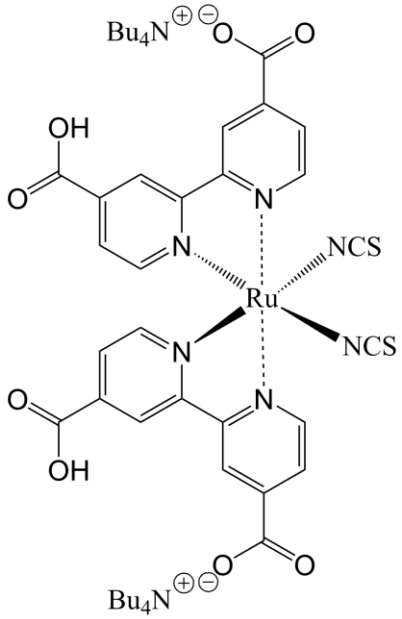

Figure 9: Structure of N-719 dye

These electron donating groups can also increase cell longevity if they are hydrophobic. Water can rapidly spoil a DSSC by desorbing or deactivating dye molecules.[35] Some water uptake is inevitable due to the somewhat permeable nature of current sealing methods, but its effect can be reduced if it is kept away from the TiO_2 surface by large hydrophobic groups. Additionally, these groups can be used to form a "donor-antenna" structure which significantly increases the molecule's absorbance.[36-39] Such structures can significantly increase red absorbance with thiophene and triphenylamine groups.

2.3.3 Organic Dyes

Recently attention has been given to purely organic sensitizers due to the possibility for extremely high molar absorption coefficients. The most commonly used

ruthenium dye, N-719 has a peak absorbance in the visible of 11,700 $M^{-1}cm^{-1}$ at 514 nm,[36] while purely organic dyes can have absorption coefficients easily several times higher. JK-2, an organic dye containing thiophene groups has been shown to have a peak molar absorption in the visible of 39,000 M^{-1} cm^{-1} at 452 nm. [40] Dyes of this type, such as JK-2 have been shown to be very efficient, especially in SDSCs where their high absorption coefficient is of great benefit, boosting IPCE values above 50%.[41] JK-2 is also capable of producing very high open circuit voltages, exceeding 1 V.[42] C205 dye, containing the ethylenedioxythiophene choromophore exhibits a similar absorption coefficient with excellent overlap of the visible spectrum, leading to a very high efficiency of 7.6% in a solvent-free electrolyte, as well as high stability.[43] An indoline-based dye has also been shown to have an efficiency comparable to ruthenium dyes, 9% using a volatile liquid electrolyte.[44]

Organic dyes which have significantly higher absorption coefficients will be limited in the width of their absorption however, as the product of absorption strength and the width of frequency response are constrained by the oscillator strength of the dye. Squarine dyes (so named for containing an aromatic squaric acid moity) are known to have extremely high absorption coefficients, 319,000 M^{-1} cm^{-1} at 662 nm in the case of SQ-2 dye.[45] However, SQ-2 absorbs only in a very narrow spectral window from about 550-700 nm. This omits the large portion of solar radiation present from 350-550 nm, which would otherwise be absorbed by a ruthenium-containing dye. For that matter, neither does it utilize infrared wavelengths which also contain a considerable amount of power. However, it does allow for high IPCE values at the absorption maximum with drastically thinner films than would be required for typical

dyes. Squarine dye has successfully been coupled with JK-2 dye to extend overall absorption further into the red and increase efficiency.[46] Cells containing only squarine dyes have low overall efficiencies however, limited to about 5.4%.[45]

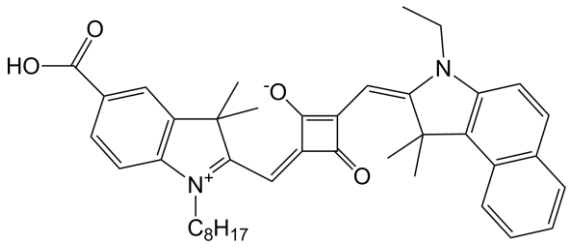

Figure 10: Structure of SQ-2 Squarine dye

Currently, the favorite types of dye used to extend absorption into the infrared region are dyes based on zinc phthalocyanine or other macrocyclic dyes. One example, chlorophyll is a magnesium chlorin, as well as a proven means of harnessing solar energy in plants. Chlorophyll derivatives have displayed an 8% efficiency in DSSCs.[47] Zinc phthalocyanines absorb in the range of 600-800 nm and cells based on these dyes have been shown to have IPCE values as high as 70-80% and an efficiency of just under 4%.[48] By using a different metal atom in the core of the macrocycle molecule (e.g. magnesium or zinc) the region of absorption can be shifted. Although light collection is efficient in the region of absorption, as with squarine dyes the region of absorption is quite small and therefore limits the overall efficiency.

2.3.4 Utilizing multiple dyes

The question then would be that, having many dyes that are efficient in a small region of the spectrum, could we perhaps combine them in such a way that makes absorption across the whole spectrum possible? This question has been explored in a few different ways. The simplest solution is to mix dyes together in the same staining solution and create a mixed monolayer of dye on the substrate.[40,49-52] Such an approach has commonly been referred to as a "dye cocktail" because the dyes are mixed together in the same staining solution. Many studies of this type have been conducted and show that although absorption can be broadened, it often comes at a price. Because different types of dye are competing for adsorption sites on the same substrate more surface area is required to accommodate both dyes. And because the open circuit voltage is heavily influenced by the characteristics of the dye, a cell employing multiple dyes will exhibit an open circuit voltage that is an average of all dyes.[53] All dyes used must therefore allow high open circuit voltages to prevent a degradation of performance. Also, the stability of the cell will be determined by the least stable dye. It is worth noting that Sony has developed a DSSC, which has an 11% efficiency and may be very likely to see commercial production, based on a dye cocktail of "black dye" (N-749) and an organic dye D131.[52] However this approach uses an active layer thickness of approximately 15 μm which is simply not feasible for solid-state cells.

Mixing different dyes can sometimes lead to unfavorable reactions between the two, such as electron injection from one type of excited dye to a neighbor of a different type.[50,52] In order to minimize such interactions there has been interest in creating

organized layers of dye having only one type of dye per layer. Bi-layer[54] and tri-layer[53] architectures have been demonstrated which do in fact show increased efficiency over a single dye structure under the condition that the substrate is thickened to allow sufficient amounts of each dye to adsorb. In the case of the tri-layered system the substrate was 25 μm thick.[53] Photocurrent was shown to increase, while open circuit voltage and fill factor were an average of the values observed when each dye was used alone. This approach, as with dye cocktails, may be appropriate only for extending response in liquid junction DSSCs where relatively thick active layers are feasible.

Another method is to use a tandem cell, in which each layer of the cell employs a different sensitizing dye. Such cells can be more efficient as the electronic properties of each individual layer are not compromised by stacking them. However, it does have the drawback of cost, as adding a layer can almost double the amount of raw materials used. Optical losses are also increased as there are more interfaces and more glass to pass through. It is likely that increases in the cost of production would offset gains in efficiency using this method.

The eventual goal is to combine the best of both worlds; to have strong, broad absorption without sacrificing electrical performance or increasing production costs. The way to overcome these hurdles may likely be Förster Resonance Energy Transfer (FRET). As described in Chapter 3, FRET works by using only one type of dye anchored to the substrate, while another type of dye with a complementary absorption spectrum is dissolved into the electrolyte. By transferring excitation at a distance, this second dye in the electrolyte sidesteps the problems of competition for adsorption sites or lowering the open circuit voltage due to unfavorable dye kinetics. It also adds almost

nothing to the cost of fabrication as a very small amount is used. Most importantly it allows very thin active layers which are compatible with low-mobility hole transport materials.

2.4 Effect of TiO_2 Electrode

The traditional design of DSSCs has employed a sintered film of TiO_2 nanocrystals approximately 10-20 nm in size. This type of electrode possesses an extremely high effective surface area 1000-2000 times that of a flat film.[55] This allows the film to adsorb very large amounts of dye which are required for complete light absorption. Its high porosity also allows excellent penetration of the liquid electrolyte, facilitating charge transport between all dye molecules and the distant hole-collecting electrode. There are several publications addressing the proper design of nanoparticulate electordes[35,55-59] but most have settled on a design incorporating an 8 μm thick layer of 12-20 nm transparent titania nanoparticles topped with a 4-5 μm thick light scattering layer comprised of 400 nm titania particles. Almost all of the dye is adsorbed to the 12-20 nm size particles, while the light scattering layer adsorbs very little dye and simply serves to increase the path length of light passing through the dye to raise the chance of absorption.

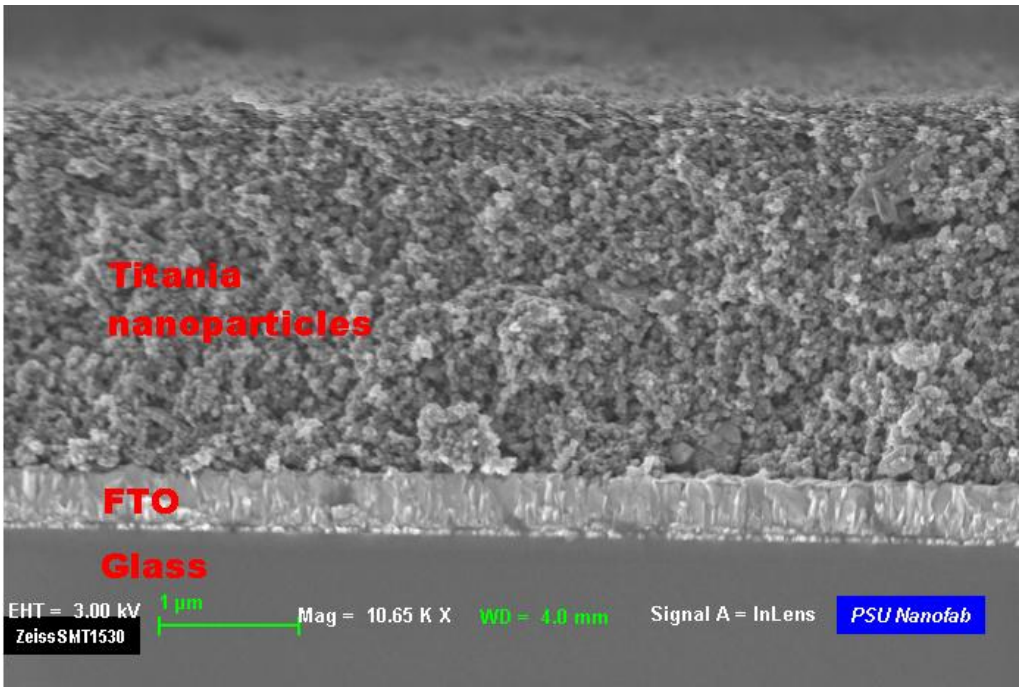

Figure 11: SEM cross section view of a 2 micron thick nanoparticle electrode.

Mobilities vary due to processing conditions but have been measured at 1.5–0.017 $cm^2V^{-1}s^{-1}$.[60-62] Mobility in TiO_2 is highly dependent on light intensity and surface characteristics (for example the presence of a dye layer). Reasonable light intensities, including solar radiation, generate large amounts of carriers in TiO_2 which serve to fill trap states. TiO_2 has many deep trap states and illumination is required for a proper measurement of mobility. Older studies of mobility in sintered TiO_2 nanoparticle films which were measured under very low or no illumination arrived at mobilities of 10^{-4}-10^{-6} $cm^2V^{-1}s^{-1}$.[63,64]

Because transport can be a limiting factor in DSSCs, an alternative substrate geometry was developed. Titania nanotube electrodes attempt to speed transport by

reducing the number of dimensions in which carriers can travel. In nanoparticle electrodes carriers diffuse in three dimensions; in nanotubes they are constrained to just one. Assuming carrier lifetimes are the same in both types of structure, diffusion should be faster in the lower dimensional structure, resulting in a higher fraction of collected electrons. Measurements have shown that electron lifetimes are an order of magnitude higher in titania nanotube arrays than in nanoparticle films, although transport times remain similar.[65] In nanoparticle films transport is limited by scattering at grain boundaries and disorder. In nanotubes however, the dominant limitation is the presence of exciton-like traps due to Ti^{3+} states.[66] These can be caused by oxygen vacancies, substitutional fluorine impurities, or Ti interstitials. It is assumed that by altering the fabrication procedure the number of these traps could be reduced, thereby significantly enhancing transport and allowing for thicker substrates without adding to transport losses.

2.5 Effect of Additives

The role of lithium salt in improving transport in Spiro-OMeTAD has been discussed above, but there are also several other additives which are used to increase performance. Tert-butyl pyridine is important to increase open circuit potential. It is believed that it fills gaps caused by imperfect packing in the dye monolayer, thereby blocking the electrolyte from contacting the substrate and eliminating short circuiting. It is used in both liquid and solid-state DSSCs.

Guanidinium Thiocyanate (GuSCN) performs a similar function. It is added to liquid junction DSSCs and adsorbs to vacant surface sites where imperfections occur in the dye layer. It has been shown to shift the potential of TiO_2 to more positive values, thereby speeding electron injection from excited dye molecules.[67] This causes an increase in short circuit current density by shifting the balance between the electron injection rate and the decay rate of the dye excited state. GuSCN also significantly increases the operational lifetime of DSSCs. The exact mechanism is unproven, although it is suggested that it is very effective at blocking access to the substrate to impurities which might degrade open circuit voltage or short circuit current over time.

Ionic liquids have also seen increasing usage in liquid junction DSSCs. Various imidazolium iodide salts have been used in small concentrations to increase the amount of available iodide in the electrolyte, thereby increasing conductivity. Beyond a certain concentration, however, their high viscosity can actually reduce performance due to mass transport limitations. Recently developed low viscosity ionic liquids coupled with tailored dyes have allowed for impressive efficiencies of up to 8.5% using only non-volatile ionic liquids as the solvent.[10]

2.6 Quantifying Solar Cell Performance

The main figure of merit for all solar cells is the power conversion efficiency (η). This figure is arrived at by measuring the current per unit area of a cell versus applied voltage. The two most significant points on a current-voltage (I-V) plot are the x and y intercepts. The voltage when current is zero is defined as the open circuit voltage, or

V_{oc}. In inorganic solar cells V_{oc} is limited by the bandgap of the absorber, minus any losses. In DSSCs the upper bound for V_{oc} is instead the difference between the conduction band of TiO_2 and the redox potential of the electrolyte. Higher V_{oc} values are desired as it indicates a reduction of loss mechanisms.

The current density when voltage is equal to zero is defined as the short circuit current, or J_{sc}. The maximum value of J_{sc} is determined by the fraction of solar radiation with an energy larger than the absorber's bandgap. In DSSCs it is determined by the overlap of the dye absorbance spectrum with the spectrum of solar power reaching the Earth's surface (see Figure 4). Differences between the theoretical value and observed value of J_{sc} represent carrier recombination inside the cell.

The power curve for the cell is the product of current and voltage plotted against voltage. The peak of this curve is taken to be the cell efficiency, and can be achieved with a properly matched load. Ideally, the solar cell should have a good diode-like behavior. Assuming idea diode behavior, the current as a function of voltage would be

$$I(V) = I_{in} - I_s(e^{\frac{qV}{k_B T}} - 1)$$

where I_{in} is the total incident photon flux absorbed by the cell and I_s is the diode reverse saturation current. The non-idealities of solar cells are usually expressed as a diode leakage current, or dark current, a shunt resistance, and a series resistance, connected as in the equivalent circuit presented in Figure 12. In the case of DSSCs, the shunt resistance can often represent shorting between the electrolyte and TiO2 substrate, and the series resistance can include transport through all of the cell components and connections. In efficient devices R_{series} is very small and R_{shunt} is very large.

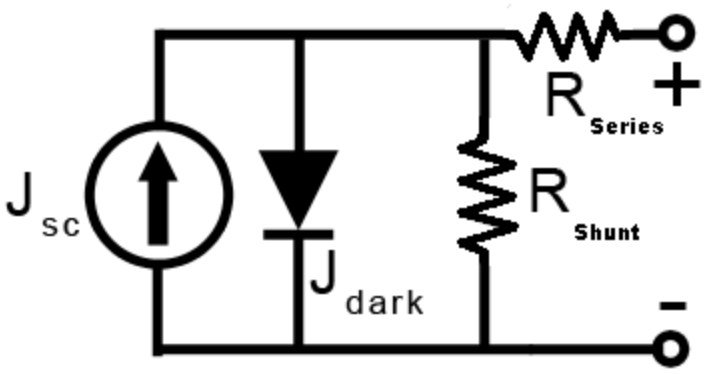

Figure 12: Simple solar cell equivalent circuit.

The fill factor (FF) measures the diode quality of a solar cell and is defined as

$$FF = \frac{\eta}{V_{oc} * J_{sc}}$$

and is expressed as a percent, although even for an ideal diode a fill factor of 100% would be mathematically impossible. High fill factors are key to efficient device performance as they indicate optimization of parasitic resistances. A measured fill factor can be used to estimate series and shunt resistances through the ideal formulas

$$FF = FF_0(1 - \frac{1}{r_{sh}})$$

$$FF = FF_0(1 - r_s)$$

$$FF_0 = \frac{\frac{V_{oc}}{k_B T} - \ln(\frac{V_{oc}}{k_B T} - 0.72)}{\frac{V_{oc}}{K_B T} + 1}$$

Where r_{sh} and r_s are the shunt and series resistances, respectively, scaled by the characteristic resistance V_{oc}/I_{sc}.

It is also common to measure the Incident Photon to Collected Electron (IPCE) yield. This is measured as a function of wavelength, measuring the current produced under short circuit conditions under a monochromatic illumination of known power. This method does not take into account photons which are reflected or transmitted by the cell. By integrating the IPCE over the solar photon flux, one can determine Jsc. The Internal Quantum Efficiency (IQE) is similar measurement, which accounts for losses. In a DSSC it would be the fraction of photons absorbed by the dye molecules which result in collected electrons, after dismissing reflective, transmissive losses, etc.

2.7 Specific design adopted for this dissertation

Given the previously mentioned benefits of SDSCs, and declining academic focus on liquid junction DSSCs due to their inherent limitations, the standard cell employed in this work is solid-state, using Spiro-OMeTAD as the hole transport material. The substrates used are transparent titania nanotube arrays 600-800 nm thick, with inner pore diameters of 22-28nm. These dimensions were chosen because by keeping the active layer thin good electrical characteristics and high process uniformity are possible. By keeping the pore diameter very small it is ensured that the donor material is placed close to the dye. The pore radius is similar to the expected Förster radius for efficient donor material. The dye of choice was SQ-2 because its strong absorption in the red and near transparency in the green region invites coupling

to a FRET donor. This window of low IPCE makes it easy to assign increased efficiency in this region to the addition of donor material only. Even with the very low active layer thickness used (about 5% as thick as liquid junction cells) reasonable IPCE values are attainable. Nanotubes were chosen over nanoparticles because of their superior transport properties. Donor materials are introduced by simply dissolving them into the Spiro-OMeTAD. The back contact is evaporated gold. Solar cell fabrication is treated in depth in Chapter 4.

Figure 13: Band diagram for SDSC.

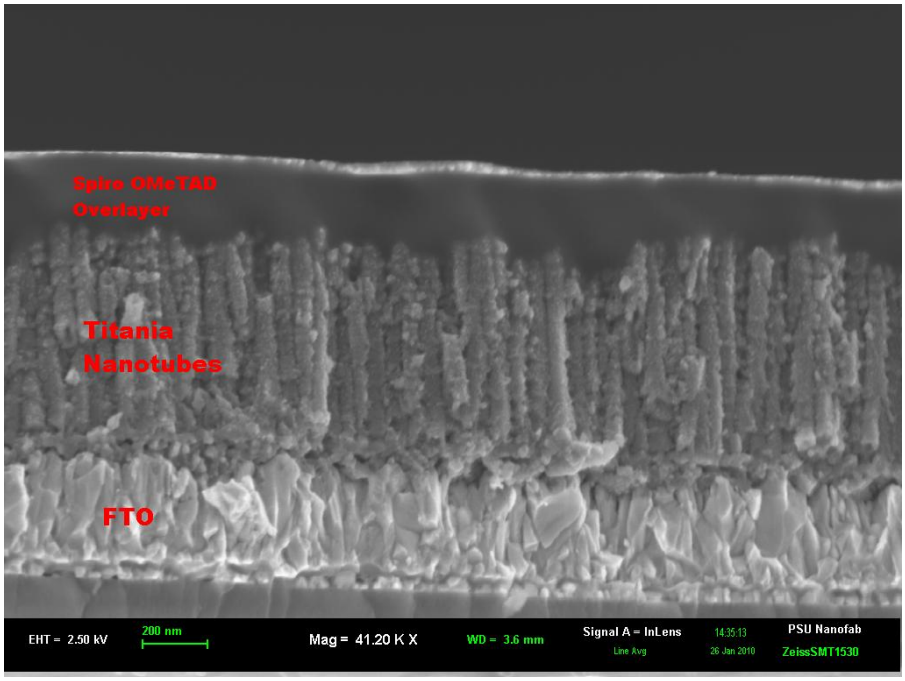

Figure 14: SEM cross section of an SDSC used in this study

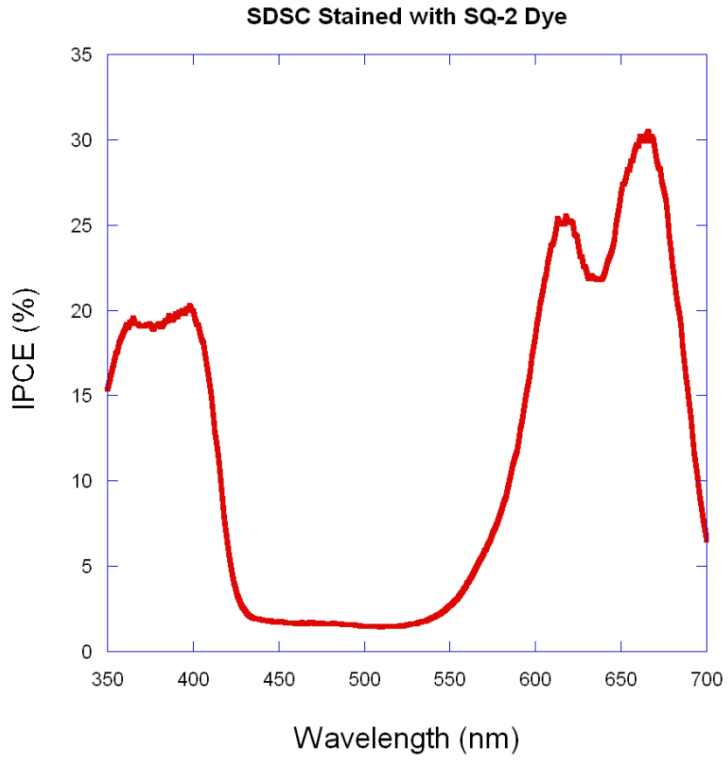

Figure 15: IPCE spectrum of a control cell containing no donor material

2.8 References

(1) Desilvestro, J. Graetzel, M. Kavan, L. Moser, J.; Augustynski, J. Highly efficient sensitization of titanium dioxide. *Journal of the American Chemical Society* **1985**, *107*, 2988-2990.

(2) O'Regan, B.; Gratzel, M. A low-cost, high-efficiency solar cell based on dye-sensitized colloidal TiO_2 films. *Nature* **1991**, *353*.

(3) Mor, G. Varghese, O. K. Paulose, M. Shankar, K.; Grimes, C.A. A review on highly ordered, vertically oriented TiO_2 nanotube arrays: Fabrication, material properties, and solar energy applications. *Solar Energy Materials and Solar Cells* **2006**, *90*, 2011-2075.

(4) Tachibana, Y. Moser, J. E. Grätzel, M. Klug, D. R.; Durrant, J. R. Subpicosecond Interfacial Charge Separation in Dye-Sensitized Nanocrystalline Titanium Dioxide Films. *The Journal of Physical Chemistry* **1996**, *100*, 20056-20062.

(5) Chen, C.-Y. Wang, M. Li, J.-Y. Pootrakulchote, N. Alibabaei, L. Ngoc-le, C.-H. Decoppet, J.-D. Tsai, J.-H. Grätzel, C. Wu, C.-G. Zakeeruddin, S. M.; Grätzel, M. Highly efficient light-harvesting ruthenium sensitizer for thin-film dye-sensitized solar cells. *ACS Nano* **2009**, *3*, 3103-9.

(6) Zakeeruddin, S. M.; Grätzel, M. Solvent-Free Ionic Liquid Electrolytes for Mesoscopic Dye-Sensitized Solar Cells. *Advanced Functional Materials* **2009**, *19*, 2187-2202.

(7) Murai, S. Mikoshiba, S. Sumino, H. Kato, T.; Hayase, S. Quasi-solid dye sensitised solar cells filled with phase-separated chemically cross-linked ionic gels. *Chemical Communications* **2003**, 1534.

(8) Kuang, D. Klein, C. Zhang, Z. Ito, S. Moser, J.-E. Zakeeruddin, S. M.; Grätzel, M. Stable, high-efficiency ionic-liquid-based mesoscopic dye-sensitized solar cells. *Small (Weinheim an der Bergstrasse, Germany)* **2007**, *3*, 2094-102.

(9) Cao, Y. Zhang, J. Bai, Y. Li, R. Zakeeruddin, S. M. Grätzel, M.; Wang, P. Dye-Sensitized Solar Cells with Solvent-Free Ionic Liquid Electrolytes. *Journal of Physical Chemistry C* **2008**, *112*, 13775-13781.

(10) Shi, D. Pootrakulchote, N. Li, R. Guo, J. Wang, Y. Zakeeruddin, S. M. Grätzel, M.; Wang, P. New Efficiency Records for Stable Dye-Sensitized Solar Cells with Low-

Volatility and Ionic Liquid Electrolytes. *Journal of Physical Chemistry C* **2008**, *112*, 17046-17050.

(11) Ito, S. Zakeeruddin, S. M. Comte, P. Liska, P. Kuang, D.; Grätzel, M. Bifacial dye-sensitized solar cells based on an ionic liquid electrolyte. *Nature Photonics* **2008**, *2*, 693-698.

(12) Huang, K.-chieh; Vittal, R.; Ho, K.-chuan Effects of crown ethers in nanocomposite silica-gel electrolytes on the performance of quasi-solid-state dye-sensitized solar cells. *Solar Energy Materials and Solar Cells* **2010**, *94*, 675-679.

(13) Chen, C.-L. Teng, H.; Lee, Y.-L. Preparation of highly efficient gel-state dye-sensitized solar cells using polymer gel electrolytes based on poly(acrylonitrile-co-vinyl acetate). *Journal of Materials Chemistry* **2011**, *21*, 628.

(14) Kim, D. Jeong, Y. Kim, S. Lee, D.; Song, J. Photovoltaic performance of dye-sensitized solar cell assembled with gel polymer electrolyte. *Journal of Power Sources* **2005**, *149*, 112-116.

(15) Senguttuvan, T.; Malhotra, L. Sol gel deposition of pure and antimony doped tin dioxide thin films by non alkoxide precursors. *Thin Solid Films* **1996**, *289*, 22-28.

(16) Bach, U. Comte, P. Moser, J. E. Weisso, F., Gratzel, M. Solid-state dye-sensitized mesoporous TiO_2 solar cells with high photon-to-electron conversion efficiencies. *Nature* **1998**, *395*, 583-585.

(17) Snaith, H. J.; Gratzel, M. Electron and Hole Transport through Mesoporous TiO_2 Infiltrated with Spiro-MeOTAD. *Advanced Materials* **2007**, *19*, 3643-3647.

(18) Fabregat-Santiago, F. Bisquert, J. Cevey, L. Chen, P. Wang, M. Zakeeruddin, S. M.; Gratzel, M. Electron transport and recombination in solid-state dye solar cell with spiro-OMeTAD as hole conductor. *Journal of the American Chemical Society* **2009**, *131*, 558-62.

(19) Ding, I.-K. Tétreault, N. Brillet, J. Hardin, B. E. Smith, E. H. Rosenthal, S. J. Sauvage, F. Gratzel, M.; McGehee, M. D. Pore-Filling of Spiro-OMeTAD in Solid-State Dye Sensitized Solar Cells: Quantification, Mechanism, and Consequences for Device Performance. *Advanced Functional Materials* **2009**, *19*, 2431-2436.

(20) Bandara, J. Shankar, K. Basham, J. Wietasch, H. Paulose, M. Varghese, O. K. Grimes, C. A.; Thelakkat, M. Integration of TiO_2 nanotube arrays into solid-state dye-sensitized solar cells. *The European Physical Journal Applied Physics* **2011**, *53*, 20601.

(21) Kuang, D. Brillet, J. Chen, P. Takata, M. Uchida, S. Miura, H. Sumioka, K. Zakeeruddin, S. M.; Grätzel, M. Application of highly ordered TiO_2 nanotube arrays in flexible dye-sensitized solar cells. *ACS nano* **2008**, *2*, 1113-6.

(22) Cai, N. Moon, S.-J. Cevey-Ha, L. Moehl, T. Humphry-Baker, R. Wang, P. Zakeeruddin, S. M.; Grätzel, M. An Organic D-π-A Dye for Record Efficiency Solid-State Sensitized Heterojunction Solar Cells. *Nano letters* **2011**, *11*, 1452-1456.

(23) Nattestad, A. Mozer, A. J. Fischer, M. K. R. Cheng, Y.-B. Mishra, A. Bäuerle, P.; Bach, U. Highly efficient photocathodes for dye-sensitized tandem solar cells. *Nature materials* **2010**, *9*, 31-5.

(24) Taguchi, T. Zhang, X.-tong; Sutanto, I. Tokuhiro, K.-ichi; Rao, T. N. Watanabe, H. Nakamori, T. Uragami, M.; Fujishima, A. Improving the performance of solid-state dye-sensitized solar cell using MgO-coated TiO_2 nanoporous film. *Chemical Communications* **2003**, 2480.

(25) Perera, V. Recombination processes in dye-sensitized solid-state solar cells with CuI as the hole collector. *Solar Energy Materials and Solar Cells* **2003**, *79*, 249-255.

(26) Kumara, G. R. A. Konno, A. Shiratsuchi, K. Tsukahara, J.; Tennakone, K. Dye-Sensitized Solid-State Solar Cells: Use of Crystal Growth Inhibitors for Deposition of the Hole Collector. *Chemistry of Materials* **2002**, *14*, 954-955.

(27) Meng, Q.-B. Takahashi, K. Zhang, X.-T. Sutanto, I. Rao, T. N. Sato, O. Fujishima, A. Watanabe, H. Nakamori, T.; Uragami, M. Fabrication of an Efficient Solid-State Dye-Sensitized Solar Cell. *Langmuir* **2003**, *19*, 3572-3574.

(28) O'Regan, B. C.; Lenzmann, F. Charge Transport and Recombination in a Nanoscale Interpenetrating Network of n-Type and p-Type Semiconductors: Transient Photocurrent and Photovoltage Studies of TiO_2 /Dye/CuSCN Photovoltaic Cells. *The Journal of Physical Chemistry B* **2004**, *108*, 4342-4350.

(29) O'Regan, B. Lenzmann, F. Muis, R.; Wienke, J. A Solid-State Dye-Sensitized Solar Cell Fabricated with Pressure-Treated P25−TiO_2 and CuSCN: Analysis of Pore Filling and IV Characteristics. *Chemistry of Materials* **2002**, *14*, 5023-5029.

(30) O'Regan, B. C.; Lenzmann, F. Charge Transport and Recombination in a Nanoscale Interpenetrating Network of n-Type and p-Type Semiconductors: Transient Photocurrent and Photovoltage Studies of TiO_2/Dye/CuSCN Photovoltaic Cells. *The Journal of Physical Chemistry B* **2004**, *108*, 4342-4350.

(31) Kumara, G. Dye-sensitized solar cell with the hole collector p-CuSCN deposited from a solution in n-propyl sulphide. *Solar Energy Materials and Solar Cells* **2001**, *69*, 195-199.

(32) Sommeling, P. M. O'Regan, B. C. Haswell, R. R. Smit, H. J. P. Bakker, N. J. Smits, J. J. T. Kroon, J. M.; van Roosmalen, J. A. M. Influence of a $TiCl_4$ post-treatment on nanocrystalline TiO_2 films in dye-sensitized solar cells. *The journal of physical chemistry. B* **2006**, *110*, 19191-7.

(33) Ding, I.-K. Melas-Kyriazi, J. Cevey-Ha, N.-L. Chittibabu, K. G. Zakeeruddin, S. M. GRATZEL, M.; McGehee, M. D. Deposition of hole-transport materials in solid-state dye-sensitized solar cells by doctor-blading. *Organic Electronics* **2010**, *11*, 1217-1222.

(34) Poplavskyy, D.; Nelson, J. Nondispersive hole transport in amorphous films of methoxy-spirofluorene-arylamine organic compound. *Journal of Applied Physics* **2003**, *93*, 341.

(35) Kroon, J. M. Bakker, N. J. Smit, H. J. P. Liska, P. Thampi, K. R. Wang, P. Zakeeruddin, S. M. GRATZEL, M. Hinsch, A. Hore, S. Würfel, U. Sastrawan, R. Durrant, J. R. Palomares, E. Pettersson, H. Gruszecki, T. Walter, J. Skupien, K.; Tulloch, G. E. Nanocrystalline dye-sensitized solar cells having maximum performance. *Progress in Photovoltaics: Research and Applications* **2007**, *15*, 1-18.

(36) Snaith, H. J. Karthikeyan, C. S. Petrozza, A. Teuscher, J. Moser, J. E. Nazeeruddin, M. K. Thelakkat, M.; Gratzel, M. High Extinction Coefficient "Antenna" Dye in Solid-State Dye-Sensitized Solar Cells: A Photophysical and Electronic Study. *Journal of Physical Chemistry C* **2008**, *112*, 7562-7566.

(37) Choi, H. Baik, C. Kim, S. Kang, M.-S. Xu, X. Kang, H. S. Kang, S. O. Ko, J. Nazeeruddin, M. K.; Gratzel, M. Molecular engineering of hybbtion rid sensitizers incorporating an organic antenna into ruthenium complex and their application in solar cells. *New Journal of Chemistry* **2008**, *32*, 2233.

(38) Nedelcu, M. Guldin, S. Orilall, M. C. Lee, J. Hüttner, S. Crossland, E. J. W. Warren, S. C. Ducati, C. Laity, P. R. Eder, D. Wiesner, U. Steiner, U.; Snaith, H. J. Monolithic route to efficient dye-sensitized solar cells employing diblock copolymers for mesoporous TiO_2. *Journal of Materials Chemistry* **2010**, *20*, 1261.

(39) Mozer, A. J. Wada, Y. Jiang, K.-J. Masaki, N. Yanagida, S.; Mori, S. N. Efficient dye-sensitized solar cells based on a 2-thiophen-2-yl-vinyl-conjugated ruthenium photosensitizer and a conjugated polymer hole conductor. *Applied Physics Letters* **2006**, *89*, 043509.

(40) Kim, S. Lee, J. K. Kang, S. O. Ko, J. Yum, J.-H. Fantacci, S. De Angelis, F. Di Censo, D. Nazeeruddin, M. K.; Grätzel, M. Molecular engineering of organic sensitizers for solar cell applications. *Journal of the American Chemical Society* **2006**, *128*, 16701-7.

(41) Moon, S.-J. Yum, J.-H. Humphry-Baker, R. Karlsson, K. M. Hagberg, D. P. Marinado, T. Hagfeldt, A. Sun, L. Gratzel, M.; Nazeeruddin, M. K. Highly Efficient Organic Sensitizers for Solid-State Dye-Sensitized Solar Cells. *The Journal of Physical Chemistry C* **2009**, *113*, 16816-16820.

(42) Chen, P. Yum, J. H. De Angelis, F. Mosconi, E. Fantacci, S. Moon, S.-J. Baker, R. H. Ko, J. Nazeeruddin, M. K.; Gratzel, M. High open-circuit voltage solid-state dye-sensitized solar cells with organic dye. *Nano letters* **2009**, *9*, 2487-92.

(43) Xu, M. Wenger, S. Bala, H. Shi, D. Li, R. Zhou, Y. Zakeeruddin, S. M. Gratzel, M.; Wang, P. Tuning the Energy Level of Organic Sensitizers for High-Performance Dye-Sensitized Solar Cells. *The Journal of Physical Chemistry C* **2009**, *113*, 2966-2973.

(44) Ito, S. Zakeeruddin, S. M. Humphry-Baker, R. Liska, P. Charvet, R. Comte, P. Nazeeruddin, M. K. Péchy, P. Takata, M. Miura, H. Uchida, S.; Grätzel, M. High-Efficiency Organic-Dye- Sensitized Solar Cells Controlled by Nanocrystalline-TiO_2 Electrode Thickness. *Advanced Materials* **2006**, *18*, 1202-1205.

(45) Geiger, T. Kuster, S. Yum, J.-H. Moon, S.-J. Nazeeruddin, M. K. Gratzel, M.; Nüesch, F. Molecular Design of Unsymmetrical Squaraine Dyes for High Efficiency Conversion of Low Energy Photons into Electrons Using TiO_2 Nanocrystalline Films. *Advanced Functional Materials* **2009**, *19*, 2720-2727.

(46) Yum, J.-H. Jang, S.-R. Walter, P. Geiger, T. Nüesch, F. Kim, S. Ko, J. Grätzel, M.; Nazeeruddin, M. K. Efficient co-sensitization of nanocrystalline TiO_2 films by organic sensitizers. *Chemical communications (Cambridge, England)* **2007**, 4680-2.

(47) Wang, X.-F. Tamiaki, H. Wang, L. Tamai, N. Kitao, O. Zhou, H.; Sasaki, S.-ichi Chlorophyll-a derivatives with various hydrocarbon ester groups for efficient dye-sensitized solar cells: static and ultrafast evaluations on electron injection and charge collection processes. *Langmuir : the ACS journal of surfaces and colloids* **2010**, *26*, 6320-7.

(48) García-Iglesias, M. Cid, J.-J. Yum, J.-H. Forneli, A. Vázquez, P. Nazeeruddin, M. K. Palomares, E. Grätzel, M.; Torres, T. Increasing the efficiency of zinc-phthalocyanine based solar cells through modification of the anchoring ligand. *Energy & Environmental Science* **2011**, *4*, 189.

(49) Zhao, W. Jun Hou, Y. Song Wang, X. Wen Zhang, B. Cao, Y. Yang, R. Bo Wang, W.; Rui Xiao, X. Study on squarylium cyanine dyes for photoelectric conversion. *Solar Energy Materials and Solar Cells* **1999**, *58*, 173-183.

(50) Ehret, A. Stuhl, L.; Spitler, M. T. Spectral Sensitization of TiO_2 Nanocrystalline Electrodes with Aggregated Cyanine Dyes. *The Journal of Physical Chemistry B* **2001**, *105*, 9960-9965.

(51) Cid, J.-J. Yum, J.-H. Jang, S.-R. Nazeeruddin, M. K. Martínez-Ferrero, E. Palomares, E. Ko, J. Grätzel, M.; Torres, T. Molecular cosensitization for efficient panchromatic dye-sensitized solar cells. *Angewandte Chemie (International ed. in English)* **2007**, *46*, 8358-62.

(52) Ogura, R. Y. Nakane, S. Morooka, M. Orihashi, M. Suzuki, Y.; Noda, K. High-performance dye-sensitized solar cell with a multiple dye system. *Applied Physics Letters* **2009**, *94*, 073308.

(53) Lee, K. Park, S. W. Ko, M. J. Kim, K.; Park, N.-gyu Selective positioning of organic dyes in a mesoporous inorganic oxide film. *Nature materials* **2009**, *8*, 665-71.

(54) Inakazu, F. Noma, Y. Ogomi, Y.; Hayase, S. Dye-sensitized solar cells consisting of dye-bilayer structure stained with two dyes for harvesting light of wide range of wavelength. *Applied Physics Letters* **2008**, *93*, 093304.

(55) Barbe, C. J. Arendse, F. Comte, P. Jirousek, M. Lenzmann, F. Shklover, V.; GRATZEL, M. Nanocrystalline Titanium Oxide Electrodes for Photovoltaic Applications. *Synthesis* **1997**, *71*, 3157-3171.

(56) Wang, Z. Significant influence of TiO_2 photoelectrode morphology on the energy conversion efficiency of N719 dye-sensitized solar cell. *Coordination Chemistry Reviews* **2004**, *248*, 1381-1389.

(57) Wang, Q. Ito, S. Gratzel, M. Fabregat-Santiago, F. Mora-Seró, I. Bisquert, J. Bessho, T.; Imai, H. Characteristics of high efficiency dye-sensitized solar cells. *The journal of physical chemistry. B* **2006**, *110*, 25210-21.

(58) O'Regan, B. C. Durrant, J. R. Sommeling, P. M.; Bakker, N. J. Influence of the TiCl4 Treatment on Nanocrystalline TiO_2 Films in Dye-Sensitized Solar Cells. 2. Charge Density, Band Edge Shifts, and Quantification of Recombination Losses at Short Circuit. *Journal of Physical Chemistry C* **2007**, *111*, 14001-14010.

(59) Peng, B. Systematic investigation of the role of compact TiO_2 layer in solid state dye-sensitized TiO_2 solar cells. *Coordination Chemistry Reviews* **2004**, *248*, 1479-1489.

(60) Turner, G. M. Beard, M. C.; Schmuttenmaer, C. a Carrier Localization and Cooling in Dye-Sensitized Nanocrystalline Titanium Dioxide. *The Journal of Physical Chemistry B* **2002**, *106*, 11716-11719.

(61) Wurfel, U.; Hinsch, A. Detailed Experimental and Theoretical Investigation of the Electron Transport in a Dye Solar Cell by Means of a Three-Electrode Configuration. *Journal of Physical Chemistry C* **2008**, *112*, 1711-1720.

(62) Tiwana, P. Docampo, P. Johnston, M. B. Snaith, H. J.; Herz, L. M. Electron Mobility and Injection Dynamics in Mesoporous ZnO, SnO_2, and TiO_2 Films used in Dye-Sensitized Solar Cells. *ACS Nano* **2011**, null.

(63) Dittrich, T. Porous TiO_2: Electron Transport and Application to Dye Sensitized Injection Solar Cells. *physica status solidi (a)* **2000**, *182*, 447-455.

(64) van der Zanden, B.; Goossens, A. The Nature of Electron Migration in Dye-Sensitized Nanostructured TiO 2. *The Journal of Physical Chemistry B* **2000**, *104*, 7171-7178.

(65) Zhu, K. Neale, N. R. Miedaner, A.; Frank, A. J. Enhanced charge-collection efficiencies and light scattering in dye-sensitized solar cells using oriented TiO_2 nanotubes arrays. *Nano letters* **2007**, *7*, 69-74.

(66) Richter, C.; Schmuttenmaer, C. a Exciton-like trap states limit electron mobility in TiO_2 nanotubes. *Nature nanotechnology* **2010**, *5*, 769-72.

(67) Kopidakis, N. Neale, N. R.; Frank, A. J. Effect of an adsorbent on recombination and band-edge movement in dye-sensitized TiO_2 solar cells: evidence for surface passivation. *The journal of physical chemistry. B* **2006**, *110*, 12485-9.

3. Förster Resonance Energy Transfer

3.1 Introduction

Förster Resonance Energy Transfer (FRET) is a process by which excitation can be transferred at a distance from one fluorescent chromophore to another which absorbs at a longer wavelength. It is a special case of energy transfer in which there is neither charge exchange nor physical contact. Through this mechanism one material, by the aid of another, can be excited by wavelengths to which it would normally be insensitive. FRET is of interest to solid-state dye-sensitized solar cells (SDSCs) because it offers a way to increase spectral response without degrading performance by increasing the active layer thickness.

3.2 Mechanism and Theory

The simplest example of FRET includes two materials: one donor and one acceptor. The donor material must have an optical bandgap somewhat larger than the acceptor material, and must be fluorescent. The main requirement for FRET to occur is that the fluorescence spectrum of the donor material must overlap with the absorption spectrum of the acceptor material. Light absorbed by the donor material promotes an electron from the ground state to the excited state. Because the donor fluorescence spectrum and acceptor absorbance spectrum overlap, the two materials are coupled through the electromagnetic field by a dipole-dipole interaction. Through this interaction

the donor transfers its excitation energy to the acceptor non-radiatively. The excited electron in the donor returns to the ground state while an electron in the ground state of the acceptor is promoted to an excited state by the transferred energy.

This process occurs by the exchange of a virtual photon between donor and acceptor. This is a directed process mediated by the dipole-dipole interaction, and not to be confused with normal radiative decay of the donor excited state resulting in the emission of a photon propagating in a random direction, which simply happens to hit the acceptor. While radiative transfer could indeed occur, the efficiency of that process would be quite low, being based on the fraction of the donor's field of view covered by the acceptor. Also, the time scale for FRET is much faster than the time scale of normal radiative decay. FRET allows the two materials to be separated by some distance, because charge transfer does not occur between the two materials. The process also allows the acceptor material to indirectly absorb a photon to which it would not be sensitive to in the absence of the donor.

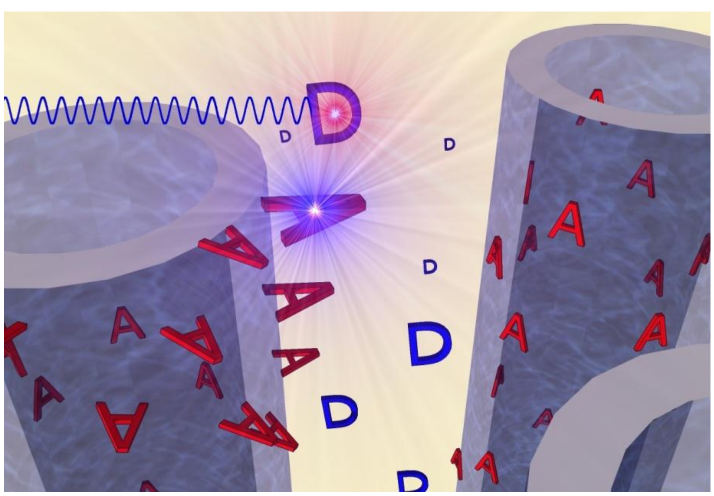

Figure 16: Schematic depicting energy transfer from dissolved donor to acceptor anchored to titania nanotubes.

The most important physical parameter to consider is the Förster radius, defined as the separation distance, R_0, at which excitation transfer efficiency reaches 50%. The Förster radius is given by the equation[1]

$$R_0^6 = \frac{9000 \ln(10) \mathrm{k}^2 \Phi_\mathrm{D}}{128\pi^2 N_A n^4} \int_0^\infty F_d(\lambda)\epsilon_A(\lambda)\lambda^4 \, d\lambda$$

where k is the orientation factor between donor and acceptor dipoles, Φ_D is the donor fluorescence quantum yield in the absence of the acceptor, N_A is the Avagadro Constant ($6.022*10^{23}$), n is the index of refraction for the medium surrounding donor and acceptor. For an arbitrary alignment of donor and acceptor dipoles the orientation factor, k is given by

$$k = cos\Phi_{DA} - 3\cos\Phi_D * cos\Phi_A$$

Where Φ_{DA} is the angle between transition moment vectors of donor and acceptor, and Φ_D and Φ_A are the angles between these vectors and the direction D → A.

k^2 is equal to 2/3 for random orientation. The overlap integral is the most important term because it is the resonance term and is the overlap between the fluorescence of the donor, normalized to unity area ($F_D(\lambda)$) and the molar absorption spectrum of the acceptor ($\epsilon_A(\lambda)$) scaled by wavelength to the fourth power. The stronger this resonance term, the more efficient energy transfer will be. Once the Förster radius has been determined, it can be used to calculate other quantities, such as the rate of excitation energy transfer, given by K_{ET}:

$$K_{ET} = \frac{1}{\tau_D}\left(\frac{R_0}{r}\right)^6$$

Where τ_D is the lifetime of the donor exited state in the absence of the acceptor, and r is the physical distance separating donor and acceptor choromophores. The expression for excitation transfer efficiency (ETE) is given by

$$ETE = \frac{R_0^6}{R_0^6 + r^6}$$

The ETE measures the fraction of excitons in the donor material which are transferred to the acceptor. ETE falls off rapidly for separation distances over one Förster radius, and is near 100% inside much of that radius.

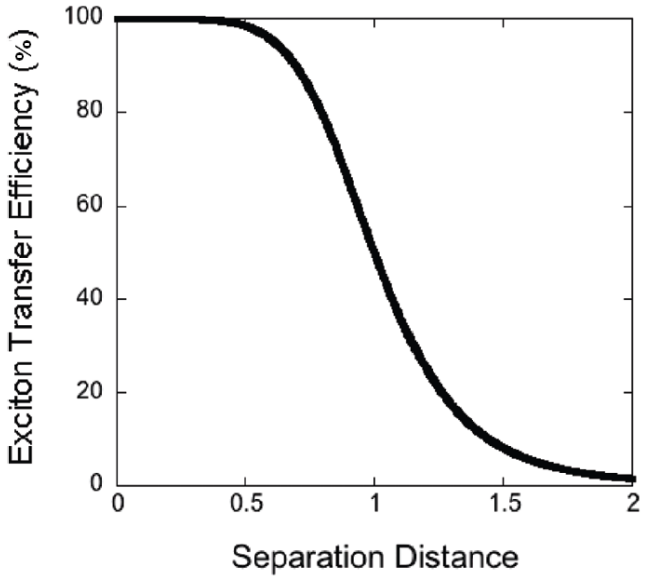

Figure 17: ETE vs donor-acceptor seperation distance, in units of Forster radii

3.3 Requirements for efficient FRET in Real Systems

The Theory of FRET is indeed quite simple. There are also some simple guidelines for employing FRET in real systems. The basic approach is to maximize the value of R_0, from which efficient energy transfer will follow. Firstly, it is imperative that the donor material have a reasonable fluorescence quantum yield, Φ_D, because R_0 scales linearly with Φ_D. A value of 100% is not necessary for FRET to occur, a reasonable Förster radius can still be accomplished with a value of 50%. However materials with a fluorescence quantum yield close to zero simply cannot be used. Also, while Φ_D is often measured while the material is very dilute in a high-purity solvent, for our case it must be measured as it will be employed in the system, i.e. at high concentration in the presence of impurities. Such conditions can lead to concentration quenching, caused by aggregation of the donor material, or by FRET between donor molecules until the energy is lost to thermalization or radiative decay. A balance must be struck such that donor concentration is high enough to afford near complete absorption of light, but low enough to prevent significant concentration quenching.

Additionally there must be good spectral overlap between the donor emission spectrum and acceptor absorbance spectrum. The larger the value of this integral, the larger the Förster radius. In practical terms that means the acceptor must have a very high absorption coefficient, and the peaks of the donor emission and acceptor absorption must coincide. In the case of DSSCs this must also take into account the

redshifts expected by absorbing the acceptor onto TiO_2 and placing the donor in a thin solid film.

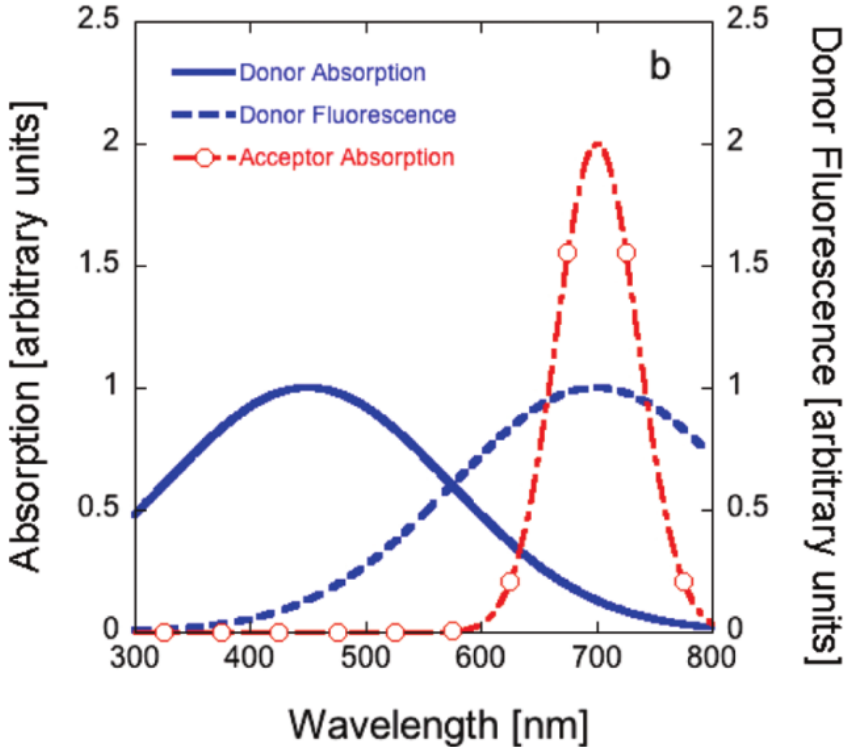

Figure 18: Example of ideal absorption/emission relationship. Reprinted from ref. [2]

Positioning of the donor material is important. Ideally, all donor material should be within a Förster radius of an acceptor. In DSSCs this is accomplished by using a nanoporous substrate where the typical pore radius is comparable to one Förster radius.

3.4 Utility in DSSCs

Because many practical dyes used in SDSCs are either weakly absorbing over a broad range, or strongly absorbing over a limited range, FRET can be a means to strengthen absorption over what is possible with a single material. By dispersing donor materials in the electrolyte of a DSSC much more space is made available for absorbing materials, increasing the optical density of a cell without the need to increase cell thickness. Without utilizing the bulk of the electrolyte, absorbing materials are constrained to the surface of TiO_2. Additionally, because the donor is isolated from the acceptor, there can be relaxed rules for compatibility. It is required to be mostly inert and not be quenched by the lithium salt dopant or to interfere with charge transport. Because SDSCs normally require very pure materials for good efficiency, degradation of charge transport is an eventuality if too much donor material is added. Therefore one must find an optimal concentration which allows for acceptable transport and is below the threshold for concentration quenching.

Because the expression for the Förster radius given above considers point-to-point energy transfer, it does not fit the case of SDSCs where there is a continuous organized layer of acceptors. It is more closely approximated by transfer from a point donor to an infinite sheet of acceptors, for which ETE falls off as r^{-4} instead of r^{-6}.[3] This provides a significant increase in Förster Radius and ETE over an unorganized distribution of acceptor molecules.

An analytical expression has recently been derived by Hoke and co-workers which gives the Förster radius for donors transferring energy to a monolayer of acceptor

dye adsorbed to the surface of a cylinder,[4] the arrangement used in a titania nanotube array. The Förster radius for a cylindrical system is given as

$$R_c = \left(\frac{C_A R_0^6}{1 + \tau_0 \sum_j K_{q_j} Q_j} \right)^{\frac{1}{4}}$$

Where C_A is the surface concentration, or packing density, of the acceptor on the surface of the cylinder, R_0 is the same expression as given above, τ_0 is the lifetime of the donor excited state in isolation. The summation is performed over the total number of quenching species indexed by j. K_{qj} is the bimolecular quenching coefficient for quenching of donor fluorescence by species j, and Q_j is the molar concentration of species j.

In order to achieve an ETE of 90% in a nanotube system, Rc must be 0.3 times the nanotube inner diameter. For the nanotubes used in this study with an average pore diameter of 24 nm, this would mean an R_c of 7.2 nm. An ETE of 50% is still possible with an R_c of only 2.9 nm.

3.5 Precedent

FRET has been observed in many systems and was first explained comprehensively in 1959.[1] FRET is especially important in photosynthetic systems, in which a large amount of choromphores surround a chemical reaction center to which they transfer absorbed energy via FRET. FRET was suggested as means to enhance light harvesting in P3HT/fullerene blends in 2005.[5] In 2007 Siegers et al. developed a covalently bonded donor-acceptor pair to enhance light harvesting in DSSCs.[6] FRET

was also suggested as a possible means to enable efficient use of low-gap dyes in DSSCs. [7] In 2009 FRET was first demonstrated by Shankar and coworkers in liquid-junction DSSCs using two discrete materials, ruthenium dye and a dissolved zinc phthalocyanine.[8] Although this work showed proof of concept, the overall efficiency increase was low due to the small value of the overlap integral for the Förster radius. The Gratzel group quickly followed with tailor-made perylene-based donors coupled to a phtalocyanine acceptor[9] and extended the concept to solid-state using a ruthenium-based donor and the squarine dye SQ-1 as the acceptor.[10] These systems lead to a 20-26% increase in overall photoconversion efficiency. Most recently our lab published a system for solid-state cells using DCM as the donor material and SQ-2 dye as the acceptor.[2] Encapsulated semiconductor quantum dots have also recently been used as a donor in DSSCs by Buhbut et al.[11]

3.6 References

(1) Forster, T. 10th Spiers Memorial Lecture: Transfer Mechanisms of Electronic Excitation. *Discussions of the Faraday Society* **1959**, *27*, 7-15.

(2) Basham, J. I. Mor, G. K.; Grimes, C. A. Förster resonance energy transfer in dye-sensitized solar cells. *ACS nano* **2010**, *4*, 1253-8.

(3) Kuhn, H. Classical Aspects of Energy Transfer in Molecular Systems. *The Journal of Chemical Physics* **1970**, *53*.

(4) Hoke, E. T. Hardin, B. E.; McGehee, M. D. Modeling the efficiency of Förster resonant energy transfer from energy relay dyes in dye-sensitized solar cells. *Optics express* **2010**, *18*, 3893-904.

(5) Liu, Y. Summers, M. A. Edder, C. Fréchet, J. M. J.; McGehee, M. D. Using Resonance Energy Transfer to Improve Exciton Harvesting in Organic-Inorganic Hybrid Photovoltaic Cells. *Advanced Materials* **2005**, *17*, 2960-2964.

(6) Siegers, C. Hohl-Ebinger, J. Zimmermann, B. Würfel, U. Mülhaupt, R. Hinsch, A.; Haag, R. A dyadic sensitizer for dye solar cells with high energy-transfer efficiency in the device. *Chemphyschem : a European journal of chemical physics and physical chemistry* **2007**, *8*, 1548-56.

(7) Koeppe, R. Bossart, O. Calzaferri, G.; Sariciftci, N. Advanced photon-harvesting concepts for low-energy gap organic solar cells. *Solar Energy Materials and Solar Cells* **2007**, *91*, 986-995.

(8) Shankar, K. Feng, X.; Grimes, C. A. Enhanced harvesting of red photons in nanowire solar cells: evidence of resonance energy transfer. *ACS nano* **2009**, *3*, 788-94.

(9) Hardin, B. E. Hoke, E. T. Armstrong, P. B. Yum, J.-ho; Comte, P. Torres, T. Fréchet, J. M. J. Nazeeruddin, M. K. Gratzel, M.; McGehee, M. D. Increased light harvesting in dye-sensitized solar cells with energy relay dyes. *Nature Photonics* **2009**, *3*, 406-411.

(10) Yum, J.-H. Hardin, B. E. Moon, S.-J. Baranoff, E. Nüesch, F. McGehee, M. D. Gratzel, M.; Nazeeruddin, M. K. Panchromatic response in solid-state dye-sensitized solar cells containing phosphorescent energy relay dyes. *Angewandte Chemie (International ed. in English)* **2009**, *48*, 9277-80.

(11) Buhbut, S. Itzhakov, S. Tauber, E. Shalom, M. Hod, I. Geiger, T. Garini, Y. Oron, D.; Zaban, A. Built-in quantum dot antennas in dye-sensitized solar cells. *ACS nano* **2010**, *4*, 1293-8.

4. Materials, Methods and Cell Assembly

4.1 Introduction

Titania (TiO_2) nanotubes have attracted much attention in the last decade. Since their discovery they have proven to be an excellent material for water photolysis[1-3] photocatalysis and artificial photosynthesis[4,5] anodes in dye-sensitzed[6-11] and heterojunction solar cells[12-14], drug delivery,[15,16] gas sensing,[17-22] and nanoporous membranes.[23] Titania nanotube arrays (TNTAs) excel in applications involving interfacial phenomena. Their high effective surface area make them well suited for adsorbing large amounts of chemical species, e.g. in catalysis, sensing, and dye adsorption. Titania is also a stable, transparent, wide band-gap (E_g 3.0-3.2 eV) intrinsically n-type semiconductor. Titania nanotubes are an excellent substrate for SDSCs due to their uniformity and excellent charge transport properties and are used preferentially over nanoparticulate substrates in this work.

This chapter provides a background on the materials and fabrications used, and motivation for their use.

4.2 TNTA Formation Mechanism

Anodic growth of titania nanotubes is generally carried out by applying a voltage between a titanium metal anode and a platinum cathode immersed in a fluoride-containing electrolyte. Titania nanotubes are formed by competing oxidation and etching reactions. When a voltage is applied to a piece of titanium metal submerged in the anodization electrolyte, a compact oxide layer quickly forms. This layer is formed by field assisted oxidation of the titanium metal by oxygen and hydroxide ions which are transported through the oxide under the influence of the electric field. [24] Once a thick enough oxide layer is formed, the transport of oxygen is slowed and oxide formation stops. Fluoride ions in the electrolyte begin to corrode the oxide, causing pitting. The oxide at the bottom of these pits becomes relatively thin, increasing the local electric field and the field assisted etching rate. The thinning of the oxide allows migration of oxygen again, and oxidation of the underlying metal may continue in the direction of the electric field. Due to the applied electric field, the Ti-O bond is weakened by polarization, allowing dissolution of Ti^{4+} ions into the electrolyte.[20] The remaining oxygen ions are then transported though the oxide to the metal interface where they oxidize titanium metal.[25] Field assisted oxidation also reduces the local pH by releasing H^+ ions. This increases the etching rate at the pore bottom. In viscous electrolytes a pH gradient will develop along the nanotube. In low viscosity electrolytes a ribbed structure can result due to periodic variation of the pore diameter caused by fluctuations in the local pH at the pore bottom. These fluctuations can be dampened in a viscous electrolyte, leading to smooth walls of uniform thickness.[26] The anodic oxidation and chemical etching steps are represented by the equations: [27]

$$Ti + 2H_2O \rightarrow TiO_2 + 4e^- + 4H^+$$

$$TiO_2 + 2F^- + 4HF \rightarrow TiF_6^{2-} + 2H_2O$$

From here on, nanotube growth is controlled by three competing processes: electric field assisted oxide growth, field assisted isotropic chemical etching, and anisotropic field-assisted etching. Nanotube length will increase until the rate of chemical dissolution of the walls matches the rate of new oxide formation. In some electrolytes, for example dilute hydrofluoric acid, this occurs at relatively low nanotube lengths, approximately 500nm. [28] For electrolytes with very low chemical etching rates, for example NH_4F in ethylene glycol, millimeter-long nanotubes have been realized. [23] The ending average pore radius depends mostly on anodization voltage, and is roughly equal to the thickness of the compact oxide layer which would be formed at the same voltage in the absence of fluoride. [29]

4.3 Evolution of Electrolyte Chemistry

In 1999 Zwilling et al. discovered that an ordered nanoporous structure could be formed by anodizing titanium in a chromic acid and hydrofluoric acid (HF) bath.[30] In 2001 Gong et al. discovered that the porous structure could be deepened to form discreet tubes in a dilute aqueous HF bath given an appropriate pH and anodization voltage.[28] These tubes had a pore diameter of 25-65 nm and a length of 250 nm. An example is shown in **Error! Reference source not found.**.

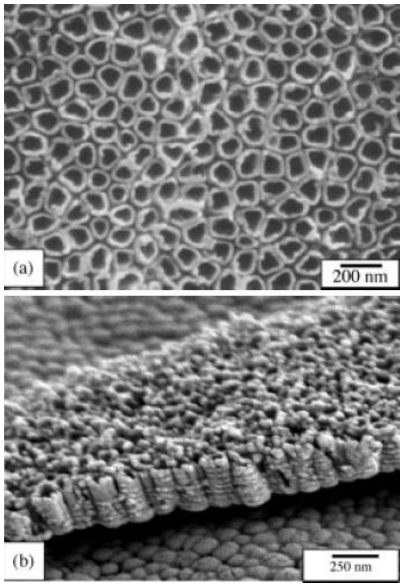

Figure 19: a) top view and b) side view of nanotubes fabricated in 0.5 wt% aqueous HF solution at 20 V for 45 minutes.[21]

The nanotube length was kept short by the powerful isotropic etching of the hydrofluoric acid bath. The reduction of the isotropic reduction rate was the next hurdle to achieving increased nanotube length. The first attempt produced a buffered HF electrolyte, in which the pH was brought closer to neutral. The greatly reduced isotropic etching rate allowed the nanotubes to reach a length of approximately 6 µm.[31] The real breakthrough came with the realization of non-aqueous electrolytes, in which the isotropic etching rate could be reduced to almost zero, while maintaining a high field-assisted etching rate. This group of electrolytes consists of a small amount of HF or fluoride-containing salt (typically NH_4F, NaF, KF or tetra(n-butyl) ammonium fluoride) dissolved in an appropriate organic solvent (e.g. DMSO, ethylene glycol, formamide).[23,32-37] A small amount of water (1-10% v/v) must be added to increase the growth rate

and inhibit the formation of pore clogging precipitates. Nanotubes formed using this recipe can in some cases be grown to arbitrary lengths because chemical etching is suppressed. [23,35] By varying the water content the barrier layer thickness and adhesion of the TNTA to the metal substrate can be varied from weak (little or no water) to strong (generally >5% water). Weakly adhered TNTAs can be separated from the substrate by various means to form a free-standing nanotube membrane. [23,35,38] It has recently been discovered that nanotubes with a high initial degree of crystallinity can be grown using polyethylene glycol as a solvent.[39]

4.4 Post fabrication crystallization

Nanotubes made by electrochemical anodization are typically amorphous, and must be annealed to a more useful, crystalline form. Of the three crystalline phases of TiO_2, anatase, brookite and rutile, the most useful form for most applications is anatase due to its superior charge transport characteristics. Anatase nanotubes show markedly higher efficiencies. Amorphous titania can be converted to anatase by annealing in an oxygen ambient. An oxygen ambient is required to prevent the formation of nonstoichiometric titania. In general, the crystalline fraction and grain size will increase with annealing time and temperature until about 580 °C, after which the anatase phase can convert to rutile. Annealing generally takes place in a tube furnace with a constant to flow of oxygen to flush away any contaminants released from the sample, such as organic residue left over from the anodization process. Short exposure to very high temperatures, such as during flame annealing, may lead to the sintering of

adjacent nanotubes. [2] Long exposure to very high temperatures (above 820° C) will lead to a total collapse of the nanotubular structure. [40] Annealing also leads to the formation of a rutile barrier layer between the metal substrate and the nanotube array due to oxidation. This barrier layer can cause unwanted reductions in charge transport due to series resistance, and it is important to minimize its thickness. To this end, rapid thermal annealing has been investigated in order to minimize the amount of barrier layer growth while maintaining good crystallization of the above nanotube array. Such treatments were able to increase photoconversion efficiencies to 13.13% under bandgap illumination versus 10% for an optimal thermally annealed sample. [41]

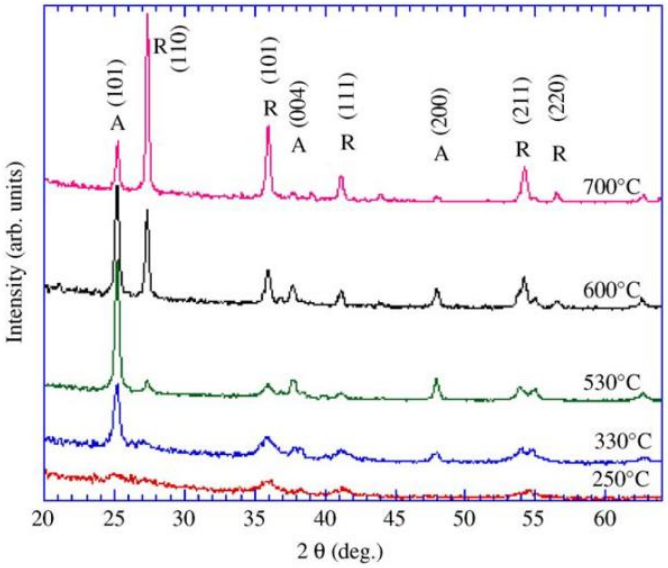

Figure 20: X-ray diffraction patterns for TiO_2 nanotubes annealed at various temperatures, showing anatase (A) and rutile (R) peaks. Reprinted from ref. [27]

4.5 Transparent Nanotube Arrays

Although titania itself is transparent, normally TNTAs formed by anodization of metal foil substrates are not transparent due to the thick layer of unconsumed metal remaining. Some applications which benefit from front-side illumination (i.e. illumination through the substrate), such as DSSCs, require a transparent substrate. For this reason transparent TNTAs were developed by sputtering a thin film of titanium metal on conductive oxide coated glass.[6,11,42] This film can then be anodized in the normal manner until only a thin, semi-transparent of layer metal is left between the nanotubes and the glass substrate. At this point the anodization is abruptly stopped. When the film is annealed the remaining metal will be oxidized, giving full transparency. State of the art transparent TNTAs have recently been fabricated on conductive oxide coated glass up to a length of 33 µm.[6]

Figure 21: Stages of TNTA fabrication showing thick titanium film (top), anodized film with semitransparent metal later (middle), and fully annealed transparent film (bottom). Reprinted from Ref [8]

In this work a thin film of titanium is sputtered onto a 2 mm thick glass substrated coated with fluorine-doped tin oxide (FTO), a common transparent conductive oxide. This film is then anodized in an electrolyte containing 2 vol% hydrofluoric acid in dimethyl sulfoxide. The anodization voltage was 8 V and the cathode was platinum foil. When only a thin, semitransparent layer of metal remained the anodization was stopped and the film was washed in isopropanol. The films were then annealed in a tube furnace under flowing oxygen at a temperature of 400 C for 6 hours. The lowest possible temperature is used which will lead to crystallization in order to prevent unnecessary degradation of the FTO layer.

4.6 Titanium Tetrachloride Treatment

It is common to treat nanotube arrays with titanium tetrachloride ($TiCl_4$) after the annealing step. The treatment consists of soaking the electrode in a 20 mM aqueous solution of $TiCl_4$ for 12-16 hours followed by a short anneal at 450 °C. This is a technique borrowed from the fabrication of nanoparticulate TiO_2 electrodes in which it was intended to create a stronger connection between adjacent particles. [43] This is not the desired effect in nanotubular electrodes, but the open circuit voltage, short circuit current and dye loading are still increased considerably.[6] O'Regan, Durrant, et al found that $TiCl_4$ treatment also lowers the TiO_2 conduction band and decreases the electron recombination rate, thereby increasing quantum efficiency.[44] The end result is a sizable increase in efficiency over non-treated electrodes. This may be attributed to the fact that during processing the surface of the TiO_2 electrode may become contaminated.

$TiCl_4$ treatment produces a pristine surface which has improved electrical characteristics and more favorable trap distribution. [44] By adjusting process variables this new layer of TiO_2 can take the form of a conformal layer, particles several nanometers in size, or a combination of the two. A great increase in dye uptake, especially for short nanotubes, can be observed after $TiCl_4$ treatment [6,7] likely due to the increased surface area attributed to the layer of TiO_2 nanoparticles deposited on the nanotube surface.

4.7 Use in Dye-Sensitized Solar Cells

One of the most exciting applications of TNTAs is their use as electrodes for DSSCs. Titania has long been the material of choice for making DSSCs due to its transparency, photostability, favorable band positions, and electron conductivity. For efficient light absorption the titania must possess a nanostructure which enables it to be coated with the equivalent of several hundred monolayers of dye. For efficient regeneration of the dye, the pore structure must also allow free flow of the electrolyte. Conventional DSSCs are made using a layer of sintered titania nanoparticles. Electron transport through such structures is governed by diffusion, and electrons move from their generation point to the collection point via a random walk. In the process they undergo many thousands of scattering events at grain boundaries and impurity sites. Every scattering event is an opportunity for the electron to recombine, and can be a significant loss mechanism. When the nanoparticulate structure is replaced by a TNTA the random walk is constrained into one dimension, achieving vectorial charge transport directed along the length of the nanotubes. Transport studies conducted by Frank et.al

show that recombination in nanotubular electrodes is an order of magnitude slower than in nanoparticulate electrodes.[45] This means that much thicker active layers could be used in TNTAs, leading to more complete red absorption.

Interest in titania nanotubes for DSSC anodes began with the use of disordered nanotube or nanowire pastes which were deposited in a similar manner to titania particle films. [46,47] The objective was to improve charge transport in the anode although success was mixed. Anodes formed by randomly aligned 1D structures are not a true one dimensional network. They are perhaps more analogous to a well-connected three dimensional network. In order to have true one dimensional transport an organized array of vertically aligned 1D nanostructures must be utilized. The use of ordered titania nanotubes in DSSCs was first reported in 2006. [8] Transparent TNTAs on conductive glass were used to achieve an efficiency of 2.9% using 360nm long nanotubes. Efficiency was limited by the length of nanotubes and the thin film deposition techniques used at the time, however it was much higher than would be expected for a DSSC using a sintered nanoparticle electrode of similar thickness. It was found that the $TiCl_4$ treatment had an enormous effect on the photocurrent. Treated electrodes generated five times more current than untreated electrodes. [8] It has been shown that this increase in current can be correlated to the increased amount of dye adsorbed following $TiCL_4$ treatment.[7] This increase is especially large for short nanotubes because of their initial small surface area. Treatment can increase surface roughness considerably and strengthen bonding between titania and dye. [48] Even after treatment they can still have a low optical absorption.

The obvious road to improvement was to use longer nanotubes in order to provide more complete absorption of light. Due to the difficulty in preparing long TNTAs on glass, metal foil substrates were first investigated. [10] These provided the benefit of unrestricted nanotube length, but with the drawback that due to the metal substrate the cell must be illuminated in an inverted manner (backside illuminated), i.e. light must pass through the platinized electrode and electrolyte before reaching the dye. Nonetheless, efficient cells can still be made by reducing the iodine content of the electrolyte, which absorbs a significant amount of short wavelength light. By using high absorption coefficient Ru-TPA-NCS dye coupled with an electrolyte containing 0.01M iodine, an efficiency of 6.1% was realized. [7]

Advances in the growth of TNTAs on transparent substrates recently led to the ability to grow nanotubes roughly 20 times longer than initial attempts, and an optimized nanotube array length led to a 6.9% efficient front side illuminated cell. [6] These efficiencies are still well below record efficiencies for nanoparticle-based devices. It is believed that at long lengths the diffusion of electrolyte inside the nanotube pore can be restricted, slowing regeneration of the dye molecules and leading to decreased efficiency. It has been shown that this limitation can be overcome by detaching the nanotube array from the substrate, etching the pore bottom, and reattaching the resulting membrane atop a thin layer of TiO_2 nanoparticle paste.[49] This arrangement, despite using TNTAs with a relatively low roughness factor, was reported to achieve an efficiency or 9.1% in a liquid junction DSSC.

4.8 Dye adsorption process

Many dye molecules are designed with a carboxylic acid functional group which will coordinate to oxygen vacancies on the surface of TiO_2. All that is needed to form a self-assembled monolayer on the surface of TiO_2 is to soak the substrate in a solution of the sensitizer. Typically the solvent used is one in which the dye is very highly soluble as this has been observed to lead to higher dye loading than when a poorer solvent is used. The solvent must also be free of any water, as many dyes react with water. Surface adsorbed water on TiO_2 also competes with dye molecules for attachment sites and must therefore be minimized by careful drying of the substrate prior to dye coating, often by heating.

In this work the squarine dye SQ-2[50] was used exclusively as the acceptor dye due to its high molar absorption coefficient and the fact that its absorption occurs in the red region of the spectrum (550-700nm). For dye coating a 0.3 mM solution of SQ-2 (Solaronix) was dissolved in dry ethanol (Koptec). The substrate was dried either by removing from the furnace immediately after $TiCl_4$ treatment at a temperature of approximately 80 °C and placing directly into the dye solution (the preferred method) or by heating above 100 °C on a hotplate for 30 minutes before cooling to 80 °C and immersing in dye solution. The bottle was then sealed tightly and placed in the dark to soak for 17 hours. After this time the sample was rinsed with excess quantities of pure ethanol to remove unattached dye molecules and dried under a nitrogen stream. The substrate was then immediately transferred to a nitrogen-filled glovebox for deposition of the hole transport material.

4.9 Deposition of Hole Transport Material

The materials and deposition procedure for the hole transport material can be quite sensitive to ambient temperature, humidity and oxygen. For this reason deposition was always carried out under controlled conditions in a nitrogen-filled glovebox using materials which were stored either in the glovebox or a dessicator. The hole transport material consisted of 12 mg of Spiro-OMeTAD (Merck) dissolved in 100 µl of cholrobenzene (99.8%, Sigma Aldrich) to which was added 1.2 µl tert-butyl pyridine (98%, Sigma Aldrich) and 2.5 µl of 0.592 M $Li[CF_3SO_2]_2N$ salt in cyclohexanone (99%, Sigma Aldrich). This solution was heated on a hotplate inside the glovebox for 20 minutes at 70°C to help fully dissolve the Spiro-OMeTAD. After heating, any donor material solution was then added from a concentrated stock solution.

It is highly preferred that the donor material be soluble in chlorobenzene, the same solvent used for spin casting, in order to ensure that a uniform film is formed. If it is not, using a different solvent can lead to phase separation during spin casting, leaving small islands of the donor material instead of having it uniformly dispersed through the Spiro-OMeTAD layer. To prevent phase separation upon spin casting, the donor material must be dissolved in a solvent which is highly miscible with chlorobenzene and has a similar boiling point. The author has found empirically that many donor materials which are not soluble in chlorobenzene can be dissolved in dimethylformamide (DMF) and a continuous film can be cast as a mixture of Spiro-OMeTAD in chlorobenzene and donor material in DMF. Adding too much donor material can dilute the solution, resulting in a thinner film. To avoid this, when adding large amounts of donor material solution

the amount of chlorobenzene added was reduced to keep the total solution volume to 120 μl or less.

Substrates were first prepared by depositing 50 μl of xylene (Sigma Aldrich) onto the surface and then spin coating. This step helps to remove dust and unattached dye molecules and also helps the Spiro-OMeTAD solution to penetrate deeper into the nanotube pores. Immediately following this step 50 μl of the Spiro-OMeTAD solution was dispensed onto the substrate and spin coated. For both steps the spin program consisted of a 60 second wait to allow the solution to penetrate the nanotube pores, followed by a 4 second ramp to 2000 rpm and a total spin time 40 seconds. At the end of this time spinning was abruptly stopped. The cells were then left to dry in the glove box for one hour before removing.

4.10 Deposition of back contact

After deposition of the hole transport material, the cells were fitted to a shadow mask having rows of circular holes 2mm in diameter. Masked cells were placed in a home built thermal evaporator and pumped down to < $5x10^{7}$ Torr using a cryogenic pump. Gold of four nines (99.99%) purity was thermally evaporated at a rate of 2-4 Å/sec to a thickness of 400 Å. A throwing distance of 18 centimeters was used. Substrate temperature was maintained below 40 °C.

Figure 22: Photograph of a completed cell. Substrate is 15 mm x 25 mm. Contacts have a radius of 1 mm.

4.11 References

(1) Mor, G. K. Shankar, K. Paulose, M. Varghese, O. K.; Grimes, C. A. Enhanced photocleavage of water using titania nanotube arrays. *Nano letters* **2005**, *5*, 191-5.

(2) Shankar, K. Paulose, M. Mor, G. K. Varghese, O. K.; Grimes, C. A. A study on the spectral photoresponse and photoelectrochemical properties of flame-annealed titania nanotube-arrays. *Journal of Physics D: Applied Physics* **2005**, *38*, 3543-3549.

(3) Varghese, O. K. Paulose, M. Shankar, K. Mor, G. K.; Grimes, C. A. Water-Photolysis Properties of Micron-Length Highly-Ordered Titania Nanotube-Arrays. *Journal of Nanoscience and Nanotechnology* **2005**, *5*, 1158-1165.

(4) Roy, S. C. Varghese, O. K. Paulose, M.; Grimes, C. A. Toward solar fuels: photocatalytic conversion of carbon dioxide to hydrocarbons. *ACS Nano* **2010**, *4*, 1259-78.

(5) Varghese, O. K. Paulose, M. Latempa, T. J.; Grimes, C. A. High-rate solar photocatalytic conversion of CO_2 and water vapor to hydrocarbon fuels. *Nano letters* **2009**, *9*, 731-7.

(6) Varghese, O. K. Paulose, M.; Grimes, C. A. Long vertically aligned titania nanotubes on transparent conducting oxide for highly efficient solar cells. *Nature nanotechnology* **2009**, *4*, 592-7.

(7) Shankar, K. Bandara, J. Paulose, M. Wietasch, H. Varghese, O. K. Mor, G. K. LaTempa, T. J. Thelakkat, M.; Grimes, C. A. Highly efficient solar cells using TiO_2 nanotube arrays sensitized with a donor-antenna dye. *Nano letters* **2008**, *8*, 1654-9.

(8) Mor, G. K. Shankar, K. Paulose, M. Varghese, O. K.; Grimes, C. A. Use of highly-ordered TiO_2 nanotube arrays in dye-sensitized solar cells. *Nano letters* **2006**, *6*, 215-8.

(9) Paulose, M. Shankar, K. Varghese, O. K. Mor, G. K.; Grimes, C. A. Application of highly-ordered TiO_2 nanotube-arrays in heterojunction dye-sensitized solar cells. *Journal of Physics D: Applied Physics* **2006**, *39*, 2498-2503.

(10) Paulose, M. Shankar, K. Varghese, O. K. Mor, G. K. Hardin, B.; Grimes, C. A. Backside illuminated dye-sensitized solar cells based on titania nanotube array electrodes. *Nanotechnology* **2006**, *17*, 1446-1448.

(11) Mor, G. K. Varghese, O. K. Paulose, M.; Grimes, C. A. Transparent Highly Ordered TiO_2 Nanotube Arrays via Anodization of Titanium Thin Films. *Advanced Functional Materials* **2005**, *15*, 1291-1296.

(12) Mor, G. K. Kim, S. Paulose, M. Varghese, O. K. Shankar, K. Basham, J.; Grimes, C. A. Visible to near-infrared light harvesting in TiO_2 nanotube array-P3HT based heterojunction solar cells. *Nano letters* **2009**, *9*, 4250-7.

(13) Mor, G. K. Shankar, K. Paulose, M. Varghese, O. K.; Grimes, C. A. High efficiency double heterojunction polymer photovoltaic cells using highly ordered TiO_2 nanotube arrays. *Applied Physics Letters* **2007**, *91*, 152111.

(14) Shankar, K. Mor, G. K. Prakasam, H. E. Varghese, O. K.; Grimes, C. A. Self-assembled hybrid polymer-TiO_2 nanotube array heterojunction solar cells. *Langmuir : the ACS journal of surfaces and colloids* **2007**, *23*, 12445-9.

(15) Popat, K. C. Eltgroth, M. Latempa, T. J. Grimes, C. A.; Desai, T. A. Decreased Staphylococcus epidermis adhesion and increased osteoblast functionality on antibiotic-loaded titania nanotubes. *Biomaterials* **2007**, *28*, 4880-8.

(16) Popat, K. C. Eltgroth, M. LaTempa, T. J. Grimes, C. A.; Desai, T. A. Titania nanotubes: a novel platform for drug-eluting coatings for medical implants? *Small (Weinheim an der Bergstrasse, Germany)* **2007**, *3*, 1878-81.

(17) Paulose, M. Varghese, O. K. Mor, G. K. Grimes, C. A.; Ong, K. G. Unprecedented ultra-high hydrogen gas sensitivity in undoped titania nanotubes. *Nanotechnology* **2006**, *17*, 398-402.

(18) Varghese, O. K. Yang, X. Kendig, J. Paulose, M. Zeng, K. Palmer, C. Ong, K. G.; Grimes, C. A. A Transcutaneous Hydrogen Sensor: From Design to Application. *Sensor Letters* **2006**, *4*, 120-128.

(19) Yoriya, S. Prakasam, H. E. Varghese, O. K. Shankar, K. Paulose, M. Mor, G. K. Latempa, T. J.; Grimes, C. A. Initial Studies on the Hydrogen Gas Sensing Properties of Highly-Ordered High Aspect Ratio TiO_2 Nanotube-Arrays 20 μm to 222 μm in Length. *Sensor Letters* **2006**, *4*, 334-339.

(20) Mor, G. Varghese, O. Paulose, M.; N Fabrication of tapered, conical-shaped titania nanotubes. *Journal of Materials Research* **2003**, *18*, 18-20.

(21) Varghese, O. K. Gong, D. Paulose, M. Ong, K. G. Dickey, E. C.; Grimes, C. A. Extreme Changes in the Electrical Resistance of Titania Nanotubes with Hydrogen Exposure. *Advanced Materials* **2003**, *15*, 624-627.

(22) Varghese, O. Hydrogen sensing using titania nanotubes. *Sensors and Actuators B: Chemical* **2003**, *93*, 338-344.

(23) Paulose, M. Varghese, O. K. Peng, L. Popat, K. C. Prakasam, H. E. Mor, G. K. Desai, T. a; Grimes, C. a TiO_2 Nanotube Arrays of 1000 μm Length by Anodization of Titanium Foil: Phenol Red Diffusion. *Journal of Physical Chemistry C* **2007**, *111*, 14992-14997.

(24) Parkhutik, V. P.; Shershulsky, V. I. Theoretical modelling of porous oxide growth on aluminium. *Journal of Physics D: Applied Physics* **1992**, *25*, 1258-1263.

(25) Siejka, J.; Ortega, C. An O18 Study of Field-Assisted Pore Formation in Compact Anodic Oxide Films on Aluminum. *Journal of The Electrochemical Society* **1977**, *124*, 883.

(26) Macak, J. M. Tsuchiya, H. Taveira, L. Aldabergerova, S.; Schmuki, P. Smooth anodic TiO_2 nanotubes. *Angewandte Chemie (International ed. in English)* **2005**, *44*, 7463-5.

(27) MOR, G. Varghese, O. K. PAULOSE, M. Shankar, K.; Grimes, C. A. A review on highly ordered, vertically oriented TiO_2 nanotube arrays: Fabrication, material properties, and solar energy applications. *Solar Energy Materials and Solar Cells* **2006**, *90*, 2011-2075.

(28) Gong, D. Grimes, C. A. Varghese, O. K. Chen, Z. Hu, W.; Dickey, E. Titanium oxide nanotube arrays prepared by anodic oxidation. *Journal of Materials Research* **2001**, *16*, 3331-3334.

(29) Yasuda, K. Macak, J. M. Berger, S. Ghicov, A.; Schmuki, P. Mechanistic Aspects of the Self-Organization Process for Oxide Nanotube Formation on Valve Metals. *Journal of The Electrochemical Society* **2007**, *154*, C472.

(30) Zwilling, V. Aucouturier, M.; Darque-ceretti, E. Anodic oxidation of titanium and TA6V alloy in chromic media . An electrochemical approach. *Electrochimica Acta* **1999**, *45*, 921 - 929.

(31) Cai, Q. Paulose, M. Varghese, O. K.; Grimes, C. A. The effect of electrolyte composition on the fabrication of self-organized titanium oxide nanotube arrays by anodic oxidation. *Journal of Materials Research* **2005**, *20*, 230-236.

(32) Ruan, C. Paulose, M. Varghese, O. K. Mor, G. K.; Grimes, C. A. Fabrication of highly ordered TiO_2 nanotube arrays using an organic electrolyte. *The journal of physical chemistry. B* **2005**, *109*, 15754-9.

(33) Paulose, M. Shankar, K. Yoriya, S. Prakasam, H. E. Varghese, O. K. Mor, G. K. LaTempa, T. J. Latempa, T. A. Fitzgerald, A.; Grimes, C. A. Anodic growth of highly ordered TiO_2 nanotube arrays to 134 microm in length. *The journal of physical chemistry. B* **2006**, *110*, 16179-84.

(34) Yoriya, S. Paulose, M. Varghese, O. K. Mor, G. K.; Grimes, C. a Fabrication of Vertically Oriented TiO_2 Nanotube Arrays Using Dimethyl Sulfoxide Electrolytes. *Journal of Physical Chemistry C* **2007**, *111*, 13770-13776.

(35) Prakasam, H. E. Shankar, K. Paulose, M. Varghese, O. K.; Grimes, C. A. A New Benchmark for TiO_2 Nanotube Array Growth by Anodization. *Journal of Physical Chemistry C* **2007**, *111*, 7235-7241.

(36) Shankar, K. Mor, G. K. Prakasam, H. E. Yoriya, S. Paulose, M. Varghese, O. K.; Grimes, C. A. Highly-ordered TiO_2 nanotube arrays up to 220 μm in length: use in water photoelectrolysis and dye-sensitized solar cells. *Nanotechnology* **2007**, *18*, 065707.

(37) Yoriya, S. Mor, G. K. Sharma, S.; Grimes, C. A. Synthesis of ordered arrays of discrete, partially crystalline titania nanotubes by Ti anodization using diethylene glycol electrolytes. *Journal of Materials Chemistry* **2008**, *18*, 3332.

(38) Albu, S. P. Ghicov, A. Macak, J. M. Hahn, R.; Schmuki, P. Self-organized, free-standing TiO_2 nanotube membrane for flow-through photocatalytic applications. *Nano letters* **2007**, *7*, 1286-9.

(39) Allam, N. K.; Grimes, C. A. Room temperature one-step polyol synthesis of anatase TiO_2 nanotube arrays: photoelectrochemical properties. *Langmuir : the ACS journal of surfaces and colloids* **2009**, *25*, 7234-40.

(40) Varghese, O. K. Gong, D. Paulose, M. Grimes, C. A.; Dickey, E. Crystallization and high-temperature structural stability of titanium oxide nanotube arrays. *Journal of Materials Research* **2003**.

(41) Allam, N. K.; Grimes, C. A. Effect of Rapid Infrared Annealing on the Photoelectrochemical Properties of Anodically Fabricated TiO 2 Nanotube Arrays. *The Journal of Physical Chemistry C* **2009**, *113*, 7996-7999.

(42) Chen, P. Brillet, J. Bala, H. Wang, P. Zakeeruddin, S. M.; Gratzel, M. Solid-state dye-sensitized solar cells using TiO_2 nanotube arrays on FTO glass. *Journal of Materials Chemistry* **2009**, *19*, 5325.

(43) Barbe, C. J. Arendse, F. Comte, P. Jirousek, M. Lenzmann, F. Shklover, V.; Gratzel, M. Nanocrystalline Titanium Oxide Electrodes for Photovoltaic Applications. *Synthesis* **1997**, *71*, 3157-3171.

(44) O'Regan, B. C. Durrant, J. R. Sommeling, P. M.; Bakker, N. J. Influence of the $TiCl_4$ Treatment on Nanocrystalline TiO_2 Films in Dye-Sensitized Solar Cells. 2. Charge Density, Band Edge Shifts, and Quantification of Recombination Losses at Short Circuit. *Journal of Physical Chemistry C* **2007**, *111*, 14001-14010.

(45) Zhu, K. Neale, N. R. Miedaner, A.; Frank, A. J. Enhanced charge-collection efficiencies and light scattering in dye-sensitized solar cells using oriented TiO_2 nanotubes arrays. *Nano letters* **2007**, *7*, 69-74.

(46) Adachi, M. Murata, Y. Okada, I.; Yoshikawa, S. Formation of Titania Nanotubes and Applications for Dye-Sensitized Solar Cells. *Journal of The Electrochemical Society* **2003**, *150*, G488.

(47) Adachi, M. Murata, Y. Takao, J. Jiu, J. Sakamoto, M.; Wang, F. Highly efficient dye-sensitized solar cells with a titania thin-film electrode composed of a network structure of single-crystal-like TiO_2 nanowires made by the "oriented attachment" mechanism. *Journal of the American Chemical Society* **2004**, *126*, 14943-9.

(48) Sommeling, P. M. O'Regan, B. C. Haswell, R. R. Smit, H. J. P. Bakker, N. J. Smits, J. J. T. Kroon, J. M.; van Roosmalen, J. A. M. Influence of a $TiCl_4$ post-treatment on nanocrystalline TiO_2 films in dye-sensitized solar cells. *The journal of physical chemistry. B* **2006**, *110*, 19191-7.

(49) Lin, C.-J. Yu, W.-Y.; Chien, S.-H. Transparent electrodes of ordered opened-end TiO2-nanotube arrays for highly efficient dye-sensitized solar cells. *Journal of Materials Chemistry* **2010**, *20*, 1073.

(50) Geiger, T. Kuster, S. Yum, J.-H. Moon, S.-J. Nazeeruddin, M. K. Gratzel, M.; Nüesch, F. Molecular Design of Unsymmetrical Squaraine Dyes for High Efficiency Conversion of Low Energy Photons into Electrons Using TiO_2 Nanocrystalline Films. *Advanced Functional Materials* **2009**, *19*, 2720-2727.

5: Donor Materials

5.1 Introduction

Because the purpose of this work is to demonstrate working FRET systems, the largest part of the effort includes identifying appropriate donor materials. For practical purposes attention is focused on existing materials available for dye lasers, OLEDs and fluorescent markers, rather than taking the more complicated approach of synthesizing new materials. In this way it was possible to survey many materials with differing characteristics and observe trends among them. Because the types of solar cells investigated vary only in the type and quantity of donor material used, there are three main concerns when choosing a donor material.

First, it must exhibit FRET to the acceptor dye in a pure system. This is verified if fluorescence of the donor is quenched in a solution containing the acceptor.

Second, it must not be deactivated by other compounds in the cell, namely the lithium salt used to dope Spiro-OMeTAD. Compatibility is verified if fluorescence of the donor is not quenched in a solution containing the lithium salt.

Lastly, test cells are produced and the effect of the donor is quantified in terms of an increase of photons harvested in the energy range corresponding to absorption by the donor. The amounts of donor added are referred to by the amount of solution volume added to the hole transport material layer, as is described in Chapter 4. For each substrate used 50 μl of Spiro-OMeTAD solution was mixed with the indicated amount of donor solution. In some cases, when large volumes of donor solution were

used, the Spiro-OMeTAD solution was prepared in a more concentrated form to keep the total volume including donor solution constant.

This Chapter profiles a number of materials which were selected because they were known to be efficient fluorescent compounds, and their absorption spectra roughly matched the window of the solar spectrum which SQ-2 dye does not absorb, namely blue to green light from 400-550nm. At the outset it was not certain which compounds might be compatible with SDSC architecture, and therefore all compounds had to be subjected to each of the tests mentioned above. This chapter includes measurements of quenching due to the presence of SQ-2 Dye and the lithium salt dopant used to increase conductivity in Spiro-OMeTAD. Being quenched by SQ-2, and not being quenched by the lithium salt are good indicators that a particular donor material may work in a FRET system. They do not guarantee it, however. The real proof comes when the material is employed in a test cell and Incident Photon to Collected Electron (IPCE) spectrum is measured.

It is worth mentioning that, at the outset, there was no precedent for using any of these materials as FRET donors in SDSCs. Their utility was totally unknown for that purpose, although they were known to be efficient materials for OLEDs, dye lasers, or fluorescent markers. They were selected due to their performance in these related fields as well as their high absorption coefficients and appropriate matching of absorption spectra to SQ-2.

5.2 Methods

Fluorescence measurements were made using a spectrofluorimeter (Jobin Yvon). 5 μM solutions were prepared in either dry ethanol (Koptec) or acetonitrile (Sigma Aldrich). Solution temperature was maintained at 22 °C. A stock solution of $Li(CF_3SO_2)_2N$ in cyclohexanone (170 mg/ml, 0.59 M) was prepared and added stepwise to the donor solutions and well mixed as fluorescence was measured. Likewise, a stock solution of saturated SQ-2 dye (about 6.8 mM as determined by optical absorption) in dry ethanol was prepared and added stepwise. UV-Vis absorption spectra were measured using a Perkin Elmber Lambda 950.

Electrical characterizations were made using a scanning potentiostat (CH Instruments 600C). The potential was scanned at 10 mV/second after holding at short circuit for 10 seconds. The light source was a 500 W Spectra Physics lamp fitted with AM 1.5G optical filters. The intensity was calibrated to 1 sun (100 mW/cm2) using an NREL-calibrated silicon solar cell fitted with a KG-5 filer (Newport m465440). The irradiance spectrum was verified using an optical spectrometer (Newport OSM2—400DUV-U). After calibration a UV-cutoff filter was installed which removed wavelengths shorter than 380 nm, and reduced intensity in the 400-800 nm region by approximately 10%. This was not accounted for in calculations of efficiency. Neither were other losses such as reflection or absorption by the substrate adjusted for. IPCE measurements were made using a 300 W xenon lamp (Spectra Physics) focused by a parabolic reflector, and a computer controlled monochromator (Oriel Cornerstone 130, 1/8 monochromator). The lamp power spectrum was measured using an oriel calibrated silicon photodiode (Model 71580). The characteristics presented for each

type of cell represent the best cell from a series of 6 or more devices. In most cases efficiencies were reproducible to within 10-15% in a series.

5.3 Nile Red

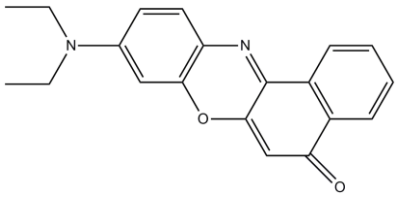

Figure 23: Chemical structure of Nile Red

Nile red is a well known as a fluorescent lipid stain.[1] It has also been used as a dopant for OLEDs.[2] It has an absorbance maximum of 41,000 $LM^{-1}cm^{-1}$ at 534 nm. It displays excellent overlap of its fluorescence spectrum with the absorbance of SQ-2, suggesting that FRET is likely. Quenching experiments indicate that lithium salt has limited effect on the emission of Nile Red while SQ-2 dye readily quenches Nile Red. Nile Red (Sigma Aldrich, technical grade) was dissolved in cholorbenzene to form a 35 mM stock solution (11 mg/ml). This stock solution was added to the Spiro-OMeTAD solution in the amount per cell indicated.

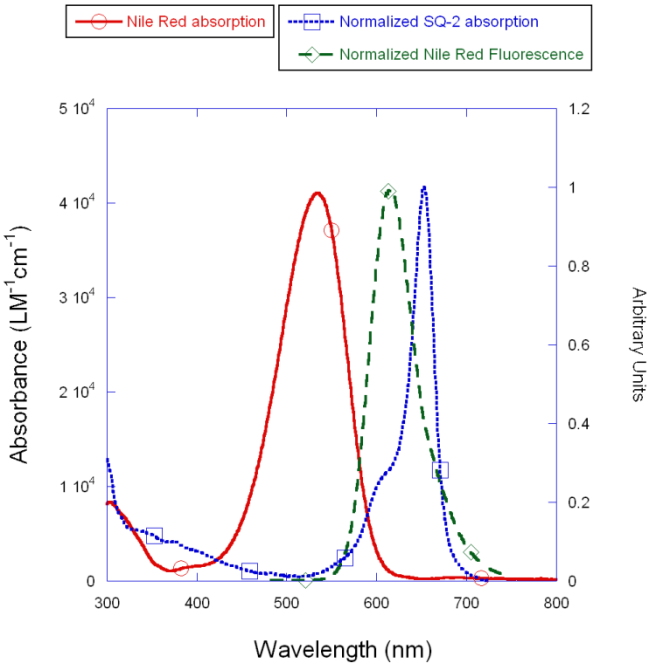

Figure 24: Absorbance and emission of Nile Red

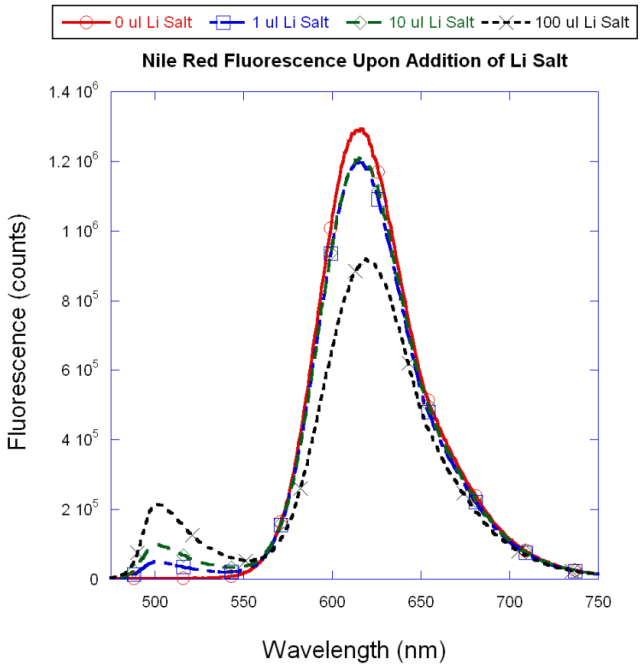

Figure 25:Quenching of Nile Red by Li salt

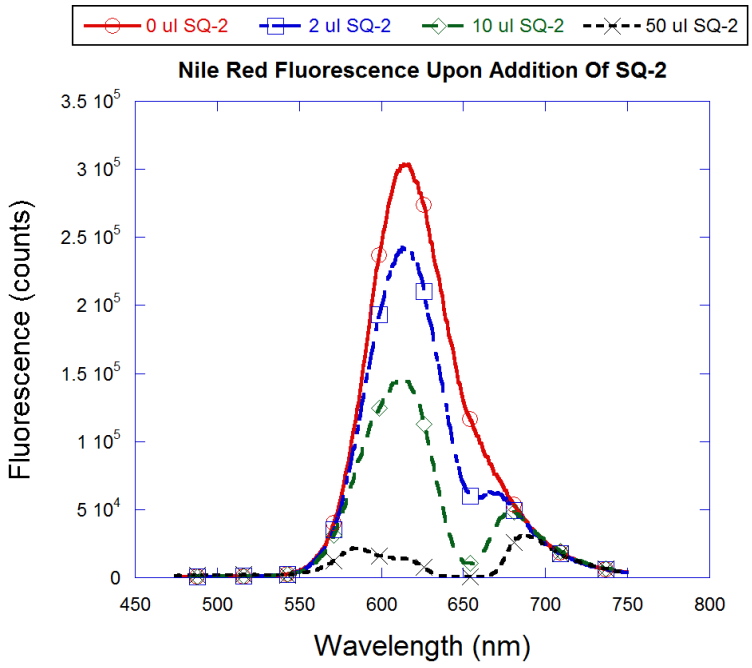

Figure 26: Quenching of Nile Red by SQ-2

Electrical characterization shows that addition of nile red has a negative effect on fill factor and short circuit current. Nile red increases cell series resistance significantly. IPCE shows that although spectral response is increased due to absorption and FRET by nile red, this gain is offset by reduced collection efficiencies across the whole spectrum. This is likely due to degraded transport though the hole transport layer. This may be due to nile red acting as a trap. It may also be due to impurities present in nile red. The exact purity is unknown, although the material used is technical grade. It is possible that purification may reduce the degradation of fill factor and carrier collection, allowing for greater efficiency.

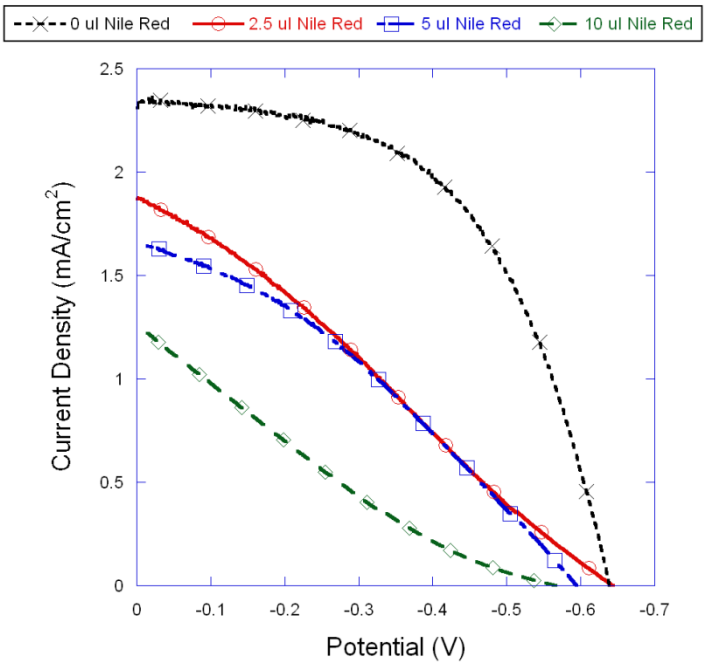

Figure 27:Current vs. Voltage for Nile Red-containing cells

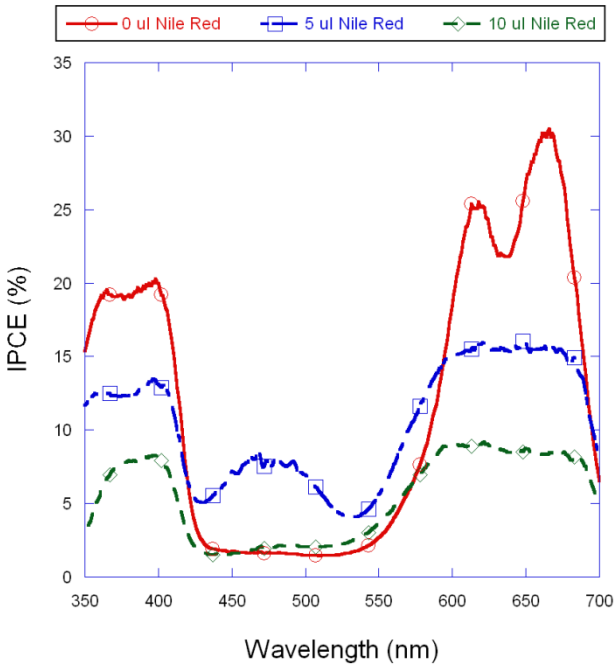

Figure 28: IPCE for Nile Red-containing cells

5.4 Merocyanine 540

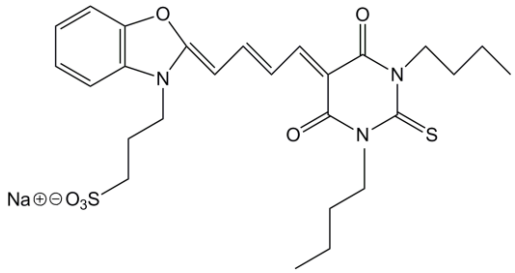

Figure 29: Chemical structure of Merocyanine 540.

Merocyanine 540 (M540) has been used as a marker for biological materials, especially cancer cells and viruses.[3,4] It has notably be used as a sensitizer for TiO_2, albeit with very low efficiencies and a peak IPCE of 7%.[5] M540 exhibits strong absorption from 500-600 nm with a peak absorbance of 98,600 $LM^{-1}cm^{-1}$ at 558 nm. Its fluorescence spectrum overlaps well with the absorption of SQ-2. It is notable that its fluorescence actually increases upon addition of lithium salt with no indication of quenching.

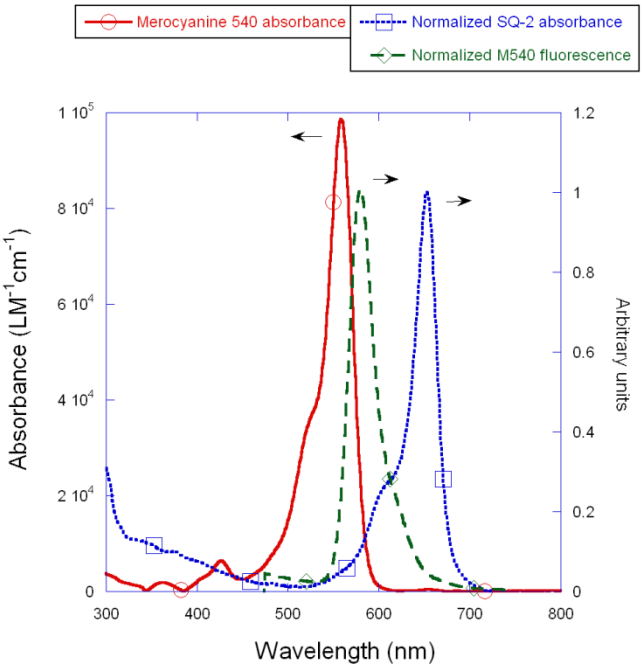

Figure 30: Absorbance and emission spectra for M540

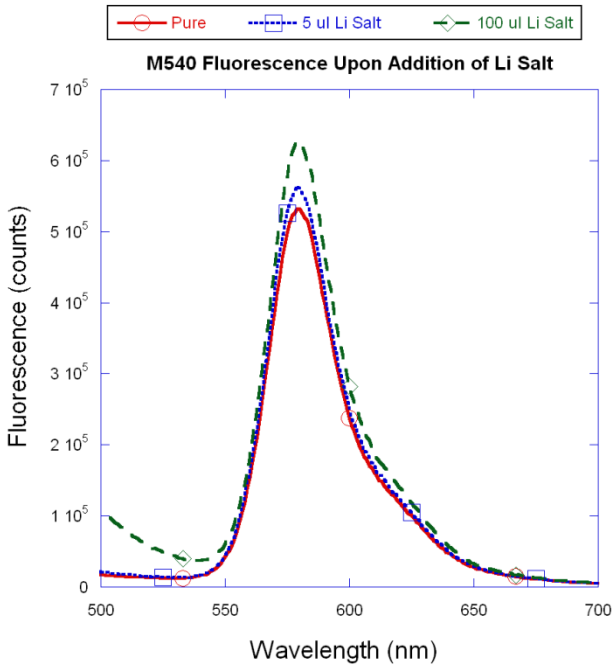

Figure 31: Quenching of M540 by Li salt

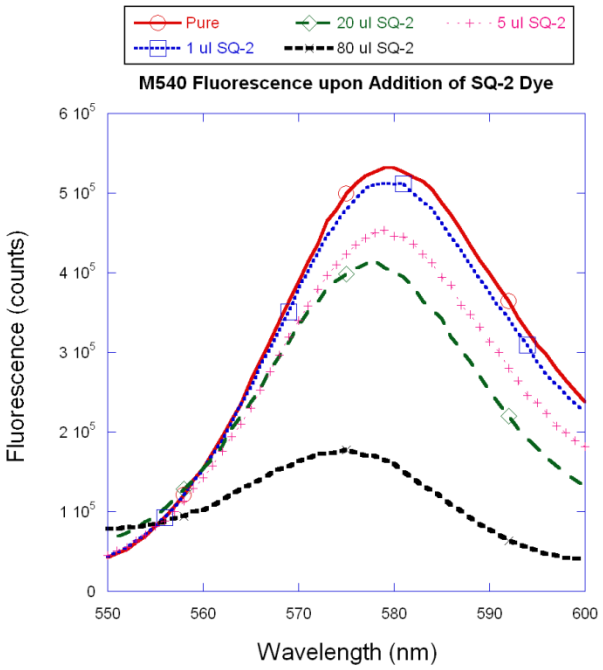

Figure 32:Quenching of M540 by SQ-2

M540 is weakly soluble in chlorobenzene. Instead, M540 (Sigma, 90%) was dissolved in dimethyl formamide (DMF) at a concentration of 10 mg/ml (17.5 mM). This solution was miscible with the Spiro-OMeTAD solution and high quality homogeneous films could be spun from this mixture. Phase separation did not occur upon drying. It was discovered that when added at a rate of 10 μl per cell, current was significantly improved. Voc was lowered upon any addition of M540, however. Due to the dramatic increase of current with the addition of 10 μl M540 solution per cell, despite the drop in fill factor and Voc, efficiency is increased by a third over the control cell. The IPCE spectrum shows that the increase in current arises from 450-600 nm region, coinciding with the absorption of M540. The lowest concentration of M540 used shows an

unexpectedly severe, though reproducible drop in current across the whole spectrum. This phenomenon reoccurs with many of the materials used. It is surprising that fill factor and Voc were still high for the 10 μl cell despite the fact that the purity of M540 was only 90%. The Excitation Transfer Efficiency (ETE) as described in Chapter 3 can be estimated by comparing the increase in IPCE due to increase in light absorption due to M540. Compared at 525 nm IPCE increases by 8.1% while an additional 13.8% of the total light is absorbed. This results in an ETE of 58%. Consulting fig. 2c reference [6] the energy transfer distance (R_c, dicussed in Chapter 3) can be estimated at 3.6 nm.

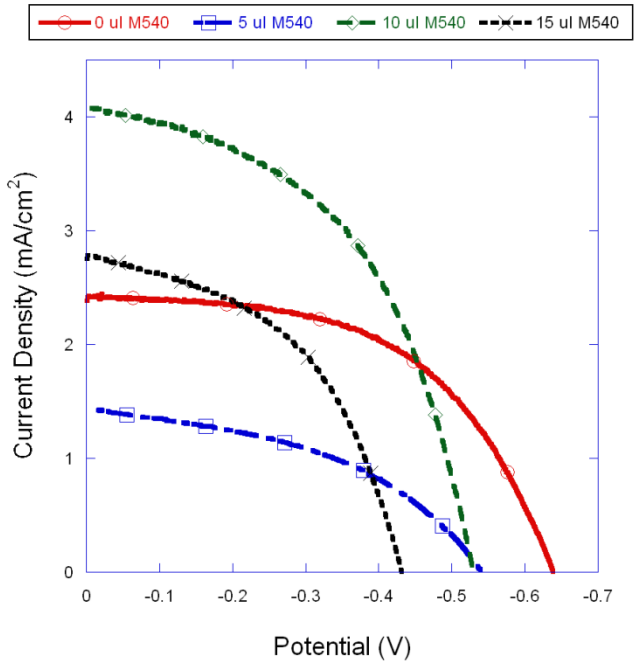

Figure 33:Current vs. Voltage for M540-containing cells

	Efficiency	Jsc (mA/cm^2)	Voc (mV)	Fill Factor
0 µl M540	0.82 %	2.4	640	53%
5 µl M540	0.34 %	1.4	542	43%
10 µl M540	1.1%	4.0	530	52%
15 µl M540	0.57%	2.7	432	48%

Table 1:Electrical properties of M540-containing cells

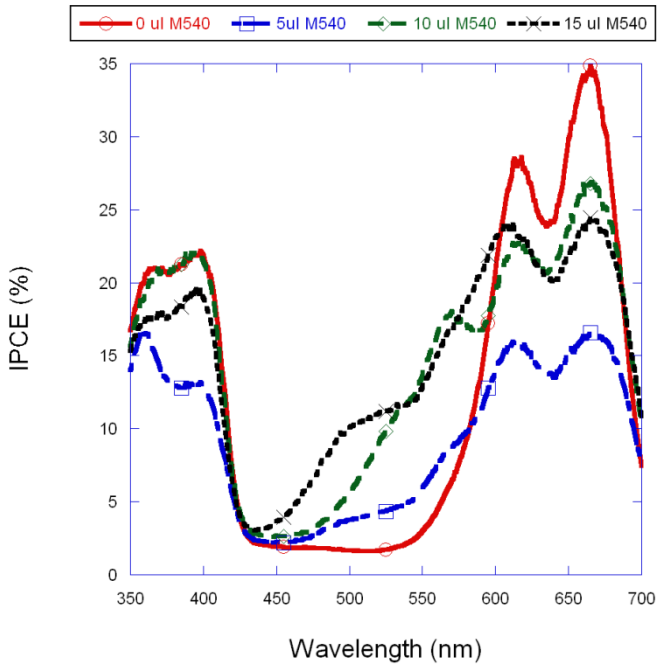

Figure 34: IPCE of M540-containing cells

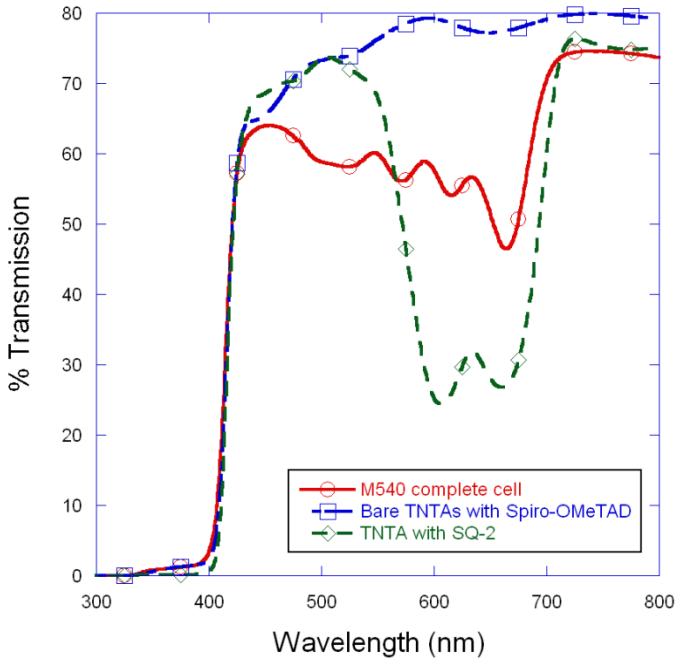

Figure 35: Transmittance of cell containing 10 μl M540

5.5 Rhodamine 640

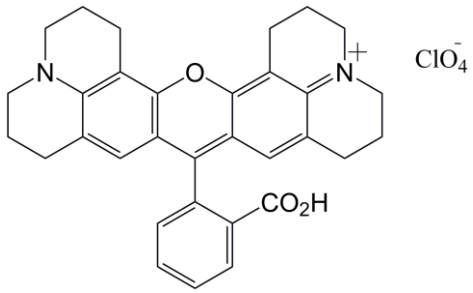

Figure 36: Chemical structure of R640

Rhodamine 640 (R640) was developed for use in dye lasers.[7] It has an absorbance maximum of 6000 $LM^{-1}cm^{-1}$ at 577 nm in acetonitrile. It is the weakest absorber which

was investigated. It is well matched to SQ-2 with broad emission overlapping the entire absorbance range of SQ-2. The tail of R640 absorbance overlaps the onset of absorbance of SQ-2. R640 experiences a significant increase in fluorescence upon addition of lithium salt. R640 is weakly soluble in acetonitrile and it is possible that the addition of lithium salt improves solubility. Quenching by SQ-2 is easily observed as the emission spectrum of R640 is replaced by that of SQ-2.

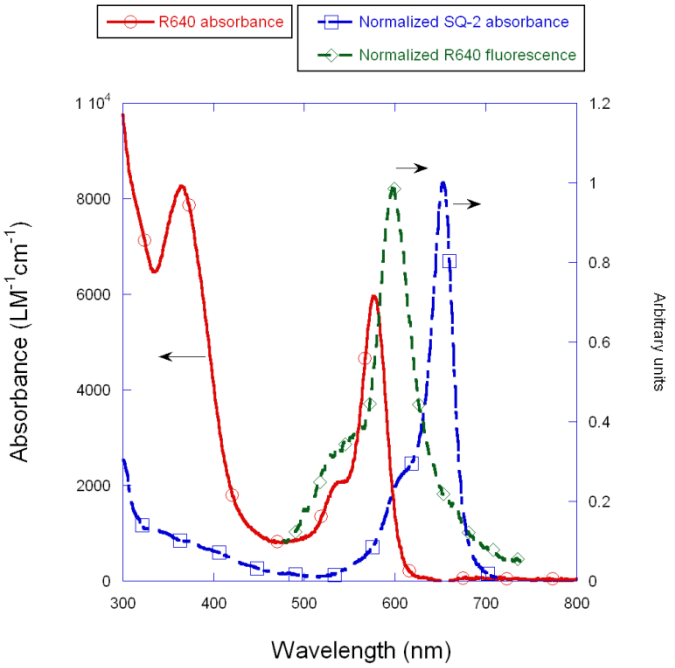

Figure 37: Absorbance and emission spectra of R640 in acetronitrile

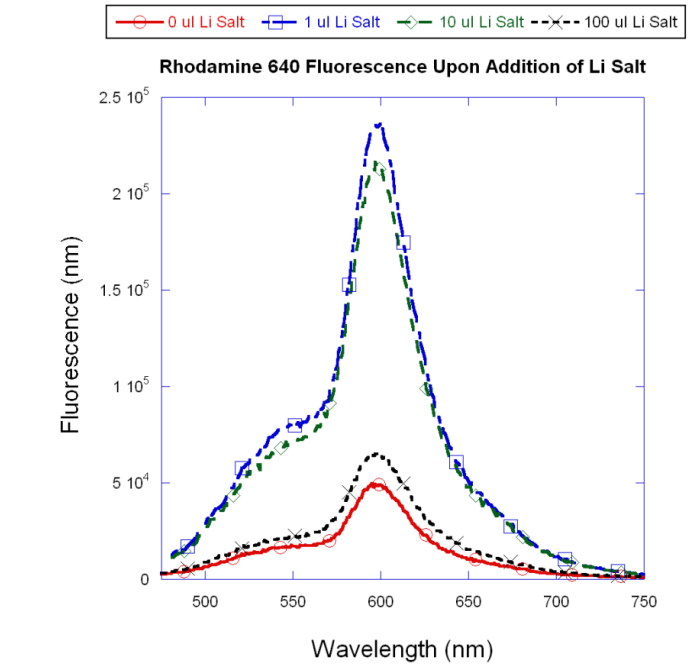

Figure 38: Quenching of R640 due to Li salt in acetonitrile

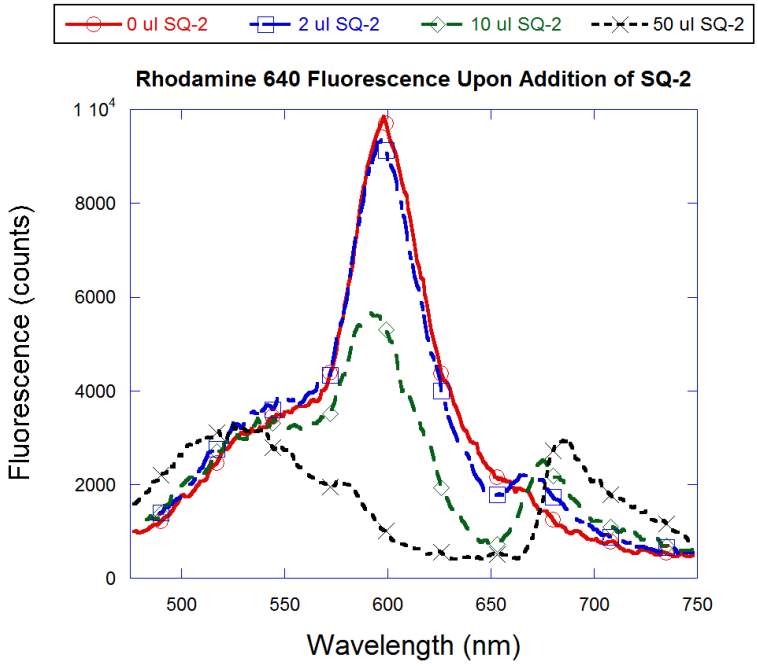

Figure 39: Quenching of R640 due to SQ-2 in acetonitrile

Rhodamine 640 was purchased from Exciton, Inc. R640 is weakly soluble in chlorobenzene and was therefore dissolved in dichlorobenzene as a saturated solution (7 mg/ml, 21 mM). Due to the similarities between the two solvents there were no problems with miscibility or phase separation upon spin casting. Electrical characterizations show that high open circuit voltages and fill factors could still be achieved upon addition of R640. IPCE shows that current increases correlate to increased response from 500-600 nm, the absorption range for R640.

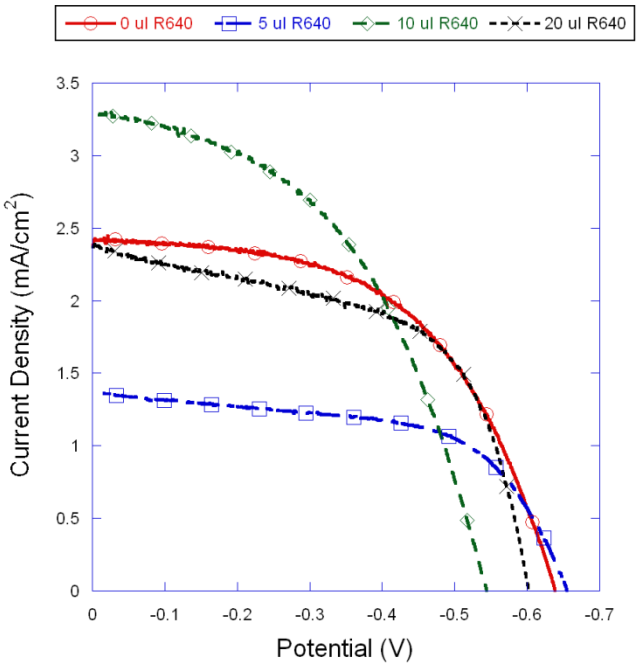

Figure 40: Current vs. Voltage for R640-containing cells

	Efficiency	Jsc (mA/cm^2)	Voc (mV)	Fill Factor
0 µl R640	0.82 %	2.4	640	53%
5 µl R640	0.53 %	1.4	654	58%
10 µl R640	0.85%	3.3	544	47%
20 µl R640	0.82%	2.4	602	57%

Table 2:Electrical properties of R640-containing cells

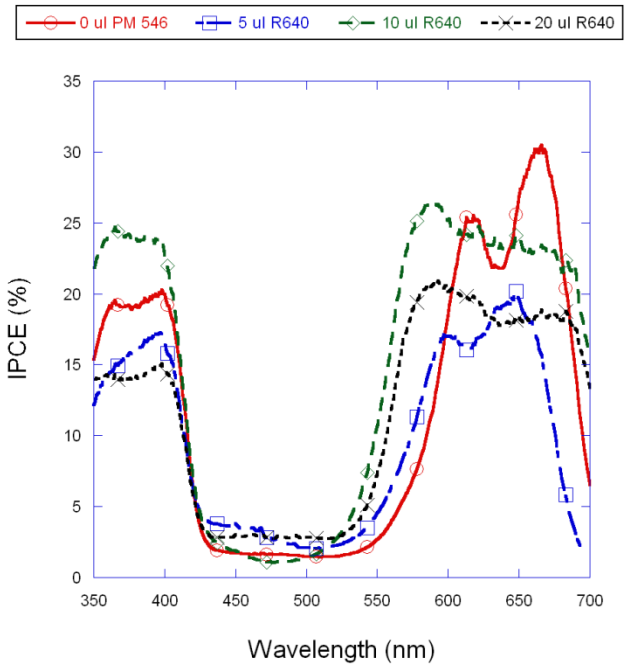

Figure 41:IPCe of R640-containing cells

5.6 Pyrromethene 546

Figure 42:Chemical structure of PM546

Pyrromethene 546 (PM546) has been used in dye lasers and solid state polymer lasers. It has a fluorescence quantum efficiency of 99% in methanol.[8] Its fluorescence is almost unaffected by the addition of lithium salt, even at very high concentrations. PM 546 has a relatively high peak absorbance of 77,800 $LM^{-1}cm^{-1}$ at 494 nm. Although its fluorescence does not overlap greatly with the absorbance of SQ-2, it still manages to transfer energy efficiently in an SDSC.

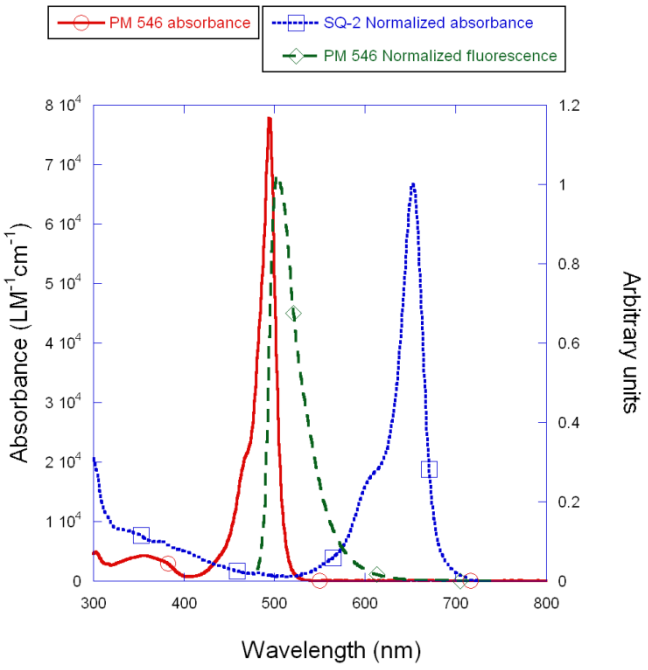

Figure 43:Absorbance adn emission of PM546

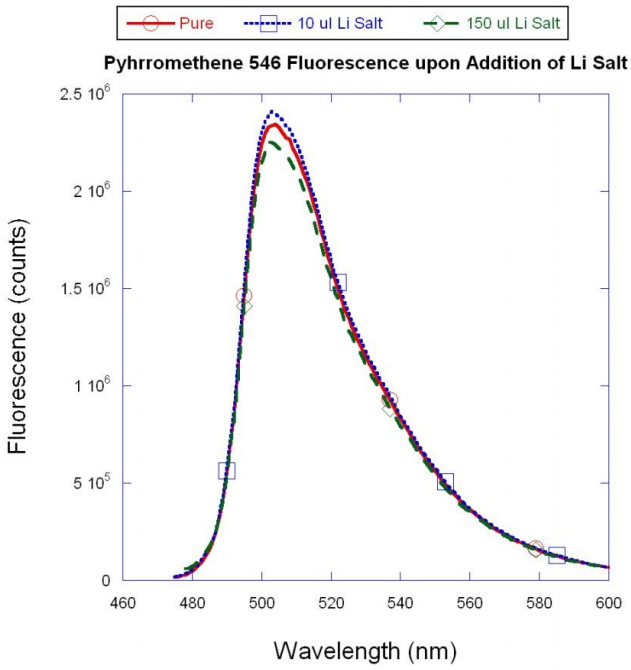

Figure 44: Pyrromethene 546 fluorescence upon addition of Li salt

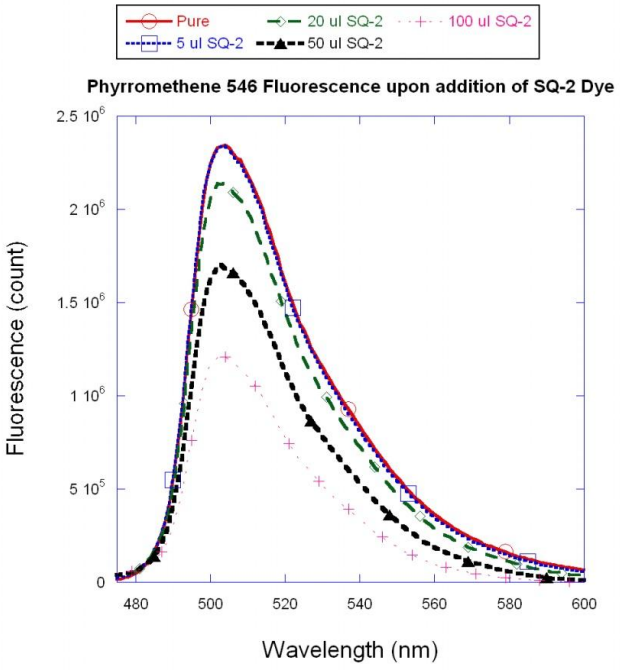

Figure 45: Pyrromethene 546 fluorescence upon addition of SQ-2 dye

PM546 was acquired from Exciton, Inc. It is soluble in chlorobenzene, and a stock solution of 10 mg/ml (38 mM) was prepared. PM546 is able to provide a considerable boost to the short circuit current in test cells. When used in the amount of 10 μl per cell a 37% increase in current was realized without significant degradation of V_{oc} and a small change in fill factor. Efficiency was increased by 27% over the control cell. IPCE shows clearly that this gain comes from absorption in the 425-550 range for cells adding 15 μl of donor. For the lesser amounts, however, the increase was mostly caused by increasing absorption by a small amount all the way to 600 nm,

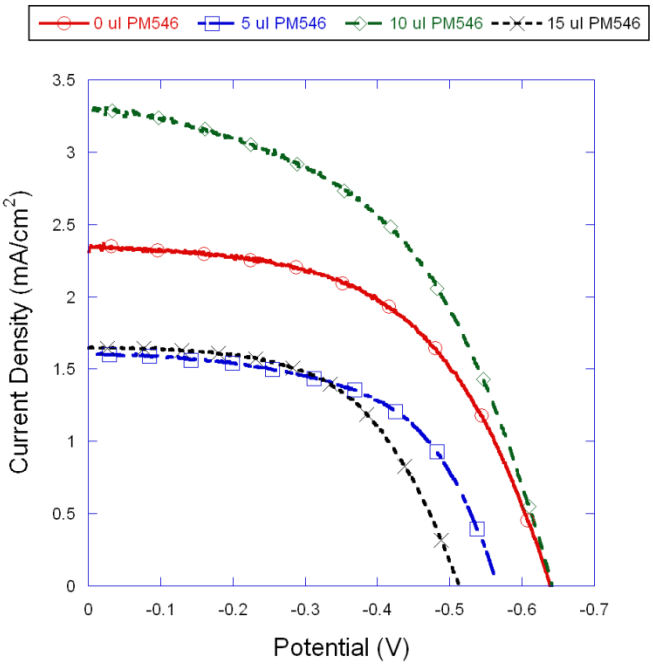

Figure 46: Current vs voltage characteristics for PM 546 test cells

	Efficiency	Jsc (mA/cm^2)	Voc (mV)	Fill Factor
0 µl PM546	0.82 %	2.4	640	53%
5 µl PM546	0.52 %	1.6	515	63%
10 µl PM546	1.04%	3.3	642	49%
15 µl PM546	0.42%	1.7	512	48%

Table 3:Electrical properties of PM546-containing cells

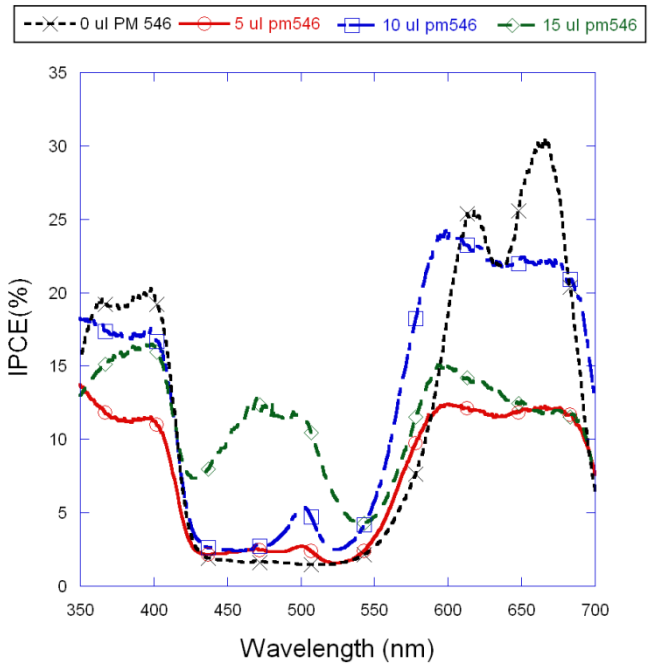

Figure 47:IPCE of PM546-containing cells

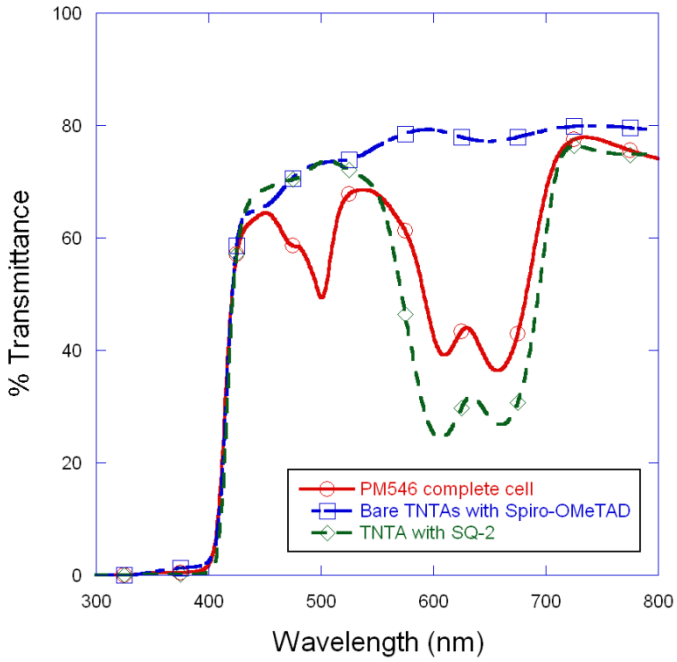

Figure 48: Transmittance for 10 μl PM 546 cell.

If the change in the transmittance at the peak of PM546 absorbance is compared to the increase in IPCE an estimation of ETE can be made. Transmittance decreases by 24% while IPCE increases by 4%, suggesting an ETE of 16.7%. For the 15 ul sample the change in IPCE is much higher, reaching 11.8% at 500 nm. If it is assumed that absorption due to PM546 increases linearly with concentration, the change in transmittance due to PM 546 would be 33%. This would correspond to an ETE of 35% for cells using 15 μl PM546. Normally ETE is assumed to be a function of Förster radius. In cases where the donor fluorescence has overlap with donor absorbance, as is the case for PM546, it is possible for FRET to occur between donor molecules. In this way excitation may migrate between PM546 until is comes within a Förster radius of an SQ-2 molecule, effective increasing the distance over which excitation may be collected. It may be possible that the concentration in 15 μl cells is sufficient to allow this excitation migration, while below this level the average separation of donors is too low. At this concentration PM546 molecules in Spiro-OMeTAD are estimated to be 2.6 nm apart on average.

5.7 Pyrromethene 605

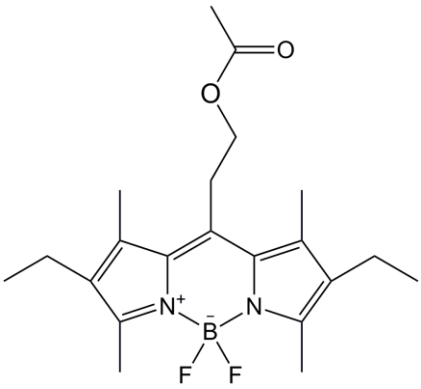

Figure 49: Structure of PM 605

Pyrromethene 605 (PM605) is similar in structure and in purpose to PM546. It has a peak absorbance of 62,000 Lm-1cm-1 at 541 nm. Its absorbance profile is also similar to PM546, though redshifted. It does provide a more favorable match in its fluorescence and the absorbance of SQ-2, suggesting that it should have a larger Förster radius than PM546. It demonstrates strong quenching by SQ-2 as well as limited quenching by lithium salt.

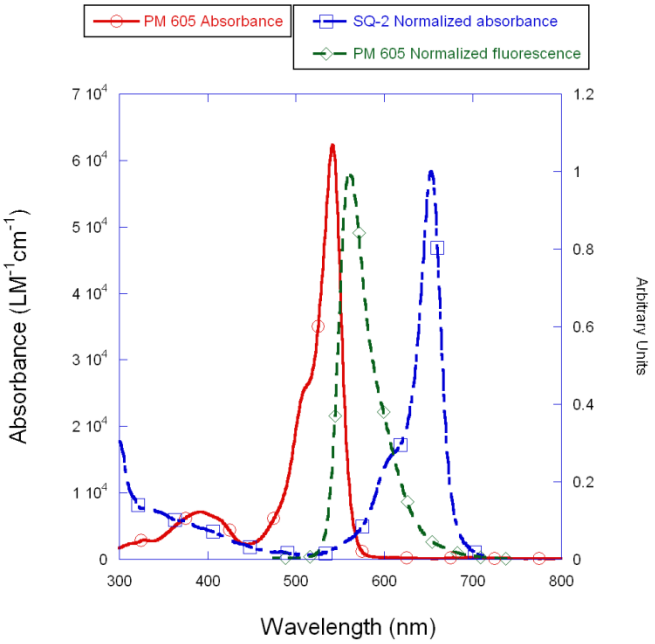

Figure 50: Absorbance and emission of PM 605

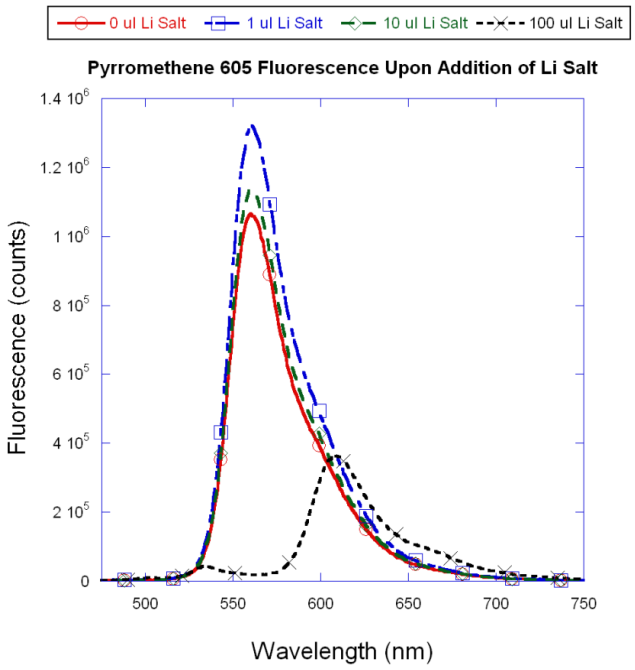

Figure 51: Quenching of PM 605 by Li salt

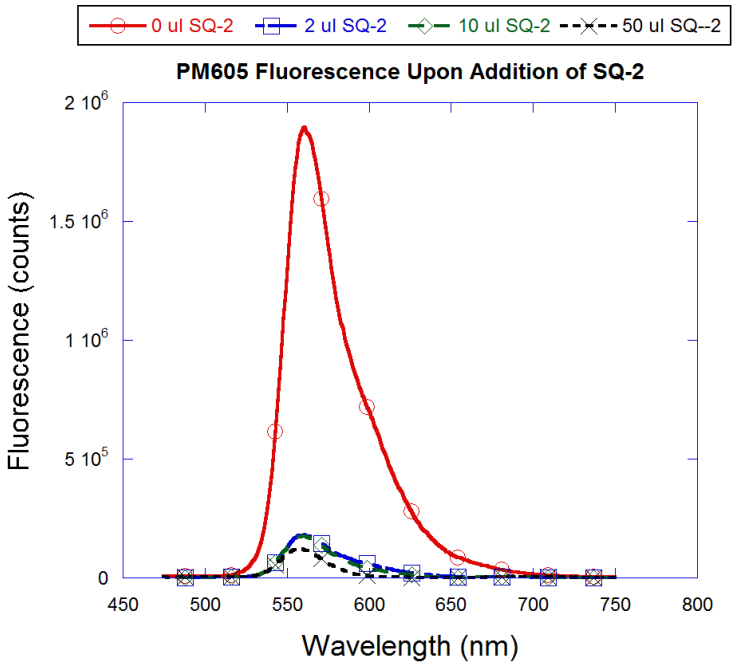

Figure 52: Quenching of PM 605 by SQ-2

PM605 was obtained from Exciton, Inc., and a stock solution of 10mg/ml (26mM) was prepared in chlorobenzene. Current vs voltage measurements, however show that that the addition of PM605 degrades cell performance. Although IPCE spectra show that response is indeed increased from 425-550 nm, these gains are offset by reductions in fill factor and open circuit voltage.

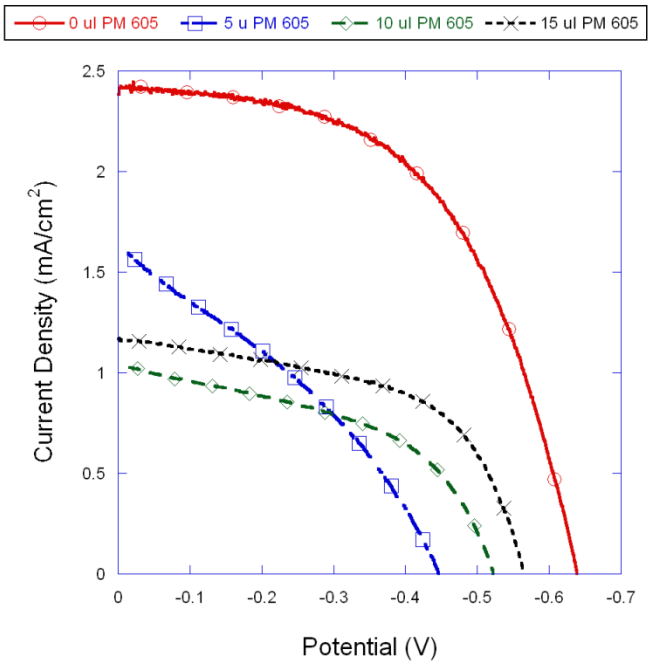

Figure 53: Current vs. Voltage for PM605-contaning cells

	Efficiency	Jsc (mA/cm^2)	Voc (mV)	Fill Factor
0 μl PM605	0.82 %	2.4	640	53%
5 μl PM605	0.24 %	1.6	446	33%
10 μl PM605	0.26%	1.04	522	48%
15 ul PM605	0.36%	1.17	565	54%

Table 4: Electrical properties of PM605-containing cells

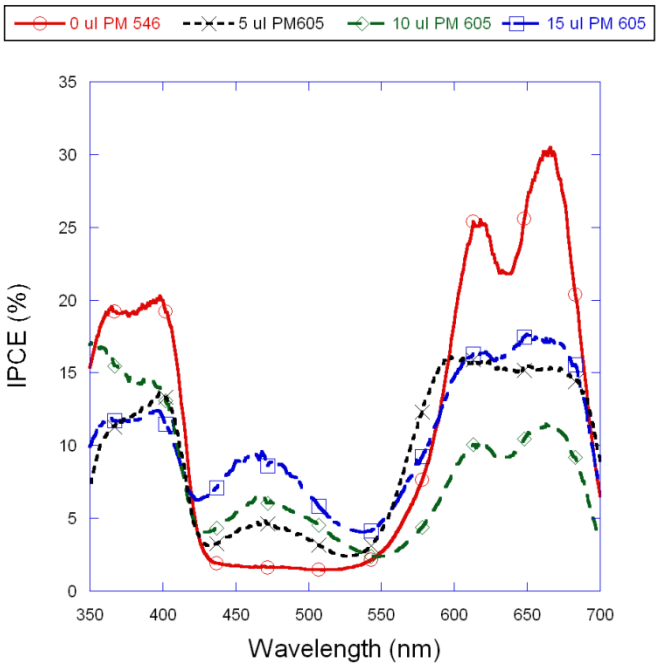

Figure 54: IPCE spectra for PM605-containing cells

5.8 Pyrromethene 650

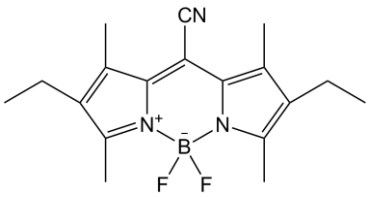

Figure 55: Chemical structure of PM 650

Pyrromethene 650 (PM650) is used in dye lasers and solid-state dye lasers. It is not as efficient a material as PM546, with a fluorescence quantum efficiency of 54%.[8] It does,

however, have a very favorable overlap in its fluorescence with the absorbance of SQ-2. It has a peak absorbance of 40,500 $LM^{-1}cm^{-1}$.

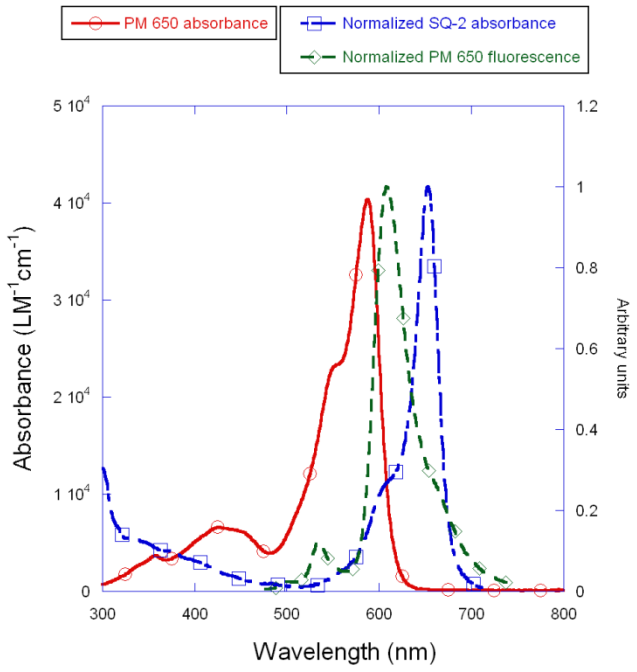

Figure 56: Absorbance and emission spectra of PM 650

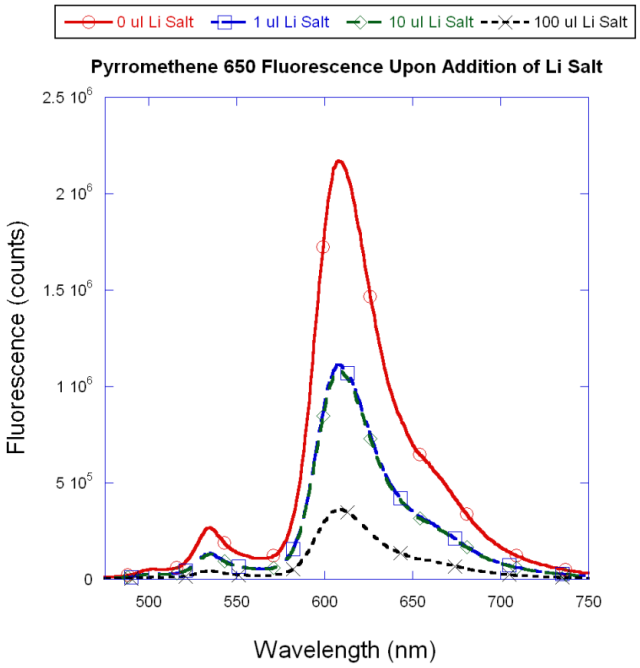

Figure 57: Quenching of PM650 by Li salt

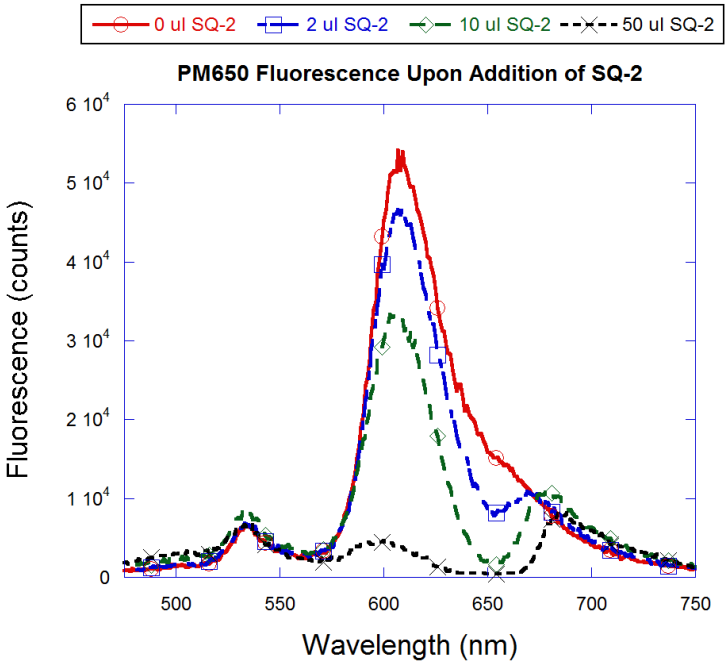

Figure 58: Quenching of PM 650 by SQ-2

PM650 was obtained from Exciton, Inc., and a stock solution of 10mg/ml (33mM) was prepared in chlorobenzene. One might expect the performance of PM 650 in test cells to be better that that of PM546 or PM605 because its emission is the most favorably aligned of the three with respect to the absorbance on SQ-2. PM650 severely degrades performance however, leading to extremely low efficiencies. It is possible that PM 650 acts as a trap and greatly increases the resistivity of the hole transport layer. Measurements of the HOMO/LUMO levels of all three pyrromethenes would be useful in determining this.

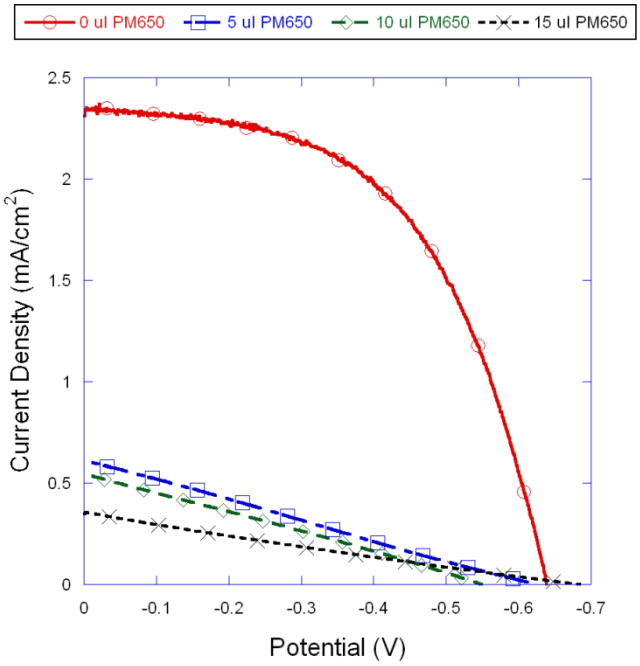

Figure 59: Current vs Voltage for PM650-containing cells

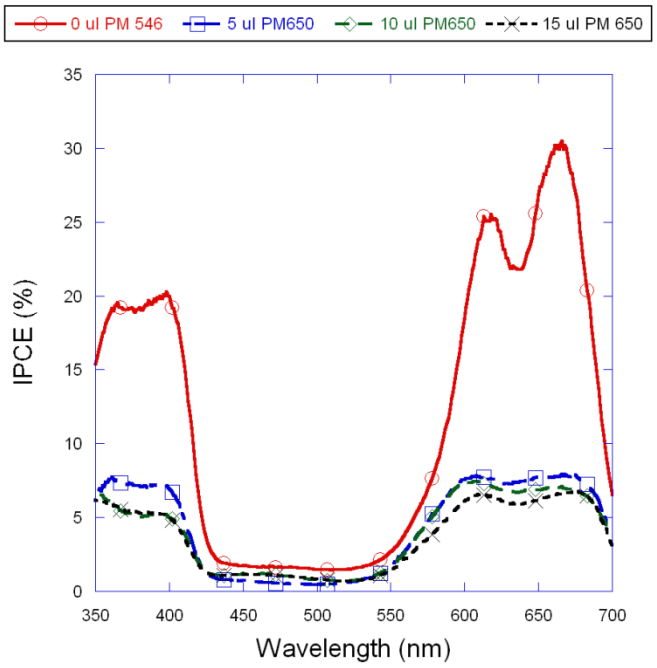

Figure 60: IPCE spectra for PM 650-containing cells

5.9 DCM Pyran

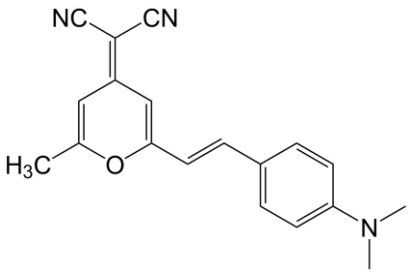

Figure 61:Chemical structure of DCM

DCM is a widely used dye for solid state dye lasers. Its peak absorbance is 28,000 $LM^{-1}cm^{-1}$ at 420 nm which is somewhat lower than most of the other molecules investigated. However, it absorbs more broadly than other molecules investigated. Its fluorescence exhibits ideal overlap with the absorbance of SQ-2. DCM (Sigma Aldrich, 98%) was dissolved in chlorobenzene for a 24 mM (7.3 mg/ml) stock solution. Quenching experiments show that DCM fluorescence is not quenched by lithium salt and actually increases for small concentrations. Fluorescence is quenched by SQ-2. UV-Vis absorption data in Figure 67 suggest that the absorption maximum of DCM is significantly shifted from 420 nm in acetonitrile to approximately 490 nm in a thin film of Spiro-OMeTAD.

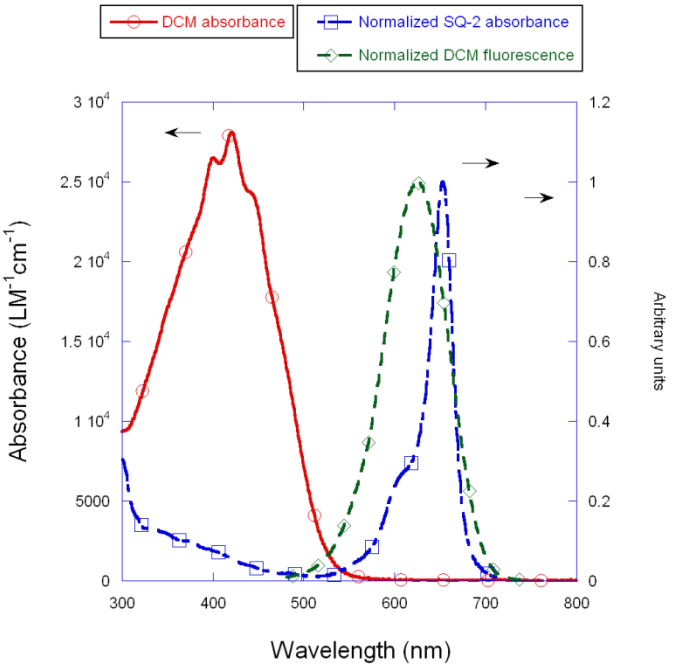

Figure 62:Absorption and emission spectra for DCM dissolved in acetonitrile

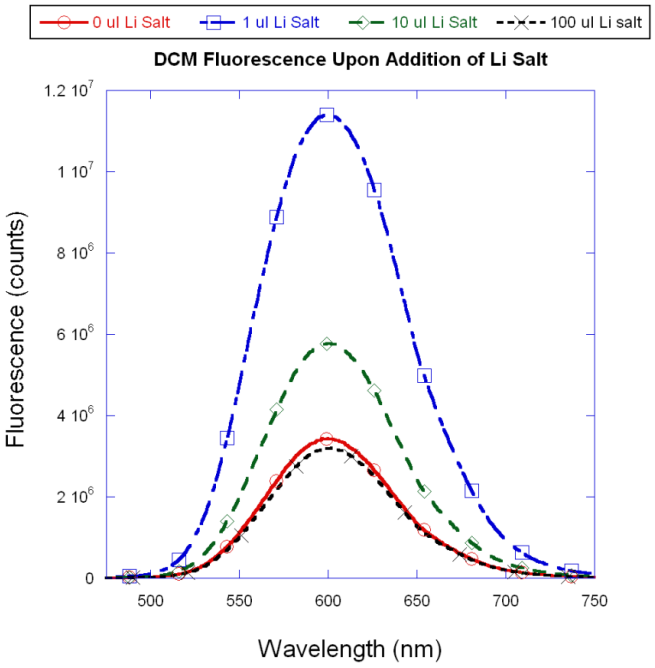

Figure 63: Quenching due to SQ-2

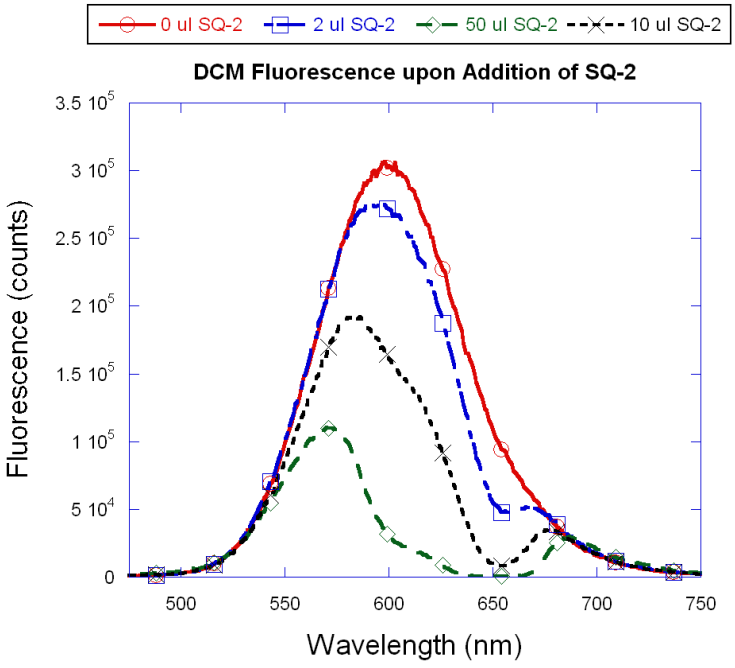

Figure 64: Quenching of DCM by SQ-2

DCM is able to be used in larger proportions than other materials without degrading cell electrical parameters. In fact, for cells containing 30 μl DCM solution open circuit voltage, short circuit current and fill factor are all improved. For concentrations above this reductions in overall efficiency were seen. In the 30 μl case, overall efficiency was increased by 34% over the control cell. IPCE at 492 nm was increased by 3.9% while light absorption was increased by 27.6%. This results in an ETE of 14%. At lower concentrations, however, IPCE was higher in this region despite lower light absorption. For cells containing 20 μl DCM, ETE was approximately 30%.

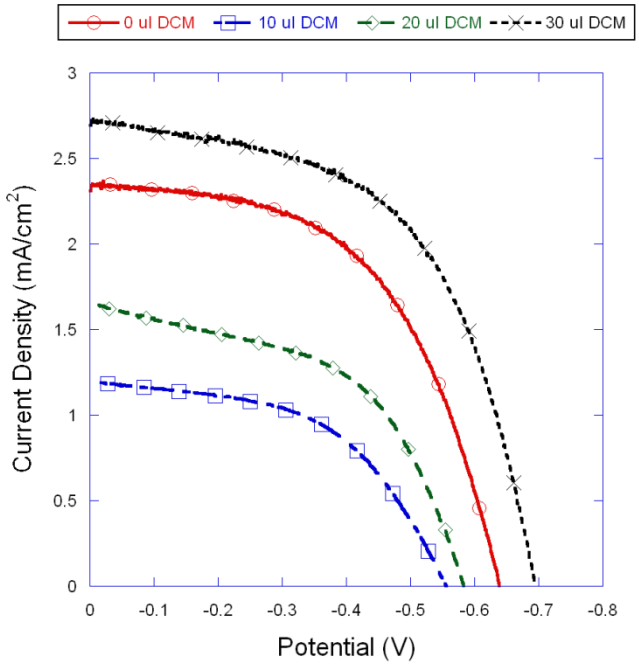

Figure 65: Current vs. Voltage for DCM-containing cells

	Efficiency	Jsc (mA/cm^2)	Voc (mV)	Fill Factor
0 µl DCM	0.82 %	2.4	640	53%
10 µl DCM	0.34 %	1.2	555	51%
20 µl DCM	0.5%	1.6	583	54%
30 µl DCM	1.1%	2.7	694	56%

Table 5: Electrical properties of DCM-containing cells

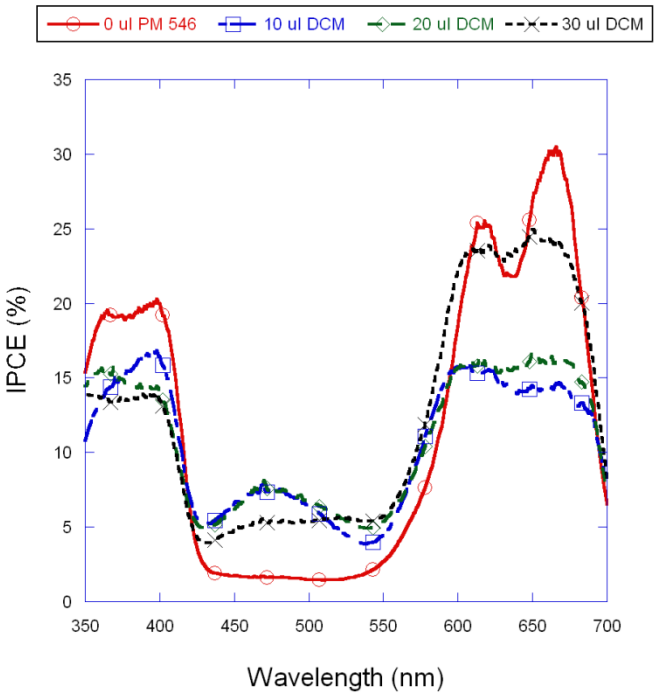

Figure 66: IPCE spectra of DCM-containing cells

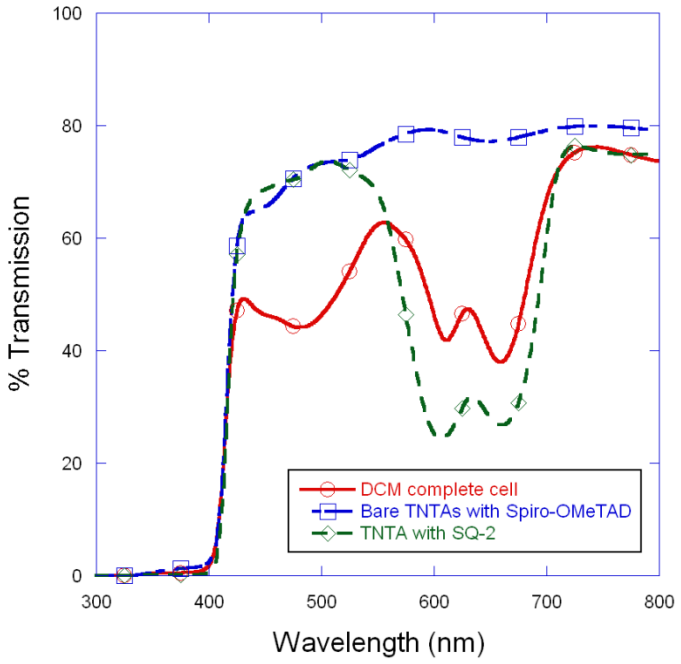

Figure 67:Transmittance for a cell containing 30 μl DCM

DCM was also investigated using SQ-1 instead of SQ-2 as the acceptor dye. The absorbance maximum of SQ-1 is slightly blue-shifted relative to SQ-1. It was found that ETE was more efficient in this system, as high as 67%. Results are published in ref. [9].

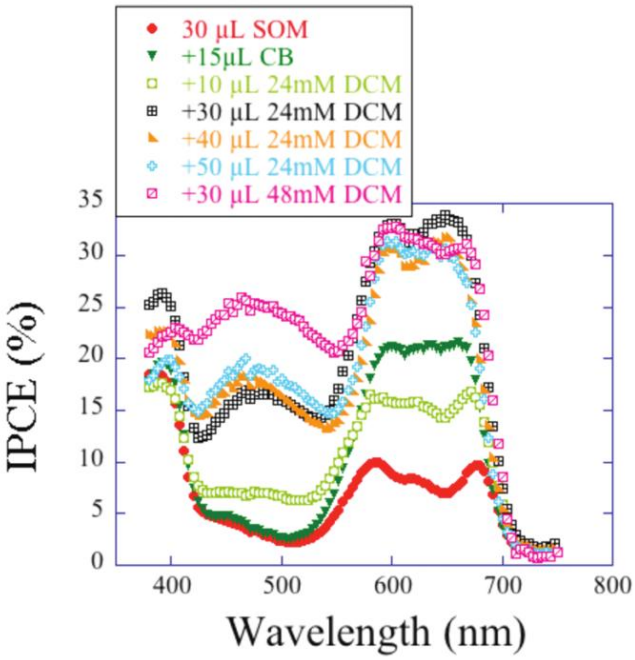

Figure 68: IPCE for cells using SQ-1 as acceptor. Reprinted from ref [9]

5.10 References

(1) Greenspan, P. Mayer, E. P.; Fowler, S. D. Nile red: a selective fluorescent stain for intracellular lipid droplets. *The Journal of cell biology* **1985**, *100*, 965-73.

(2) Pschenitzka, F.; Sturm, J. C. Three-color organic light-emitting diodes patterned by masked dye diffusion. *Applied Physics Letters* **1999**, *74*, 1913.

(3) Salama, G.; Morad, M. Merocyanine 540 as an optical probe of transmembrane electrical activity in the heart. *Science* **1976**, *191*, 485-487.

(4) Williamson, P. Mattocks, K.; Schlegel, R. Merocyanine 540, a fluorescent probe sensitive to lipid packing. *Biochimica et Biophysica Acta (BBA) - Biomembranes* **1983**, *732*, 387-393.

(5) Khazraji, A. C. Hotchandani, S. Das, S.; Kamat, P. V. Controlling Dye (Merocyanine-540) Aggregation on Nanostructured TiO_2 Films. An Organized Assembly Approach for Enhancing the Efficiency of Photosensitization. *The Journal of Physical Chemistry B* **1999**, *103*, 4693-4700.

(6) Hoke, E. T. Hardin, B. E.; McGehee, M. D. Modeling the efficiency of Förster resonant energy transfer from energy relay dyes in dye-sensitized solar cells. *Optics express* **2010**, *18*, 3893-904.

(7) Hartig, W. A high power dye-laser pumped by the second harmonic of a Nd-YAG laser. *Optics Communications* **1978**, *27*, 447-450.

(8) Boyer, J. H. Haag, A. M. Sathyamoorthi, G. Soong, M.-L. Thangaraj, K.; Pavlopoulos, T. G. Pyrromethene-BF2 complexes as laser dyes: 2. *Heteroatom Chemistry* **1993**, *4*, 39-49.

(9) Mor, G. K. Basham, J. Paulose, M. Kim, S. Varghese, O. K. Vaish, A. Yoriya, S.; Grimes, C. A. *High-Efficiency Forster Resonance Energy Transfer in Solid-State Dye Sensitized Solar Cells.* 2010.

6. Conclusions and Future Work

6.1 Conclusions

The purpose of this dissertation has been to investigate the possibility for employing FRET in order to broaden the spectral response of solid-state dye-sensitized solar cells. The materials investigated in chapter 5 prove that FRET can indeed be used to increase solar cell performance. Several compounds discussed, along with several others investigated but not discussed, did not show increases in efficiency for various reasons. These reasons included poor solubility in the spin casting solvent, quenching by other cell components, or insufficient overlap of donor fluorescence with acceptor absorbance.

Four compounds were able to increase overall cell efficiency over the control: Merocyanine 540, Pyrromethene 546, Rhodamine 640 and DCM. One feature that all these materials had in common was that they were largely unaffected by the presence of lithium salt. In fact, it seems that lithium salt actually increased their solubility and fluorescence efficiency. Three of these compounds also exhibited nearly ideal overlap in their fluorescence with the absorbance of SQ-2

Pyrromethene 546 was an unexpected success for two reasons. Firstly, its fluorescence only slightly overlaps with the absorbance of SQ-2, yet it still displays an excitation transfer efficiency of up to 35%. The fact that ETE seems to increase with donor concentration suggest that excitons may be hopping between donors until they migrate close enough to transfer to an SQ-2 molecule. This effectively increases the distance over which excitation can be harvested. Secondly, it belongs to a family of

materials, including pyrromethene 605 and 650, which would be expected to be better donor materials as one fluorescence redshifts. The expected trend is opposite to the observed trend, however, in which the electrical properties become significantly degraded in pyrromethene 605 ad 650. One possible cause may be that the HOMO level of pyrromethene 546 is only slightly more positive that then HOMO level of Spiro-OMeTAD. The decrease in optical bandgap in these materials may be realized by moving the HOMO level to more negative potentials, until in pyromethene 650 it could be more negative than the HOMO level of Spiro-OMeTAD, creating traps and increasing recombination. This theory could be tested by measuring the HOMO/LUMO levels of the three pyrromethenes.

The most interesting material for further study was Merocyanine 540. It exhibited the largest increase in short circuit current density, meaning the largest increase in the number of photons harvested. It also exhibited the largest excitation transfer efficiency, 58%. It is surprising that this is possible from the lowest purity material used. This excellent result proves not only that FRET can be harnessed to broaden the spectral response of SDSCs, but that it can do so efficiently. With the proper donor and doping levels, it can be utilized without sacrificing other important cell parameters, namely V_{oc} and fill factor.

6.2 Future Work

There are many areas in which the solar cells, as fabricated in this dissertation, could be improved. The most ready improvement would be a moderate increase in the active layer thickness. The cells in this work have an active layer thickness of 600-800nm, while the maximum useful thickness is about 2 microns. While it is more difficult to optimize the fabrication process close to this limit, it is very possible once a specific system has been chosen and would lead to higher efficiencies. The lower thickness used in this work was justified by greater uniformity between the wide variety of samples.

Efficiency could also be increased by using a dye which can produce a greater open circuit voltage. SQ-2 dye produces a relatively low open circuit voltage of 650-700 mV, while up to 1 V is possible in SDSCs.[1] Unlike inorganic solar cells where the open circuit voltage is limited by the band gap of the absorber, the upper limit of open circuit voltage in DSSCs in instead the difference between the conduction band of TiO_2 and the redox potential of the electrolyte or hole transport material. This is about 1.2 V for SDSCs using Spiro-OMeTAD, and about 0.8V for DSSCs using a liquid I^-/I_3^- redox couple. Losses can be due to dye kinetics, such as high rates for interfacial recombination. By using a dye with better kinetics which raises V_{oc}, efficiency could be increased. It has also been shown that dyes which increase the surface charge on TiO_2 can push its conduction band to more negative potentials, thereby increasing the open circuit potential. Therefore a dye with a larger dipole moment would also increase efficiency and V_{oc}.[2]

Additionally, because SQ-2 has an energy gap of about 1.6 eV while the maximum extractable voltage is only 1.2 V, dyes with slightly lower energy gaps could be used to harvest lower energy photons to increase short circuit current without degrading V_{oc}. Some overpotential is still necessary, however, to drive transport and exciton separation. If an energy gap of 1.4 eV could be uitilized, as well as a good IPCE across the spectrum between 350 nm – 900 nm, roughly 50% more solar power would be available for conversion than for a typical cell using N-719 dye.

Extending the range of the acceptor dye to longer wavelengths could also mean that the donor materials must cover a larger band of the solar spectrum. It may be necessary to couple two or more donor materials which would transfer energy in a cascade ending with the acceptor dye. By using multiple donors it would likely be easier to achieve uniformly high IPCE instead of two strong peaks for absorption.

The structure of donors must also be specially designed to increased efficiency. Practical concerns such as high solubility in cholorbenzene can be met by adding functional groups. HOMO/LUMO levels can also be adjusted to decrease interaction with lithium salt dopants and to reduce the effect on charge transport. Bulky pendant groups may also be added in order to increase physical separation from any quenchers. The materials found in this work to be the best suited for use in SDSCs could be used as a starting point, with these modifications to their structure to increase efficiency even further.

Additionally, the purity of donors is extremely important, as impurities can adversely affect transport. It is well known that using high purity dyes and other materials greatly improves solar cell efficiency. It is possible that in this work the purity

of donor materials may have limited the amount of donor that could be used before transport degradation offset any gains made. For example, the highest grade of merocyanine 540 readily available was only 90% pure. It is likely that using very high purity donors would increase cell performance at similar loadings of donor material by removing impurities which may act as traps and recombination centers. By enabling higher loading of donor molecules it would also be possible to achieve nearly complete light absorption by the donor.

It would also be very useful to do a full characterization of the effect of any of the four best donors on cell parameters such as electron lifetime, transport time and mobility. The most useful techniques would be open circuit voltage decay, intensity modulated photocurrent spectroscopy, and intensity modulated photovoltage spectroscopy.

The ideal culmination of this work would be a thick cell employing several tailor-made donor materials which transfer energy in a cascade to an IR-absorbing dye which exhibits a high open circuit voltage and low rates of recombination and back injection. Currently neither such donors nor such dyes exist, so the remaining task is largely the work for an organic synthetic chemist.

6.3 References

(1) Chen, P. Yum, J. H. De Angelis, F. Mosconi, E. Fantacci, S. Moon, S.-J. Baker, R. H. Ko, J. Nazeeruddin, M. K.; Gratzel, M. High open-circuit voltage solid-state dye-sensitized solar cells with organic dye. *Nano letters* **2009**, *9*, 2487-92.

(2) Rühle, S. Greenshtein, M. Chen, S.-G. Merson, A. Pizem, H. Sukenik, C. S. Cahen, D.; Zaban, A. Molecular adjustment of the electronic properties of nanoporous electrodes in dye-sensitized solar cells. *The journal of physical chemistry. B* **2005**, *109*, 18907-13.

Curriculum Vitæ

Education

The Pennsylvania State University (2007-Present)
University Park, PA. 16802

- PhD in Electrical Engineering, concentration in Semiconductor Design and Device Physics (VLSI).

Rensselaer Polytechnic Institute (2003-2007)
110 8th St. Troy, NY 12180

- BS in Applied Physics, specialization in nanomaterials.

Awards and Honors

- Member of Sigma Pi Sigma, national physics honor society. Awarded 2007.
- President of the Society of Physics Students, RPI chapter. (2005-2007)

Teaching Experience

Recitation instructor for an undergraduate circuits course, EE211 AY 2010-2011.

Selected Publications

Bandara, J., Shankar, K, Basham, J, Thelakkat, M. et al.. Integration of TiO_2 nanotube arrays into solid-state dye-sensitized solar cells. *The European Physical Journal Applied Physics* **53**, 20601(2011).

Basham, J.I., Mor, G.K. and Grimes, C.A. Förster resonance energy transfer in dye-sensitized solar cells. *ACS Nano* **4**, 1253-8(2010).

Mor, G.K., Basham, J.I., and Grimes, C.A. High-Efficiency Forster Resonance Energy Transfer in Solid-State Dye Sensitized Solar Cells. *Nano letters* (2010).doi:10.1021/nl100415q

Feng, X., LaTempa, T., Basham, J.I., et al. Ta_3N_5 nanotube arrays for visible light water photoelectrolysis. *Nano letters* **10**, 948-52(2010).

Shankar, K., Basham, J.I., et al. Recent Advances in the Use of TiO2 Nanotube and Nanowire Arrays for Oxidative Photoelectrochemistry. *The Journal of Physical Chemistry C* **113**, 6327-6359(2009).

Mor, G.K., Kim, S., Paulose, M., Varghese, O.K., Shankar, K., Basham, J., Grimes, C.A. Visible to near-infrared light harvesting in TiO2 nanotube array-P3HT based heterojunction solar cells. *Nano letters* **9**, 4250-7(2009).